UNIVERSITY OF CALIFORNIA

Los Angeles

Regulation of Neuronal Excitability by the RNA-Binding Protein Rbfox1

A dissertation submitted in partial satisfaction of the requirements

for the degree Doctor of Philosophy in Molecular Biology

by

Celine Kim Vuong

2017

ABSTRACT OF THE DISSERTATION

Regulation of Neuronal Excitability by

The RNA-Binding Protein Rbfox1

by

Celine Kim Vuong

Doctor of Philosophy in Molecular Biology

University of California, Los Angeles, 2017

Professor Douglas L. Black, Chair

Dysfunction of the neuronal RNA binding protein RBFOX1 has been linked to epilepsy and autism spectrum disorders. Rbfox1 loss in mice leads to neuronal hyperexcitability and seizures, but the physiological basis for this is unknown. We identify the vSNARE protein Vamp1 as a major Rbfox1 target using high throughput RNA-seq and CLIP-seq in adult mouse brain. Vamp1 is strongly downregulated in Rbfox1 Nes-cKO mice due to loss of 3' UTR binding byRbfox1. Using viral induction by AAVs and reporter assays in primary cultured neurons, we show that cytoplasmic Rbfox1 stimulates Vamp1 expression in part by blocking microRNA-9. We find that Vamp1 is specifically expressed in inhibitory neurons in vivo and in cultured neurons using immunofluorescence. Electrophysiological analyses in acute hippocampal slices

show that both Vamp1 knockdown and Rbfox1 loss lead to decreased inhibitory synaptic transmission and E/I imbalance. To assay whether the inhibitory defects in the Rbfox1 cKO are due to Vamp1 loss, we then use stereotaxic injection of AAVs to re-express Vamp1 selectively within Rbfox1 cKO interneurons. Remarkably, re-expression of Vamp1 rescues the electrophysiological changes in the Rbfox1 cKO, indicating that Vamp1 loss is a major contributor to the Rbfox1 Nes-cKO phenotype. The regulation of interneuron-specific Vamp1 by Rbfox1 provides a paradigm for broadly expressed RNA-binding proteins performing specialized functions in defined neuronal subtypes.

The dissertation of Celine Kim Vuong is approved.

Arnold Berk

Kelsey C. Martin

Thomas J. O'Dell

Douglas L. Black, Chair

University of California, Los Angeles

2017

DEDICATION

This dissertation is dedicated to my parents, without whose hard work and sacrifice I would not have been able to pursue and succeed in my education; to Luis de la Torre-Ubieta, my other half, confidante, and truest friend; to my mentor Doug Black, in whose lab I was so lucky to be supported, encouraged and free to explore new ideas; to all the members of the Black lab, for making lab feel like my second home; to the collaborators and friends I had the good fortune to meet at UCLA; and to my committee, for their guidance throughout my graduate work.

TABLE OF CONTENTS

LIST OF FIGURES

ACKNOWLEDGEMENTS

Chapter 1 includes, with permission, material from a published review:
Vuong CK, Black DL, Zheng S (2016). The neurogenetics of alternative splicing. Nat. Rev. Neurosci. Apr 20;17(5): 265-281. PMID: 27094079. PMCID: PMC4861142.

Chapters 2 through 4 are a manuscript that is in preparation:
Vuong CK, Wei W, Lee JA, Lin CH, Damianov A, de la Torre-Ubieta L, Halabi R, Otis KO, Martin KC, O'Dell TJ, Black DL (2017). Rbfox1 regulates synaptic transmission through the inhibitory neuron specific v-SNARE Vamp1. *In preparation.*

W. Wei performed and analyzed all electrophysiology presented in this work, under the supervision of T.J. O'Dell. C.H. Lin performed bioinformatic analysis of RNAseq and iCLIPseq data, and A. Damianov performed Rbfox1 iCLIP in adult mouse brain, under supervision of D.L. Black. J.A. Lee performed Rbfox1 iCLIP in primary neurons, under the supervision of K.C. Martin. L. de la Torre-Ubieta performed logistic regression on RNAseq data. R. Halabi and K.O. Otis contributed to molecular biology and electrophysiology experiments, respectively.

This work was supported by the Cellular and Molecular Biology Training Grant at UCLA (NIH T32 GM007185) and the Ruth L. Kirschstein Pre-Doctoral National Research Service Award (F31 NS093923).

VITA

EDUCATION

Brown University — Providence, RI

B.A., Biology — 2009

PUBLICATIONS

1) Ying Y, Wang XJ, Vuong CK, Lin CH, Damianov A, Black DL (2017). Cell. A tyrosine-rich domain mediates higher order assembly of Rbfox proteins to regulate splicing.
2) Vuong CK, Black DL, Zheng S (2016). The neurogenetics of alternative splicing. Nat. Rev. Neurosci. Apr 20;17(5): 265-281. PMID: 27094079. PMCID: PMC4861142.

PRESENTATIONS

1) Vuong CK, Wei W, Lin CH, Lee JA, Damianov A, Halabi R, Martin KC, O'Dell TJ, Black DL. Rbfox1 regulation of inhibitory synaptic transmission. Oral presentation Sep, 2017 at the CSHL Meeting: Eukaryotic mRNA Processing, Cold Spring Harbor, NY.
2) Vuong CK, Wei W, Lee JA, Damianov A, Martin KC, O'Dell TJ, Black DL. Rbfox1 regulation of inhibitory synaptic transmission. Oral presentation Sep, 2016 at the CSHL Meeting: Axon Guidance, Synapse Formation & Regeneration, Cold Spring Harbor, NY.

3) Vuong CK, Otis KO, Martin CK, Black DL. The role of Rbfox1 in neuronal excitability. Poster presentation Aug, 2014 at the Gordon Research Seminar & Conference: Synaptic Transmission, Waterville Valley, NH
4) Vuong CK and Black DL. Uncovering the role of alternative splicing in regulation of neuronal activity. Poster presentation Dec, 2012 at the HHMI Meeting: Neurobiology, Ashburn, VA

Chapter 1: INTRODUCTION

Part 1: Post-transcriptional regulation by RNA-binding proteins

RNA-binding proteins (RBPs) direct every step of an mRNA transcript's life by controlling transcript splicing, stability, translation and localization. In the nucleus, constitutive splicing involves the removal of introns from pre-mRNA by the spliceosomal complex to produce the mature RNA (mRNA), which is then exported to the cytoplasm for translation. RBPs outside of the spliceosome control alternative splicing at many sites along the pre-mRNA to generate multiple protein isoforms that can differ in function. Each subsequent step in the mRNA's life is also controlled by other aspects of RBP function such as mRNA export, stability, translational output and subcellular localization. Recent work has shown that many RBPs that mainly studied in the nucleus as alternative splicing regulators also play important roles in mRNA processing in the cytoplasm.

Alternative Splicing of pre-mRNA

The pre-mRNA splicing reaction is a key step in the regulation of eukaryotic gene expression. Nearly all mammalian multi-exon genes produce multiple mRNA isoforms through alterations in splice-site choice to produce proteins of different structures and functions, or to alter mRNA localization, translation or decay. In keeping with its cellular and functional complexity, the mammalian nervous system makes extensive use of splicing regulation to generate specialized protein isoforms that affect all aspects of neuronal development and function (Darnell, 2013a; Li et al., 2007; Raj and Blencowe, 2015; Zheng and Black, 2013). Splicing defects are being increasingly implicated in neurological and neurodegenerative disease, which underscores the need to better understand these regulatory processes. Alternative splicing patterns (Figure 1-1) are regulated by RBPs that alter spliceosome assembly at specific splice sites (Fu and Ares,

2014; Lee and Rio, 2015; Matera and Wang, 2014; Will and Lührmann, 2011) (Figure 1-2). These proteins are structurally diverse and can exert different effects on a target transcript depending on their binding position, their modification by signaling pathways, and their interactions with co-factors. Some regulators exhibit tissue-specific expression, whereas others are more ubiquitous, but they all regulate large overlapping programs of neuronal alternative splicing events. Although each regulatory protein can affect many different RNA targets, each transcript is usually targeted by multiple regulators (Figure 1-3). These compounded levels of complexity have challenged characterization of the biological function of splicing regulatory proteins and studies of their mechanisms of action. However, increasingly powerful mouse genetics have allowed the biological roles of splicing regulators and the cellular programs they control to be elucidated.

Alternative splicing-coupled to quality control mechanisms

Regulation of splicing can be coupled to mRNA quality control mechanisms. Briefly, mRNA decay in mammalian cells is limited by the rate of poly(A) tail shortening, whereupon reaching a critical length, mRNA decay occurs at the 5' end through decapping and 5'-to-3' exonuclease activity, or at the 3' end through continued shortening of the poly-A tail and 3'-to-5' exonuclease activity (Meyer et al., 2004; Parker and Song, 2004). Alternative splicing coupled to nonsense-mediated decay (AS-NMD) produces transcripts that encode premature termination codons (PTCs) within alternative exons or retained introns, whose inclusion in the mRNA leads to degradation during the pioneer round of translation (Figure 1-4A, Steps 1 and 2).

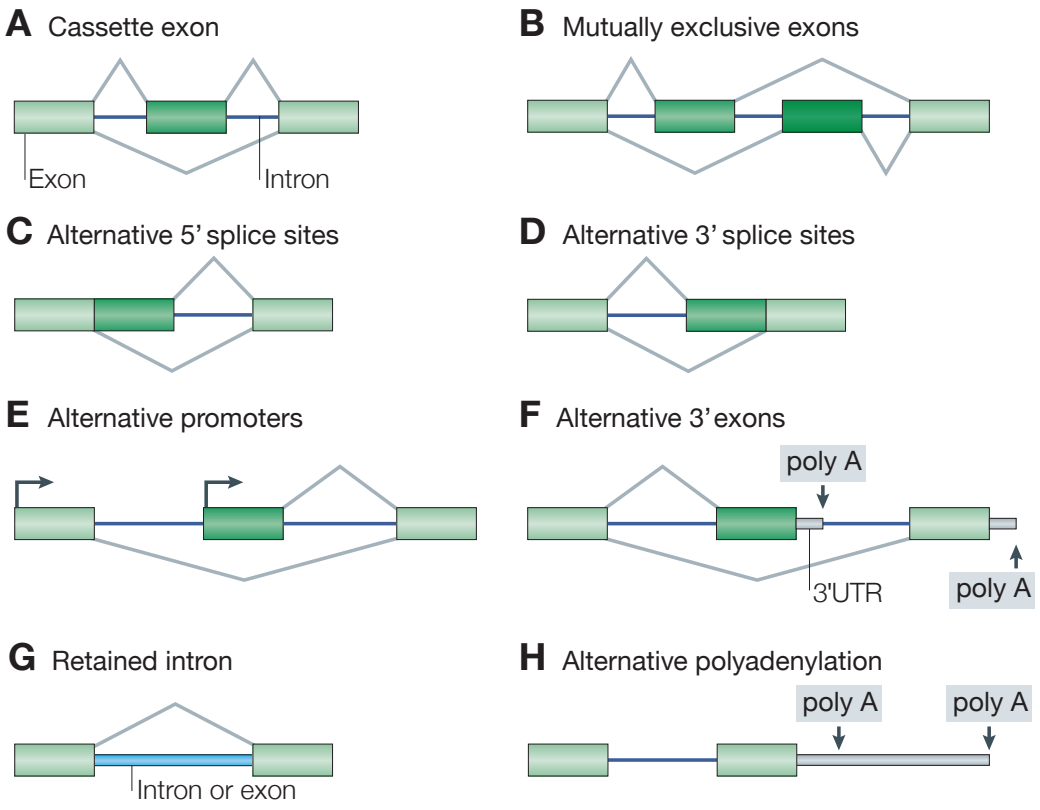

Figure 1-1: Patterns of alternative splicing.

The diversity of mRNA isoforms is generated from many different patterns of alternative splicing. Genes are segmented into introns and exons. During the pre-mRNA splicing process, introns are excised from the precursor mRNA and exons are ligated together to form the mRNA. Special sequences at the intron ends define where the cleavage and ligation reactions occur. The 5' splice site or donor site is at the 5' end of the intron. The 3' splice site or acceptor site is at the 3' end of the intron. Splicing catalysis by the spliceosome takes place in two cleavage/ligation steps. The 3' splice site has an associated branchpoint sequence, which is joined to the 5' splice site after the first cleavage step. This is followed by cleavage at the 3' splice site and ligation of the two exons. In the figure, the light green boxes indicate exons and the dark green boxes

indicate alternative exons. The v-shaped lines show the different ways in which the exons can be joined in a final mRNA. The most common change in splicing pattern is a cassette exon (skipped exon, **a** in figure) whose inclusion or skipping will insert or delete a sequence from the final mRNA. Mutually exclusive exons (figure, **b**) are a pair of consecutive cassette exons where only one of the exons is included in the mRNA. Alternative 5' splice sites (figure, **c**) are consecutive 'donor sites' that change the length of an exon at its 3' end. Conversely, alternative 3' splice sites (figure, **d**) are consecutive acceptor sites that change the 5' end of the exon. Alternative promoters (figure, **e**) and alternative 3' exons (figure, **f**) create different first exons and different last exons on the mRNA, respectively. Retained introns (figure, **g**) can be excised as a typical intron or remain in the final mRNA. Alternative polyadenylation (figure, **h**) in the last exon allows for the generation of 3'UTRs of varying lengths. A single gene can have multiple positions and patterns of alternative splicing to create a family of many different mRNAs and proteins through the inclusion or skipping of various alternatively spliced RNA segments. Modified with permission from (Li et al., 2007).

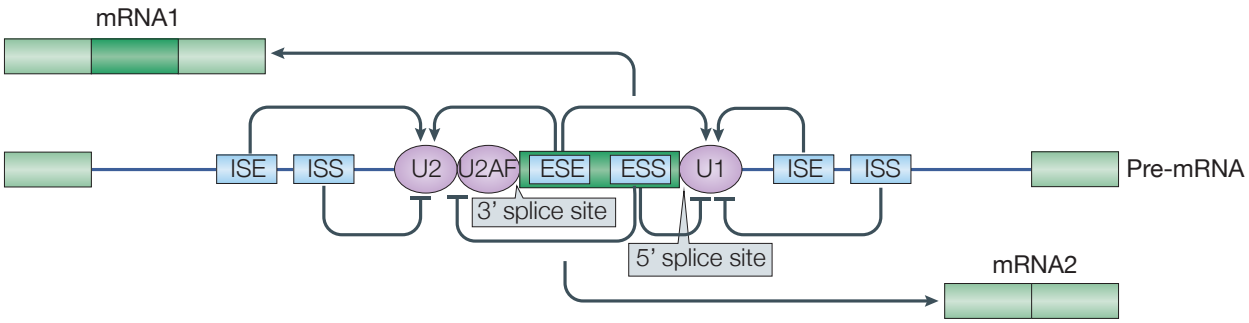

Figure 1-2: Regulation of an alternative exon by RNA-binding proteins.

Trans-acting RNA-binding proteins (RBPs) interact with cis-sequence elements in the pre-mRNA to facilitate or inhibit the assembly of the spliceosomal machinery at nearby splice sites. The 5' splice site is initially bound by U1 small nuclear ribonucleoprotein (snRNP). The U2 snRNP recognizes the branchpoint and is recruited by the U2AF protein bound to the polypyrimidine tract between the branchpoint and the 3' splice site. Binding of U1 and U2 allows recognition of an exon in a process called exon definition. These snRNPs are subsequently brought into interaction across an intron to allow further spliceosome assembly and pairing of splice sites within the catalytic center of the spliceosome. An alternative splicing event frequently involves multiple competing weak splice sites subject to dynamic regulation by neighboring cis-elements. These cis-elements include intronic and exonic splicing enhancers (ISE and ESE) and intronic and exonic splicing silencers (ISS and ESS) that recruit activator or repressor RBPs, respectively. These RBPs, through multiple modes of action not yet understood, collectively influence splice site recognition or splice site pairing within the spliceosome. The levels and activity of these trans-acting RBPs control the choice of splice sites for many different transcripts.

Activator RBPs binding to enhancer elements are shown as arrows, and repressors binding to silencer elements are shown as inhibitory arrows. Constitutive flanking exons are shown in light green, and the alternative exon is shown in dark green.

ISE, intronic splicing enhancer; **ISS**, intronic splicing silencer; **ESE**, exonic splicing enhancer; **ESS**, exonic splicing silencer.

AS-NMD is an important regulatory mechanism for RBPs to control expression of target transcripts and other RBPs as well as their own expression (Yap and Makeyev, 2013). For example, the RBP Ptbp1 auto-regulates its expression and that of its neuronal paralog Ptbp2 through exon skipping. Similarly, Ptbp1 and Ptbp2 control developmental expression of the neuronal excitatory post-synaptic scaffold protein PSD-95 (Dlg4) through repression of exon 18 (Boutz et al., 2007; Makeyev et al., 2007; Spellman et al., 2007), which causes a frame shift leading to NMD (Zheng et al., 2012). Activity-dependent AS-NMD has also been described for the NOVA and SLM proteins (Eom et al., 2013; Nguyen et al., 2016).

Nuclear mechanisms also process transcripts targeted for degradation. In alternative splicing coupled to nuclear retention and elimination (AS-NRE), incompletely spliced transcripts containing introns accumulate in the nucleus and are eventually degraded by the nuclear surveillance machinery (Yap and Makeyev, 2013) (Figure 1-4A, Step 2). As with AS-NMD, RBPs use AS-NRE to control their own expression or that of a target. For example, human SRSF1 maintains homeostatic expression levels through incomplete splicing of its own transcript (Sun et al., 2010). In another example, the transcripts of multiple proteins important for neuronal function, such as the SNARE components Stx1b and Vamp2 and the neuron-specific kinesin subunit Kif5a, are expressed in non-neuronal cells but protein expression is restricted by Ptbp1-controlled intron retention and AS-NRE (Yap et al., 2012). Recent work found that the Drosophila ortholog of NOVA1/2, pasilla, promotes splicing of a retained intron to increase expression of Orb2A, a critical factor in long-term memory (Gill et al., 2017). Activity-dependent intron retention is found in the mammalian nervous system and recent

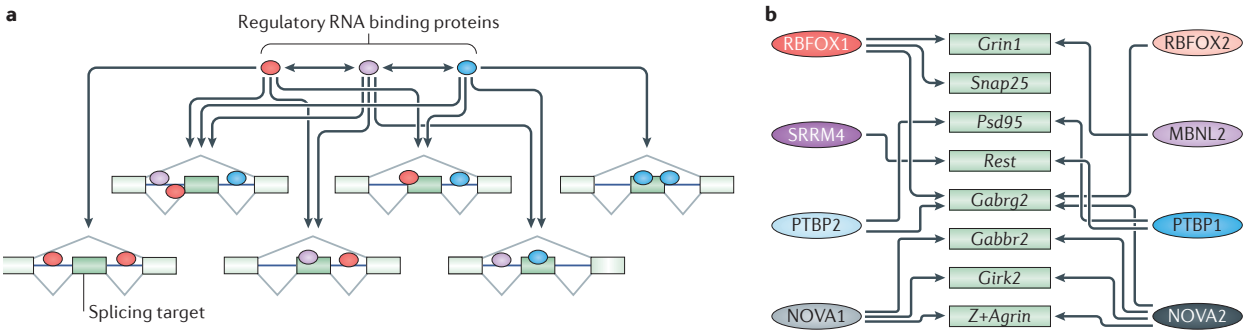

Figure 1-3: Splicing regulatory networks.

(A) Splicing regulators control large target exon sets that often overlap with those regulated by other RNA-binding proteins (RBPs). Thus, splicing of a given alternative exon can be affected by multiple RBPs. RBPs also affect their own splicing and homeostatic expression as well as that of other RBPs. The high degree of cross-regulation (indicated by arrows) between splicing regulators and their target sets creates complex splicing networks where perturbation of a single RBP can lead to pleiotropic effects. Conversely, the splicing outcome of an exon can result from combinatorial control of many RBPs. **(B)** Some of the splicing target transcripts discussed in this review (green boxes), and their cross-regulation by multiple RBPs.

work (Mauger et al., 2016) demonstrated that a number of introns are stably retained in mRNA localized to the nucleus. These introns are rapidly excised following stimulation of neuronal activity, possibly downstream of NMDA receptor and CamK signaling.

RBP regulation of mRNA stability

In the cytoplasm, RBPs regulate the stability and half-life of mRNA transcripts as well as the subcellular localization. The 3' untranslated regions (3' UTRs) of transcripts often encode instability and regulatory elements, of which the best studied are AU-rich elements (AREs) and microRNA recognition elements, and sequences directing transport to specific cellular compartments.

ARE-binding proteins (ARE-BPs) increase the rate of mRNA decay by recruiting decapping enzymes or deadenlyation factors. Their binding in the 3'UTR of a target transcript can also block the transcriptional machinery, the presence of which normally competes out deadenylation factors (Decker and Parker, 2012). RBPs such as the ELAVL (Hu) proteins function to stabilize their target transcripts by competing with ARE-BPs for binding at AU-rich elements (Brennan and Steitz, 2001; Hinman and Lou, 2008) (Figure 1-4B, Step 4). Other RBPs such as PTBP1 also regulate transcript stability in the cytoplasm besides their well-known roles in alternative splicing. In non-neuronal cells, PTBP1 translocation to the cytoplasm increases stability of the *Vegf* mRNA (Sawicka et al., 2008).

MRNA decay also occurs through internal cleavage of the transcript, essentially producing decapped and deadenylated fragments which are then subject to the respective exonucleases. Extensive base-pairing between microRNAs and their target mRNAs can induce internal cleavage by Argonaute and transcript degradation through

the pathways discussed above. Less extensive pairing results in translational repression, ultimately leading to sequestration of the mRNA in P-bodies, centers of mRNA degradation (Parker and Sheth, 2007). Stabilizing RBPs can also antagonize the binding of microRNAs to their target 3'UTRs (Figure 1-4B, Step 4). The ubiquitously expressed ELAVL protein, HuR, plays an important role in cancer through its antagonism of microRNA-mediated repression of oncogenic transcripts (van Kouwenhove et al., 2011). Members of the Rbfox family of splicing regulators also display extensive binding in 3'UTRs that is correlated with transcript abundance, and work on the cytoplasmic isoforms of Rbfox1 and Rbfox3 have demonstrated their role in transcript stability through antagonism of microRNA binding (Carreira-Rosario et al., 2016; Lee et al., 2016a; Ray et al., 2013; Weyn-Vanhentenryck et al., 2014a).

RBPs direct subcellular localization

Differential subcellular localization of mRNA transcripts (Figure 1-4B, Step 5) is crucial for the function of highly polarized cell types such as neurons. Establishment of polarity is important during cortical development, where neuronal polarity affects the proliferation of progenitor cells, commitment to a particular lineage and migration to the proper lamina (Kriegstein and Noctor, 2004). For example, zipcode binding protein1 (ZBP1) regulates the levels of β-actin present in developing dendrites, and particular levels of ZBP1 are required for the proper growth and branching of dendrites (Perycz et al., 2011). ZBP1 subcellular localization of β-actin has also been shown to be required for growth cone turning, an important factor in axon targeting (Donnelly et al., 2013; Sasaki et al., 2010). In mature neurons, consolidation of synaptic strength through local translation of mRNAs is important for the cell's response to synaptic activity. RBPs

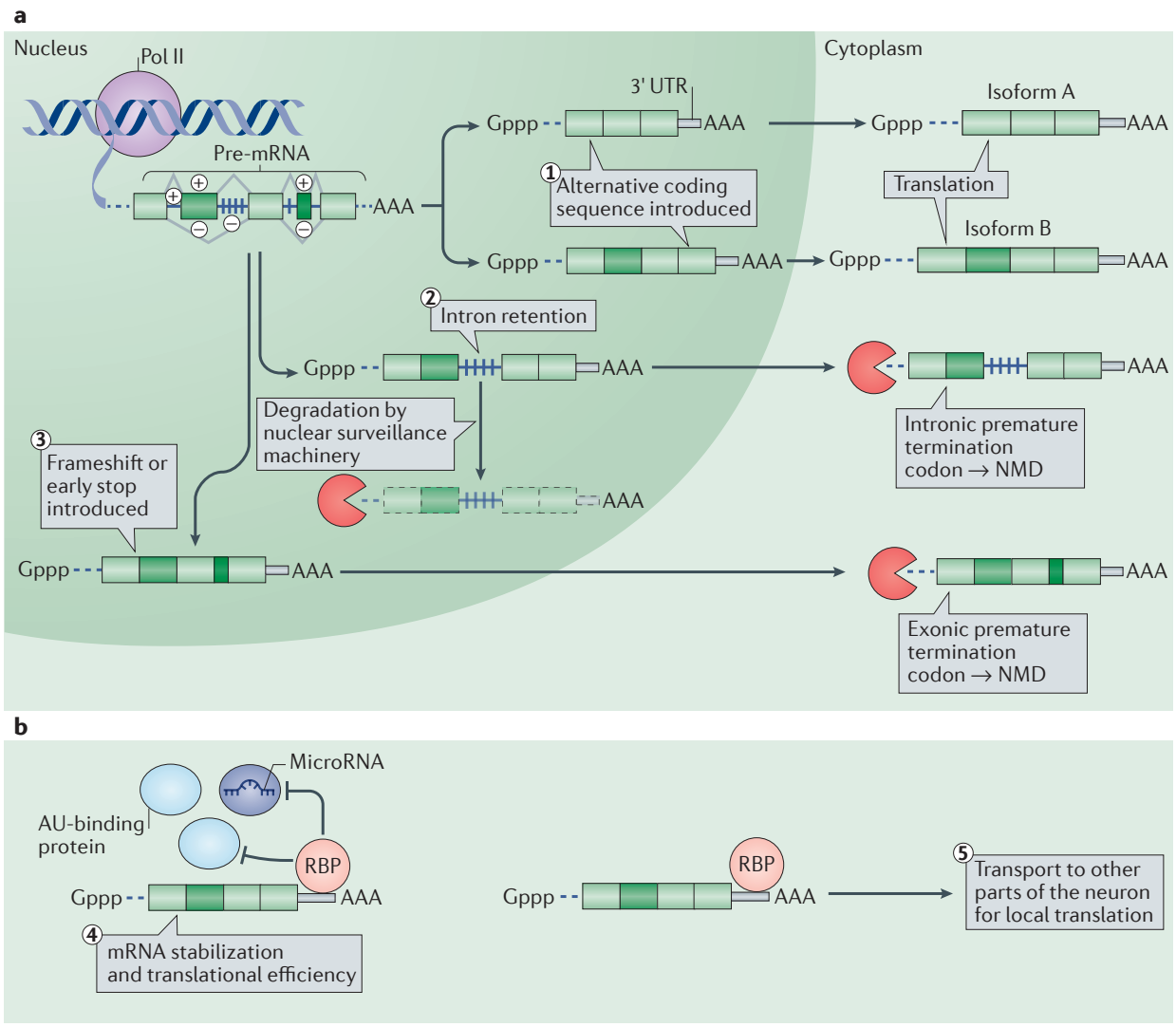

Figure 1-4: Regulatory outcomes of RNA-binding proteins.

RNA-binding proteins (RBPs) regulate transcript splicing, stability, translation and localization, and many RBPs studied as splicing regulators have extended functions in the cytoplasm affecting every subsequent step of the mRNA life cycle.

(A) *Nuclear roles of RBPs*. Step 1: RBPs control alternative splicing (AS) of pre-mRNA to generate multiple isoforms that differ in functional activity, interactions with cofactors or post-translational modifications. Step 2: Regulated intron retention targets transcript isoforms for degradation by nuclear surveillance mechanisms200,201, or by introduction

Figure 1-4 continued.

of a premature termination codon leading to nonsense-mediated decay (NMD, see below). Step 3: By shifting the reading frame or by inclusion of a 'poison exon' containing a premature translation termination codon, AS produces transcript isoforms which are degraded by NMD202. AS coupled to NMD can control the overall abundance of gene transcripts203.

(B) *Cytoplasmic roles of RBPs.* Step 4: RBPs compete with AU-binding proteins for binding at AU-rich elements in the 3'UTR to stabilize their target transcripts110,111. Other RBPs regulate transcript stability in the cytoplasm by either competing with microRNAs for their binding sites or facilitating microRNA binding131,204,205. RBP binding in both the 5' and 3' UTRs also affects translational efficiency206. Step 5: RBPs regulate the transport and differential localization of mRNA, crucial for spatial and temporal control of translation in response to activity-dependent signaling162,207,208. Establishment of neuronal polarity and consolidation of synaptic strength through local translation of mRNAs in response to synaptic activity are some well-known examples.

RBP, RNA-binding protein; **AAA**, poly-A tail; **Gppp**, 5' cap

involved in alternative splicing can also function in the cytoplasm to regulate mRNA localization. The NOVA proteins have been implicated in
localization of the mRNA of Girk2, a G-coupled potassium channel, to inhibitory post-synaptic sites (Racca et al., 2010). Similarly, Sam68 has been shown to be required for targeting of *β-actin* mRNA to post-synaptic sites (Klein et al., 2013). The RBPs Fus and TDP-43 are associated with RNA transport granules in neurons, suggesting a role in mRNA transport and localization, among many other cytoplasmic roles (Lagier-Tourenne et al., 2010).

It is important to note that nearly all RBPs are known to localize to both the nucleus and cytoplasm. Some RBPs such as Ptbp1 shuttle between the two compartments based on their phosphorylation state, while alternative splicing determines the localization of others such as Rbfox. Thus, while much of the research done on RBP mouse models focuses on the physiological consequences of splicing defects, it is almost certain that some portion of the phenotypes of these RBP mutants is due to loss of cytoplasmic mRNA regulation, in addition to those caused by mis splicing of targets in the nucleus.

Part 2: Mouse models of RNA-binding proteins affecting neuronal function

The neurogenetics of RNA binding proteins is still in its infancy and can be confounded by several factors. While changes in gene expression due to RBP loss can be attributed to loss of function, how an alteration in splicing pattern changes the function of an encoded gene product is usually not known. Nevertheless, mutation of an individual regulator often leads to a highly pleiotropic and/or lethal phenotype due to its extensive target set. This is further compounded by the dual localization of many RNA binding proteins in both the nucleus and the cytoplasm, adding the loss of cytoplasmic transcript metabolism to mis-splicing. In addition, RBPs belong to families of paralogous proteins whose partially redundant function reduces the phenotypic impact of single gene mutations. Although RBPs can be widely expressed throughout the brain, different neuronal cell types often express different combinations of regulators and exhibit distinct susceptibility to their mutation. Despite this complexity, it is clear that the splicing and gene expression regulatory programs directed by these proteins dramatically impact all aspects of neuronal development and biology, from neurogenesis to mature synaptic function.

Gene expression and alternative splicing as regulatory processes have been studied for many years at the level of individual proteins and target transcripts. The advent of whole genome analyses (Blencowe et al., 2009; Irimia and Blencowe, 2012; König et al., 2011; Nussbacher et al., 2015) brought new appreciation of the pervasiveness of their regulatory reach in metazoan organisms (Barbosa-Morais et al., 2012; Merkin et al., 2012). Genome wide analyses have allowed for the simultaneous analysis of splicing and gene expression, an important improvement given the dual roles many RBPs seem to

have in both the nucleus and the cytoplasm. Furthermore, RNA-Seq has been adapted to a multitude of other RNA metabolic processes including, but not limited to, alternative polyadenylation, translation (Ribo-Seq), and direct binding by RBPs (CLIP, iCLIP, PAR-CLIP, among others) (Darnell, 2013b). However, understanding the biology of these RNA programs and, in particular, the role of these programs in the mammalian brain needs to be addressed through a combination of genetics, neuroanatomy and physiology. While only a few of the many hundreds of potential regulatory proteins are beginning to be analyzed, the initial targeted genetic studies described here make clear that changes in posttranscriptional regulation play essential roles in nearly all aspects of neuronal development and function.

Roles of RBPs in neurogenesis

Gene expression and alternative splicing patterns change dramatically as cells progress along the neuronal lineage, directed by changes in the expression of particular RBPs, such as PTBP1, SRRM4 and NOVA 1, that affect neuronal fate and early neuronal differentiation. Though gene expression during development has been attributed to changes in transcription factor activity, the roles of RBPs are increasingly recognized in shaping neuronal development.

PTBP1 in neurogenesis

The sharply defined switch from one member of the polypyrimidine tract binding protein (PTBP) family of splicing regulators to another is a striking and essential step in progenitor commitment to the neuronal lineage. PTBP1 is abundant in neural stem cells and progenitors, but upon mitotic exit its expression is sharply reduced by induction of the neuronal microRNA miR-124 (Makeyev et al., 2007). Downregulation of PTBP1 in turn

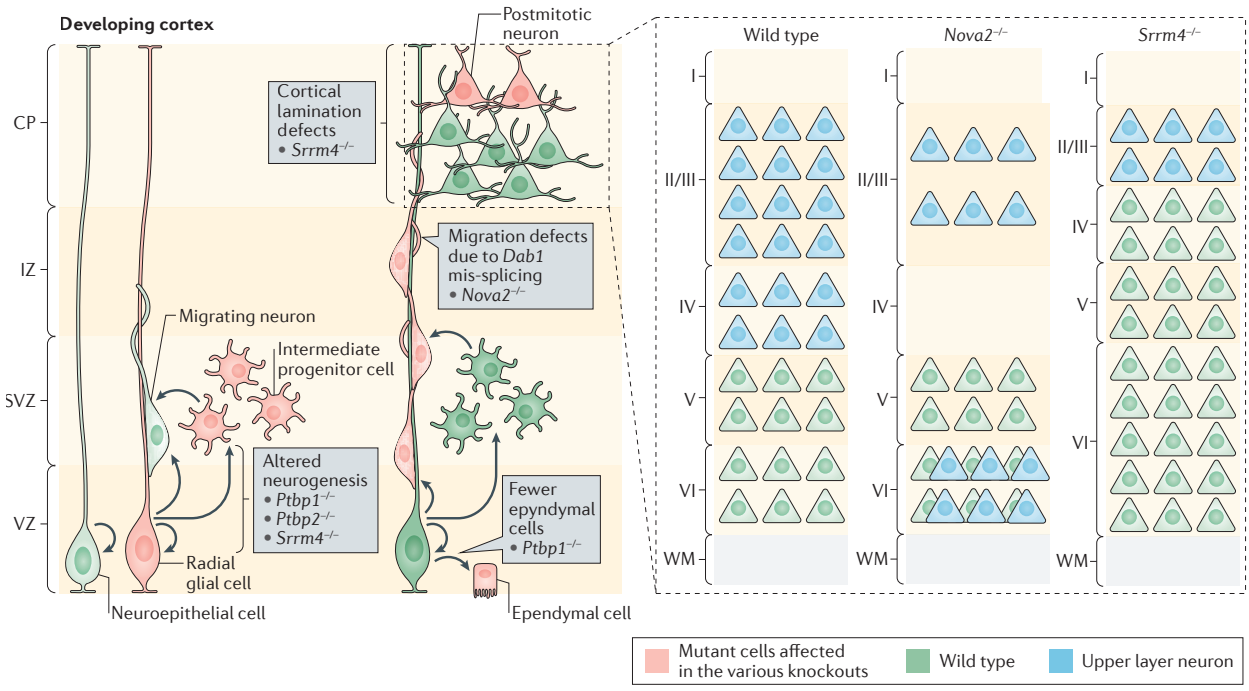

Figure 1-5: Splicing regulators in cortical development and function.

Alternative splicing controls multiple aspects of early neuronal development. Defects in neurogenesis are seen in mouse mutants of a variety of regulatory RNA-binding proteins including Ptbp1-/-, Ptbp2-/-, Nova2-/-, and Srrm4-/-. Loss of PTBP1 can cause precocious neurogenesis, deplete the neural stem cell pool and lead to fewer ependymal cells arising from radial glia later in development. PTBP2 loss may alter neural stem cell positioning and proliferation. Depletion of SRRM4 inhibits neurogenesis of upper layer neurons and causes accumulation of progenitors or lower layer neurons, resulting in abnormal cortical lamination (see inset). Defects in cortical lamination are also seen in mice lacking NOVA2, where mis-splicing of the Reelin component Dab1 leads to failure of many layer II/III and IV neurons to migrate properly (see inset).

VZ, ventricular zone; **SVZ**, subventricular zone; **IZ**, intermediate zone; **CP**, cortical plate; **WM**, white matter

Modified with permission from (Poduri et al., 2013) and (Kriegstein and Noctor, 2004).

induces expression of PTBP2, or nPTB, which is required for neuronal survival and maturation (see below). Reduced PTBP1 expression also enhances miR-124 repression of the REST transcription factor complex (Xue et al., 2013), a well-studied transcriptional repressor of neuronal gene expression (Ballas et al., 2005; Conaco et al., 2006). How the many PTBP1 splicing targets contribute to maintaining pluripotency or preventing differentiation is not yet clear. One splicing target of PTBP1 is the transcription factor *Pbx1*, where precocious expression of the neuronal PBX1 isoform leads to early induction of neurogenic genes (Linares et al., 2015). Another notable PTBP1 target is exon 10 of *Ptbp2*. Repression of exon 10 leads to nonsense-mediated mRNA decay (NMD) of the *Ptbp2* transcript and prevents its expression in PTBP1$^+$ cells (Boutz et al., 2007; Makeyev et al., 2007; Spellman et al., 2007). The induction of PTBP2 protein plays a critical role in neuronal differentiation as discussed below.

Knockout of *Ptbp1* in mice leads to early embryonic mortality (Shibayama et al., 2009; Suckale et al., 2011). Mice with pan-neuronal loss of *Ptbp1* have grossly normal brain morphology at early ages but exhibit a progressive loss of ependymal cells from the lateral ventricles with hydrocephaly and die by 10 postnatal weeks (Shibasaki et al., 2013). PTBP1 loss may induce precocious differentiation of radial glial cells (RGCs) into neurons, thereby depleting the RGC pool that later gives rise to ependymal cells (Spassky et al., 2005) (Figure 1-5). The loss of ependymal cells was restricted to the dorsal telencephalon, indicating variable roles for PTBP1 across brain regions. The lethality of the *Ptbp1* knockouts demonstrates the essentiality of this RNA-binding protein and the key roles it plays in the transition from progenitor to neuron.

An interplay between PTBP1 and SRRM4

Like PTBP1, the Serine/Arginine Repetitive Matrix protein 4 (SRRM4 or nSR100) functions during progenitor cell transition to the neuronal lineage. Despite lacking a canonical RNA binding domain, SRRM4 frequently binds UGC-rich sequences located between the polypyrimidine tract and the 3' splice site of target exons (Raj et al., 2014). The most enriched motifs surrounding SRRM4-dependent exons are typical PTBP binding elements, suggesting that SRRM4 can antagonize PTBP activity, and the regulatory programs for these two proteins are seen to significantly overlap. SRRM4 promotes splicing of the REST4 isoform, which lacks 4 of the 9 zinc fingers found in the full-length protein (Raj et al., 2011) and has reduced transcriptional repression activity (Palm et al., 1999; Shimojo et al., 2001; Tabuchi et al., 2002). REST on the other hand inhibits *Srrm4* expression in non-neuronal cells (Raj et al., 2011).

Given its interaction with REST, it is not surprising that knockdown of *Srrm4* in developing mouse cortex inhibits neuronal differentiation and leads to accumulation of $Pax6^+$ progenitor cells in the ventricular zone and depletion of differentiated cells from the cortical plate (Raj et al., 2011). Interestingly, germline deletion of *Srrm4* results in fewer $Pax6^+$ cells in the ventricular zone and fewer postmitotic, $NeuN^+$ neurons(Quesnel-Vallières et al., 2015) (Figure 1-5). The different observations of $Pax6^+$ cells may result from different effects of acute versus prolonged loss of SRRM4, or may indicate that SRRM4 plays different roles in early versus late neurogenesis. Indeed, $Srrm4^{-/-}$ mice have fewer late-born, upper layer and more early-born, lower layer neurons, suggesting either depletion of the neural stem/progenitor cell pool or alterations in neuronal subtype specification (Figure 1-5).

Together, the interplay between Srrm4 and Ptbp1 and their interactions with miR-124 and the REST complex constitute an important genetic program underlying neuronal cell fate commitment.

Regulation of neuronal migration by RBPs

Migration of neurons during brain development establishes the lamination of structures such as the cortex and cerebellum and produces the circuit organization that underlies neuronal function. In multiple brain regions, alternative splicing of components of the Reelin signaling pathway is important for proper neuronal migration. Loss of splicing regulators such as NOVA2 and RBFOX2 leads to defects in cortical and cerebellar lamination.

NOVA2 ensures proper migration of late-born cortical neurons

The neuro-oncological ventral antigen (NOVA) proteins were identified as autoantigens in patients with paraneoplastic opsoclonus-myoclonus ataxia (POMA), a human neurological syndrome characterized by motor and cognitive deficits (Darnell and Posner, 2003). The two paralogs NOVA1 and NOVA2 are expressed in a largely mutually exclusive pattern. NOVA1 is mainly found in hindbrain and ventral spinal cord, whereas NOVA2 is predominant in forebrain and dorsal spinal cord, with some overlapping expression in portions of midbrain and hindbrain (Yang et al., 1998). Genetic knockout of *Nova1*, *Nova2* or both has demonstrated important roles for the two proteins in multiple aspects of brain development (Jensen et al., 2000; Yano et al., 2010), including neuronal migration and cortical lamination.

In *Nova2* null mice, neurons displaying markers of cortical layers II/III and IV are mislocalized to lower layers (Yano et al., 2010) (Figure 1-5). Progenitor cell proliferation

and radial glia morphology are largely unaffected, suggesting a defect of neuronal migration rather than subtype specification. This contrasts with lamination defects in *Srrm4* null mice, where increased numbers of lower layer neurons are likely due to premature commitment of progenitors to neurogenesis or alterations in subtype specification. The defective migration of *Nova2*$^{-/-}$ upper layer neurons was attributed to mis-splicing of *Dab1*, a component of the Reelin signaling pathway that controls cortical neuronal migration and lamination (Ayala et al., 2007; Förster et al., 2010; Rice and Curran, 2001). In wildtype neurons, NOVA2 represses both exons 7b and 7c of the *Dab1* transcript, and the resulting DAB1∆7bc protein is subject to ubiquitylation upon Reelin activation (Arnaud et al., 2003; Bock et al., 2004; Rice et al., 1998). In *Nova2*$^{-/-}$ neurons, abnormal inclusion of these exons produces a more stable isoform that may antagonize the activity of DAB1∆7bc (Feng et al., 2007; Simo et al., 2010). Indeed, introduction of a Dab1∆7bc transgene rescued the migration defect in a subset of the layer II-IV *Nova2*$^{-/-}$ neurons. This rescue with a single spliced isoform provides an important method for validating the source for particular aspects of a pleiotropic phenotype. Notably, *Dab1* is mis-spliced in the *Nova2* null cortex only between E14 and E18. This restricted regulatory window and the limited population of affected cells reflect the complicated landscape of alternative splicing during neuronal development, where overlapping splicing regulatory programs come into play at specific times and in specific neuronal populations.

RBFOX2 is required for proper Purkinje cell radial migration

In the cerebellum, Purkinje cell migration is also affected by RBFOX2, a member of the highly-conserved RNA binding protein, fox-1 homolog (RBFOX) family of RBPs (Conboy, 2017). Although all three *Rbfox* genes are broadly expressed in the brain,

individual neuronal cell types express different combinations at different developmental times (Gehman et al., 2012; 2011; Hammock and Levitt, 2011; McKee et al., 2005; Underwood et al., 2005). For example, Purkinje cells express RBFOX2 early in development, with later onset of RBFOX1 and no expression of RBFOX3. In contrast, cerebellar granule cells switch from expressing RBFOX2 during proliferation and migration to RBFOX1 and RBFOX3 with maturation (Gehman et al., 2012). While it is not known how the different RBFOX proteins differ in activity, their complex expression patterns imply that they may serve overlapping but distinct roles.

Pan-neuronal *Rbfox2* knockout mice exhibit increased mortality with frequent hydrocephaly at one month of age (Gehman et al., 2012). The cerebellum is severely affected, with substantially reduced size and loss of foliation. Purkinje cells normally migrate outward from the ventricular zone to be arrayed in a single layer between the external (EGL) and internal (IGL) granule layers by embryonic day 18 (Hatten and Heintz, 1995; Wang and Zoghbi, 2001). The *Rbfox2*$^{-/-}$ Purkinje cells exhibit a substantial delay in migration and increased cell death, resulting in a disorganized Purkinje cell layer (Figure 1-6A). *Rbfox2*$^{-/-}$ brains exhibit altered splicing in transcripts known to control cell migration. In particular, *Lrp8*, which normally binds RELN (Reelin) to control cortical and Purkinje neuron migration, produces higher amounts of a dominant-negative isoform in *Rbfox2*$^{-/-}$ brains (Koch et al., 2002). Consistently, *Lrp8* null mice exhibit ectopic Purkinje cells similar to the *Rbfox2* null mice (Larouche et al., 2008; Trommsdorff et al., 1999). It will be interesting to test the roles of LRP8 and other components of the Reelin signaling pathway in *Rbfox2*$^{-/-}$ rescue experiments, similar to those in the *Nova2* null mouse.

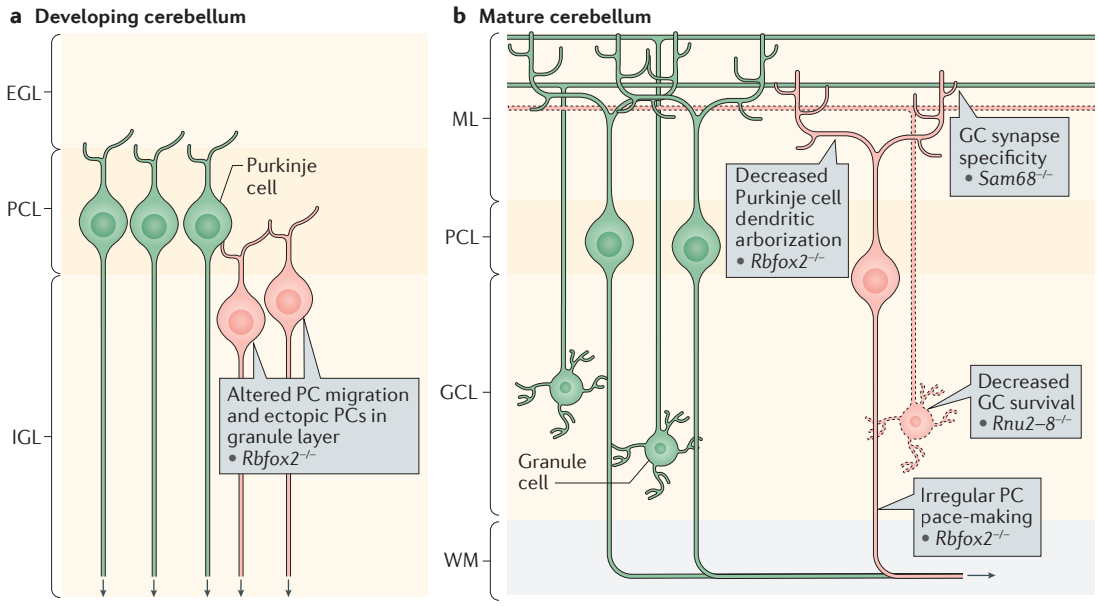

Figure 1-6: Splicing regulators in cerebellar development and function.

RBFOX2 is required for both Purkinje cell (PC) migration and mature function. The cerebellum in Rbfox2-/- mouse mutants exhibits a disorganized Purkinje cell layer (PCL) with ectopic PCs found in the internal granule cell layer (IGL), as well as reduced PC dendritic arborization later in development. In mature PCs, RBFOX2 controls the splicing and expression of sodium channel the Scn8a ($Na_v1.6$) needed for proper PC pacemaking. Splicing regulation is also required for granule neuron survival and proper synaptic specificity. Loss of the U2 snRNA, a core spliceosomal component encoded by Rnu2-8, leads to increased intron retention and progressive granule neuron death. In granule neurons, SAM68 affects trans-synaptic interactions through alternative splicing of Neurexin.

EGL, external granule layer; **IGL**, internal granule layer; **PCL**, Purkinje cell layer; **ML**, molecular layer; **GCL**; granule cell layer; **WM**, white matter; **PC**, Purkinje cell; **GC**, granule cell

Multiple components of the Reelin pathway and other signaling pathways affecting neuronal migration are expressed as alternatively spliced isoforms (Beffert et al., 2005; Gao et al., 2012). The regulators of these splicing events are largely unknown, and it is likely that other splicing regulator mutants will exhibit migration defects in particular brain structures.

Synaptogenesis and cell survival

After commitment to differentiation and migration to their proper location, neurons undergo a long period of maturation that includes the formation and maturation of synapses. Posttranscriptional regulatory mechanisms define the gene products involved in these processes, and particular RBP mutations have been shown to dramatically affect these developmental steps.

PTBP2 is required for proper neuronal maturation

Down-regulation of PTBP1 in neural stem/progenitor cells as they exit mitosis induces the PTBP2 expression required for neuronal development and survival. The essential role of PTBP2 in neuronal maturation was revealed in several different mutant mice carrying either germline null alleles or pan-neuronal conditional alleles (Li et al., 2014; Licatalosi et al., 2012). Germline mutants are paralyzed and unresponsive to touch at birth and exhibit perinatal lethality with respiratory failure, possibly due to a loss of innervation to the diaphragm. Though PTBP2 knockout brains of appear grossly normal, closer analyses reveal defects in early corticogenesis. In one analysis, small ectopic clusters of S and M phase cells were found in reverse orientation from their normal positions (Licatalosi et al., 2012) (Figure 1-5). These cellular abnormalities were possibly mediated by an observed change in the splicing of *Numb*, a known regulator of

asymmetric neural stem cell division (Cayouette and Raff, 2002; Knoblich, 2010). Early differentiation defects were not reported in another germline *Ptbp2* null allele, but these mice were not subjected to the same analyses (Li et al., 2014). This null mutant exhibited a loss of some early developing white matter tracts. Overall, the early lethality of the *Ptbp2* null alleles and of the pan-neuronal KO limited analyses of their phenotypes.

PTBP2's role in later development was revealed by its depletion from excitatory neurons of the dorsal telencephalon using an *Emx1-Cre* line (Li et al., 2014). At birth, the *Emx1-Ptbp2*$^{-/-}$ brain appears similar to wildtype in morphology, size, neuronal fate commitment and cortical lamination. However, *Emx1-Ptbp2*$^{-/-}$ cortices begin to atrophy as early as P5, and by P15 the cortex exhibits massive cell death and is almost completely degenerated. Similarly, cultured *Ptbp2*$^{-/-}$ embryonic cortical neurons initially appear normal in plating efficiency and neurite outgrowth but exhibit progressive cell death. The cell death is possibly due to a failure of synapse formation or other aspect of maturation consequently leading to a lack of activity-dependent survival signals (Figure 1-7). Because synaptogenesis occurs later in the forebrain than elsewhere in the CNS, similar defects in synaptogenesis with neuronal death may also occur in the lower brain of *Ptbp2* null mice and contribute to the perinatal lethality.

All the *Ptbp2* mutant mouse models exhibit precocious expression of many adult mRNA isoforms encoding proteins that affect a wide variety of cellular functions including regulation of transcription, synaptic transmission, synapse organization, and endocytosis (Li et al., 2014; Licatalosi et al., 2012). CLIP analysis indicates that many of these transcripts are direct PTBP2 targets (Licatalosi et al., 2012). In early development, the embryonic splicing pattern of many neuronal genes is maintained during the switch from

PTBP1 to PTBP2. Later in maturation, coincident with marked PTBP2 downregulation and synaptogenesis, adult isoforms become more prevalent (Li et al., 2014; Licatalosi et al., 2012; Zheng et al., 2012). Thus, the high expression of PTBP2 during early development extends the expression of the embryonic splicing program until late in neuronal maturation. How premature induction of the adult isoforms contributes to neuronal cell death and other phenotypes of *Ptbp2*$^{-/-}$ neurons is unclear.

One synaptic target of PTBP1 and PTBP2 is exon 18 of *Psd-95* (*Dlg4*), which encodes the major scaffold protein of excitatory synapses. The *Psd-95* transcript is expressed in many non-neuronal cells, where skipping exon 18 leads to NMD of the transcript, preventing its productive translation (Figure 1-7B). Overexpression of either PTBP1 or PTBP2 in mature neurons inhibits exon 18 inclusion, PSD-95 protein expression and excitatory synapse formation (Zheng et al., 2012). PTBP1 restricts PSD-95 protein expression to neurons, while PTBP2 controls the temporal induction of PSD-95 late in neuronal maturation. The sequential expression of PTBP1 and PTBP2 thus serves to precisely time the production of this key synaptic protein. The marked cortical degeneration phenotype of the *Ptbp2* knockout and the requirement for PTBP2 in maintaining a portion of the PTBP splicing pattern indicates that timing of synaptogenesis and its regulation by PTBP2 is critical for neuronal development and survival.

SRRM4 in synaptogenesis and development

In accordance with its paralleled function with PTBP during commitment to the neuronal lineage, Srrm4 is important for maintaining a splicing program that seems critical for neuronal survival in the inner ear, just as Ptbp2 is required in the cortex. Although the two alleles of *Srrm4* that have been analyzed exhibit different phenotypes, both mouse

mutants display defects in synaptic function. One *Srrm4* allele, the Bronx waltzer (*bv*) mouse, arose from a forward genetic screen (Nakano et al., 2012) and mutants exhibits deafness, head tossing and circling (Deol and Gluecksohn-Waelsch, 1979). A second conditional *Srrm4* allele lacking the critical RS-rich domain and splicing activity (*Srrm4*$^{\Delta 7\text{-}8}$) (Quesnel-Vallières et al., 2015) has more severe phenotypes, including defects in multiple neurodevelopmental processes. While *bv/bv* mice live to adulthood, only 15% of *Srrm4*$^{\Delta 7\text{-}8}$ mice survive beyond birth, and adult survivors exhibit severe tremors with some balance defects similar to the *bv/bv* mice.

The *bv/bv* mouse has defects in the differentiation and/or survival of inner hair cells (IHCs) and vestibular hair cells (VHCs) of the cochlea (Sobkowicz et al., 1999; Whitlon et al., 1996). In mutants, both IHCs and VHCs, which are normally densely innervated by spiral ganglion neurons, progressively degenerate and are completely lost by the first postnatal week. In contrast, outer hair cells (OHC), which normally require only sparse innervation, are unaffected (Cheong and Steel, 2002). The *bv/bv* inner ear also exhibits aberrant splicing in genes enriched in neurotransmission and secretion. This is similar to the *Srrm4*$^{\Delta 7\text{-}8}$ brain, which shows aberrant splicing in genes implicated in vesicle trafficking and recycling. Although how these splicing defects lead to decreased cell survival remains unclear, one possibility is that synaptogenesis and synaptic transmission, required for IHC and VHC survival, are impaired. As seen in the *Ptbp2*$^{-/-}$ forebrain, the *bv/bv* mouse provides evidence that correct alternative splicing is necessary for proper synaptogenesis and cell survival.

The phenotypes of *Srrm4*$^{\Delta 7\text{-}8}$ mice also have similarities to those of the *Ptbp2*$^{-/-}$ mice. *Srrm4*$^{\Delta 7\text{-}8}$ mice show no gross morphological phenotypes during embryonic

development, but most die within a few hours of birth with respiratory failure. This appears to result from insufficient phrenic innervation to the diaphragm (Quesnel-Vallières et al., 2015), as secondary branching of motor neuron axons in this region is reduced by two-fold. Although the molecular events underlying the phenotypic defects are not yet defined, one third of *in vivo* SRRM4 targets overlap with PTBP2 targets. Comparisons of these systems will provide interesting insight into how developmental alternative splicing programs control synaptogenesis.

NOVA control of motor neuron development and survival

At the neuromuscular junction (NMJ), splicing programs affecting synaptic function are also crucial for neuronal survival. Defects in muscle innervation and NMJ development and function can be seen in *Nova1* and *Nova2* double knockout mice. *Nova1*$^{-/-}$ *mice* appear normal at birth, but die in the second postnatal week with motor neuron apoptosis, profound motor failure and action-induced tremors (Jensen et al., 2000; Yang et al., 1998). *Nova1/2* double knockout (dKO) mice are born paralyzed and die from respiratory failure indicative of NMJ defects (Ruggiu et al., 2009). Indeed, the dKO mice, but neither of the single knockout mice, show fewer acetyl choline receptor (AChR) clusters and a loss of apposition between AChR clusters and phrenic nerve terminals, suggesting redundancy of the NOVA proteins in controlling NMJ development (Jensen et al., 2000; Ruggiu et al., 2009). Although NOVA1 and NOVA2 are detected in ventral and dorsal spinal cord, respectively (Yang et al., 1998), loss of NOVA1 might up-regulate NOVA2.

The impaired synaptogenesis at the NMJ in *Nova1/2* dKO mice is due primarily to aberrant *Agrn* splicing. AGRN protein promotes the clustering of AChRs within the

postsynaptic membrane of the innervated muscle. Neuronal-specific *Agrn* isoforms containing the Z exons (32 and 33) are the most potent in promoting AChR aggregation (Gesemann et al., 1995; Nitkin et al., 1987; Reist et al., 1992; Sanes and Lichtman, 1999). Targeted deletion of the Z exons leads to paralysis and perinatal lethality similar to the phenotype of *Nova* dKO mice (Burgess et al., 1999; Gautam et al., 1996). Although exon 32 is only slightly affected in single *Nova* KOs, it is almost completely skipped in dKO mice. Strikingly, restoring Z+ *Agrn* expression in dKO motor neurons via a transgene rescues AchR clustering, nerve terminal apposition, NMJ morphology and muscle responses to stimuli (Ruggiu et al., 2009). The paralysis phenotype and early mortality are unchanged by the transgene, indicating contributions of additional Nova targets and possibly in other brain regions. These studies demonstrate how the activity of a particular alternatively spliced isoform can play a crucial role in ensuring proper synaptic development.

Quaking regulates myelination of axons

In addition to synaptogenesis as described above, axonal myelination is another factor affecting neuronal development and survival. Proper myelination is important for action potential conductance and neuronal survival, and recent work has implicated the RBP Quaking and dysmyelination in schizophrenia (Aberg et al., 2006; Backx et al., 2010; Barry et al., 2014). The *quaking* (qk^{v}) mutant allele (SIDMAN et al., 1964) is an autosomal recessive deletion in Qk resulting in severe dysmyelination in the CNS, with mutant mice developing characteristic tremors starting at P10. Like many RBPs, such as those of the Rbfox family, the *Qk* transcript is alternatively spliced to produce several isoforms that differ in their subcellular localization. The levels of different *Qk* isoforms are autoregulated

by binding of one protein isoform to its cognate 3'UTR, as well as cross-regulation by different isoforms. For example, the QKI-6 protein isoform binds to the 3'UTR of the *qki-5* transcript to repress its translation(Fagg et al., 2017).

The QK proteins are highly expressed in the myelinating cells, oligodendrocytes, and some isoforms are also found in astrocytes (Hardy et al., 1996). Expression of myelin basic protein (MBP), a protein important for producing compact myelin, is drastically reduced in the qk^{v} brain (Jacque et al., 1983; Li et al., 2000). Work from multiple groups demonstrated that MBP expression is regulated through nuclear retention of the MBP transcript by the QKI-5 isoform, which binds the MBP 3'UTR and prevents transcript release into the cytoplasm for translation. The amount of nuclear QKI-5, in turn, is determined by the relative ratios of the cytoplasmic QKI-6 and 07 isoforms (Larocque et al., 2002). Loss of Qk also affects alternative splicing of another gene important for myelin formation, myelin-associated glycoprotein (MAG). In qk^{v} animals, the neonatal form of MAG persists into adulthood (Wu et al., 2002) and may contribute to dysmyelination in the mutant mouse.

Interestingly, a transgenic mouse expressing the dominant Qk isoform, QKI-6 (Lu et al., 2003), specifically in oligodendrocytes could restore compact myelin formation and MBP expression levels (Zhao et al., 2006). More recently, a conditional *Qk* mutant ($qKI^{fl/fl}$) removing *Qk* specifically from oligodendrocytes resulted in complete loss of QK protein, as well as reduced levels of MBP, hypomyelination in the CNS and defects in oligodendrocyte differentiation (Darbelli et al., 2016).

Regulation of synaptic function

Posttranscriptional regulation by RBPs contributes to many aspects of mature synaptic function, including synapse specificity through the action of the KHDRBS family, regulation of inhibitory synapse function by NOVA2, and splicing of ion channels and synaptic components by MBNL2, the neuronal ELAVLs, RBFOX1 and 2, and SCNM1.

KHDRBS proteins control alternative splicing of Neurexin

Perhaps one of the most striking alternative splicing events in mammalian neurons is that of the Neurexins (Nrxn), presynaptic cell surface proteins that promote synaptogenesis and contributes to synaptic specificity through trans-synaptic signaling (Baudouin and Scheiffele, 2010). Pre-mRNAs from the three *Nrxn* genes undergo extensive alternative splicing to produce more than three thousand protein isoforms (Baudouin and Scheiffele, 2010; Tabuchi and Südhof, 2002) presumably to increase synapse specificity (Craig and Kang, 2007; Graf et al., 2004). Regulation of *Nrxn* exon 20 generates AS4(+) or AS4(-) isoforms that exhibit differential binding to cell type-specific, postsynaptic partners (Baudouin and Scheiffele, 2010; Uemura et al., 2010). NRXNβ AS4(-) isoforms preferentially bind the NLGN1(B) concentrated at glutamatergic synapses, while NRXNβ AS4(+) isoforms preferentially bind NLGN2(A) at GABAergic and glycinergic synapses (Chih et al., 2006) (Figure 1-7A). Most interestingly, inclusion of exon 20 is negatively regulated by KHDRBS proteins, and *Khdrbs* mutant mice exhibit region-specific differential *Nrxn* splicing defects due to cell-type specific expression of the individual KHDRBS proteins. In addition, recent work showed that differences in AS4 splicing between excitatory and inhibitory neurons is driven by differential expression of a KHDRBS family member, SLM2 (Nguyen et al., 2016).

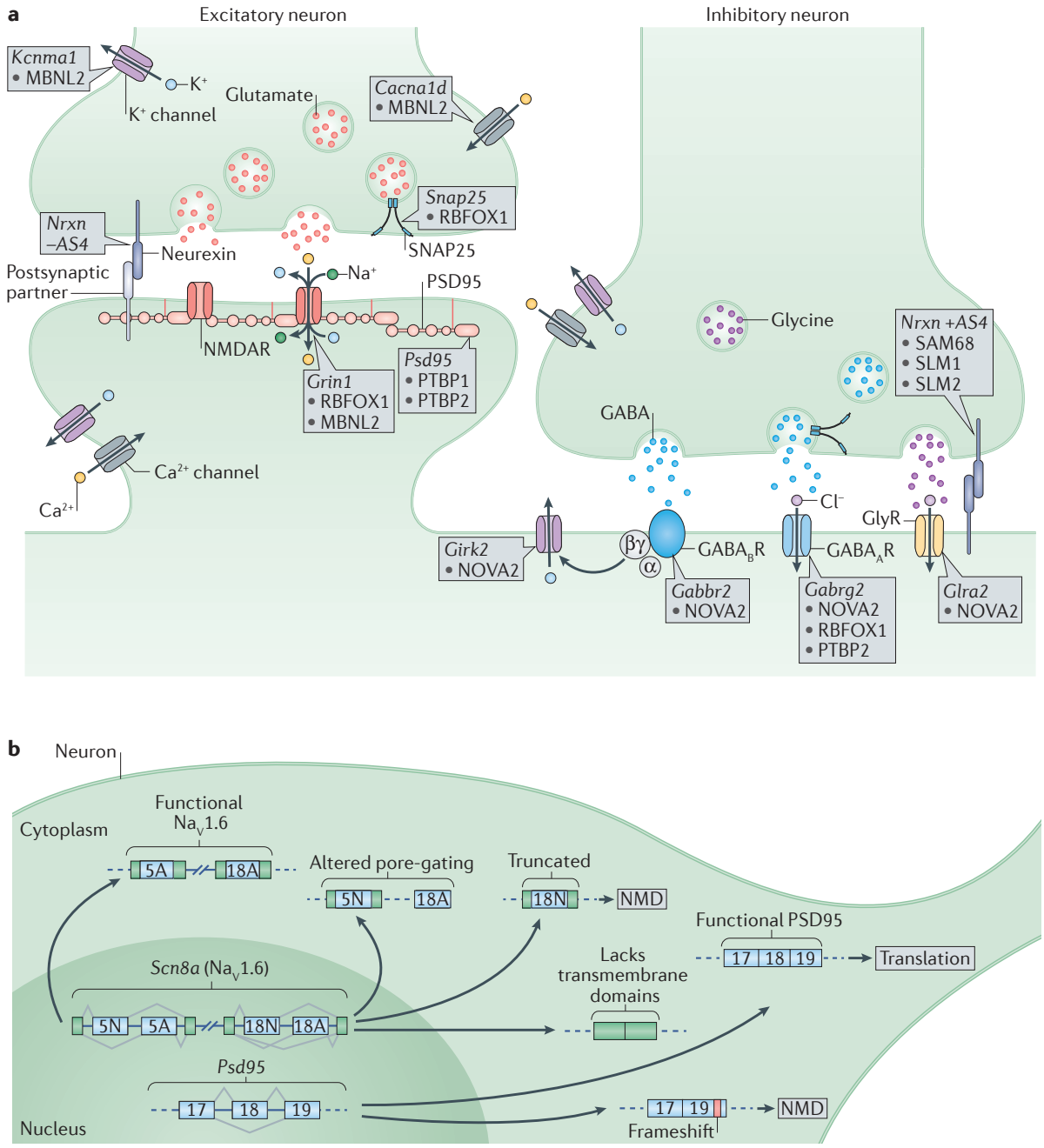

Figure 1-7: Alternative splicing regulation of synaptogenesis and synaptic function.

(A) At the presynaptic terminal, alternative splicing of Snap25 by RBFOX1 and of BK/Slo1 channel Kcnma1 by MBNL2 are important to control neurotransmitter release. Differential splicing of the pre-synaptic Nrxns at AS4 by the KHDRBS proteins controls

Figure 1-7 continued.

targeting to post-synaptic partners. At excitatory synapses, alternative splicing of the NMDA receptor alpha subunit Grin1 (GluN1) is regulated by RBFOX1 and MBNL2, while the PTBPs control productive splicing of the scaffold protein, postsynaptic density protein 95 (Psd95/Dlg4). Splicing of L-type voltage-gated calcium channels such as Cacna1d ($Ca_V1.3$) by MBNL2 may allow the voltage sensitivity, conductance, or other properties to be tuned as synapses differentiate. At inhibitory synapses, NOVA2 mediates alternative splicing of many post-synaptic components such as metabotropic $GABA_B$ receptor Gabbr2, the inwardly rectifying potassium channel Girk2 (Kir3.2) and the glycine receptor Glra2. Gabrg2 ($GABA_A$ receptor) splicing is controlled by multiple splicing regulators including NOVA2, RBFOX1 and PTBP2.

NMDAR, NMDA receptor; **SNAP25**, synaptosomal-associated protein 25; **PSD95**, postsynaptic density protein 95; **GABA**, γ-aminobutyric acid; **$GABA_BR$**, gamma-aminobutyric B receptor; **$GABA_AR$**, gamma-aminobutyric A receptor; **GlyR**, glycine receptor

(B) Alternative splicing controls the expression and function of many synaptic components. Expression of PSD-95 protein is repressed by PTBP-controlled exclusion of exon 18 until late in neuronal maturation when it is required for synaptogenesis. The voltage-gated sodium channel Scn8a ($Na_V1.6$) has multiple alternative exons (such as 5N, 5A, 18N and 18A as shown in the figure) that can change its gating properties, determine its localization or alter its overall function.

NMD, nonsense mediated decay

Modified with permission from (Li et al., 2007).

The KHDRBS (KH domain containing, RNA binding, signal transduction associated) family has three members: KHDRBS1 (SAM68), KHDRBS2 (SLM1) and KHDRBS3 (SLM2) (Di Fruscio et al., 1999). While SAM68 is found in both the nucleus and the cytosol of many cell types (Lukong and Richard, 2003), and affects a variety of cellular processes including splicing in the nucleus (Grange et al., 2004; Matter et al., 2002), SLM1 and SLM2 are more restricted to the nervous system with distinct expression patterns. For example, SLM1 is found in the dentate gyrus of the hippocampus, and in some cortical neurons and Purkinje cells. In contrast, high expression of SLM2 is present in CA1 and CA3 neurons of the hippocampus, most cortical neurons, and is also sparsely expressed in the granule and molecular layers of cerebellum (Iijima et al., 2014). The largely mutually exclusive expression pattern of SLM1 and SLM2 is enforced by their cross-regulation via alternative splicing coupled NMD, as seen with other paralogous pairs of RNA binding proteins (Boutz et al., 2007; Damianov and Black, 2010; Dredge et al., 2005; Gehman et al., 2011; Makeyev et al., 2007; Rossbach et al., 2009; Spellman et al., 2007). Specifically, SLM2 depletion shifts splicing of *Slm1* away from an NMD targeted isoform and towards a productive transcript(Traunmüller et al., 2014).

Germline *Sam68* null mice have deficits of bone metabolism, sexual organ development, motor coordination and motor learning (Lukong and Richard, 2008; Richard et al., 2005), and recent work indicates possible alterations in LTD (Klein et al., 2015). *Sam68/Slm1* dKOs were similar to *Sam68* single nulls, except for additional defects in cerebellar foliation and scattered, ectopic Purkinje cells in the molecular layer. SAM68 and SLM1 are both expressed in Purkinje cells and likely play redundant roles in their development. Since SAM68 is almost ubiquitously expressed throughout the cerebellum,

it is a question as to which neuronal subtypes contribute to the motor phenotypes, and whether *Nrxn1* is one of the relevant targets. In contrast to *Sam68* null mice, *Slm* single null mice and *Slm1/2* dKO mice are viable with no apparent anatomical defects (Ehrmann et al., 2013; Iijima et al., 2014; Traunmüller et al., 2014). Recent work found that specific deletion of Slm2 from parvalbumin+ interneurons led to increased neuronal excitability in the hippocampus, as well as defects in short-term memory (Nguyen 2016). It will be interesting to assess the *Slm2/Sam68* dKO, or the triple *Khrdbs* knockout. The interplay between the specific effects of particular KHDRBS paralogs and their partial redundancy typifies the complexity of analyzing splicing regulator mutants, and points to how a given splicing pattern may be controlled differently across different neuronal subtypes.

NOVA2 and synaptic plasticity

The differential roles of RBPs across various neuronal subtypes is highlighted by the many NOVA2 target genes are involved in inhibitory synapse function (Ule et al., 2003), including the $GABA_B$-receptor 2 (*Gabbr2*), glycine receptor α2 (*Glra2*), gephyrin (*Gphn*) and the G-coupled inwardly rectifying K+ channel *Kir3.2* (*Girk2*) (Figure 1-7A). Mis-splicing of $GABA_B$-receptors and GIRK channels likely lead to deficient long-term potentiation (LTP) of the slow inhibitory current seen in the *Nova2* null hippocampus (Huang et al., 2005). By contrast, LTP of excitatory postsynaptic currents (EPSC) is unchanged, as are basal excitatory and inhibitory synaptic transmission. This high degree of phenotypic specificity highlights the variable sensitivity of different forms of synaptic transmission and plasticity to splicing alteration. How alternative splicing of ion channels and neurotransmitter receptors changes precise physiological functions and how this regulation defines circuit function will be a rich area of investigation going forward.

MBNL2 and neurological symptoms of myotonic dystrophy

The MBNL (Muscleblind-like) family of RNA binding zinc finger proteins have been studied extensively in relation to the neuromuscular disorder myotonic dystrophy (DM). In DM, CTG or CCTG repeat expansions in expressed RNAs sequester MBNL proteins from their normal binding sites, altering MBNL-dependent splicing patterns (Du et al., 2010; Goodwin et al., 2015; Kanadia et al., 2003; Lin et al., 2006; Poulos et al., 2011). Although all three MBNLs are expressed in the brain, only *Mbnl2* null mice exhibit obvious CNS phenotypes. Germline deletion of *Mbnl2* results in abnormal sleep patterns, memory loss and learning deficits. *Mbnl2* null mice are also more susceptible to PTZ-induced seizure. Muscle function is, however, unperturbed likely due to abundant MBNL1 expression (Swanson et al., 2012). Hundreds of exons are misspliced in the *Mbnl2*$^{-/-}$ brain and overlap significantly with those known to be misspliced in DM. MBNL2 overall promotes adult-like splicing patterns, and its loss leads to continued expression of the fetal isoforms of ion channels such as *Kcnma1* (*BK/Slo1*) and *Cacna1d* (*Ca$_v$1.3*) and the NMDA receptor subunit *Grin1* (*GluN1*) (Figure 1-7A). NMDAR-mediated responses and pattern-induced LTP are impaired in the *Mbnl2* null. The observed alterations in synaptic plasticity and perturbations in neuronal excitability may be due to continued expression of fetal ion channel isoforms.

It is notable that about half of MBNL2 CLIP tags are found in 3' UTR sequences, indicating that non-splicing functions of MBNL2 (Swanson et al., 2012) perhaps contribute to the neurological defects of the mutant. Although *Mbnl2* null brains did not show major changes in transcript levels, recent studies of *Mbnl1/2* double knockouts highlight MBNL activity in controlling alternative polyadenylation events (Batra et al., 2014; Goodwin et

al., 2015; Shi and Manley, 2015). Binding in 3' UTRs is commonly observed for other splicing regulators and points to the need to distinguish phenotypes driven by splicing changes from those arising from altered mRNA stability, localization and/or translation (Figure 1-4).

ELAVL proteins regulate neuronal excitation

While recent progress in genome-wide analyses have identified new cytoplasmic roles for the MBNL proteins, RNA-seq profiling has revealed intronic binding of nELAVLs and hundreds of splicing changes in *Elavl3/4* double knockout brains. The ELAVLs have primarily been studied as regulators of mRNA stability and translation efficiency through their binding to 3' UTRs (Brennan and Steitz, 2001; Hinman and Lou, 2008; Srikantan and Gorospe, 2012). These newly defined ELAVL splicing targets are enriched for proteins involved in microtubule assembly and disassembly at synapses and axons. Interestingly, the biological processes affected at the level of splicing are different from those affected at the level of transcript abundance, suggesting that the regulatory programs of the nuclear and cytoplasmic nELAVL proteins are distinct (Ince-Dunn et al., 2012).

Like NOVA, nELAVLs are target antigens in patients with paraneoplastic neurologic disorders (Sakai et al., 1994; Szabo et al., 1991). Depletion of *nElavl* in the brain leads to multiple neurological defects (Akamatsu et al., 2005; DeBoer et al., 2014). While *Elavl3* null mice are born grossly normal and fertile, most of the adult animals show poor motor coordination. The specificity of the motor defect may be because ELAVL3 is the only nELAVL protein in Purkinje cells (Ince-Dunn et al., 2012). These mice also exhibit spontaneous cortical hypersynchrony and non-convulsive electrographic seizures. These

phenotypes are attributed to aberrant glutamate levels, based on nELAVL binding to the 3' UTRs of genes affecting glutamate synthesis. The multiple splicing regulator mutants that exhibit seizure phenotypes may reflect the large number of synaptic and membrane proteins regulated at the level of splicing, with hyperexcitability being a common consequence of their perturbation.

Cytoplasmic CELF4 functions in seizure susceptibility

CELF4, also known as Brunol4, is a member of the CUGBP, ELAV-like family of RBPs that are involved in xx functions. CELF is specifically expressed in brain tissue, and is highly enriched in neurons of the hippocampus. The frequent flyer (*Ff*) mutant allele is a transgenic insertion into the CELF4 gene leading to loss of expression. The *Ff* mutant exhibits spontaneous seizures at around 3 months of age and shows susceptibility to handling-induced seizures (Yang et al., 2007). The susceptibility to seizure is affected by genetic background and varies between mouse strains, making the *Ff* mutant a useful model for genetically complex epilepsy (Wagnon et al., 2011; Yang et al., 2007). Recent work has found that the *Ff* mutant has altered excitatory synaptic transmission, and that genetic detection of CELF4 from only excitatory neurons of the forebrain is sufficient to promote spontaneous seizures (Sun et al., 2013b; Wagnon et al., 2011). Indeed, immunofluorescence shows that CELF4 is expressed predominantly in excitatory neurons and within these cells its protein localization is restricted to the cytoplasm and the neurites. Accordingly, iCLIP of CELF4 in the cortex and hippocampus identified CELF4 binding primarily in the 3'UTRs of target transcripts, and microarray analysis found many changes in mRNA expression level, but few changes in splicing, in the CELF4 *null* brain (Wagnon et al., 2012). Interestingly, polysome fractionation showed that CELF4 is

enriched in heavy fractions associated with large RNA ribonucleotide-protein complexes, which have been shown to function in mRNA transport and local translation in neurons. Further analysis of some CELF4 mRNA targets found that loss of CELF4 resulted in a change in the local protein abundance between neurites and the soma, indicating that CELF4 might play a role in mRNA localization (Wagnon et al., 2012). The cytoplasmic function of CELF4, its specific expression in excitatory neurons and the resulting seizures in the CELF4 null brain point to an interesting cell-type specificity for RBP function.

Rbfox1 regulates neuronal excitability

Another splicing regulator whose mutation leads to a hyperexcitability phenotype is Rbfox1. Human mutations in *RBFOX1* have been identified in patients with epilepsy (Bhalla et al., 2004; Lal et al., 2015a; 2013a) and autism spectrum disorder (ASD) (Bill et al., 2013; Voineagu et al., 2011; Weyn-Vanhentenryck et al., 2014b). Pan-neuronal deletion of *Rbfox1* (*Rbfox1*$^{loxp/loxp}$; Nestin-Cre) leads to increased susceptibility to spontaneous and kainic acid-induced seizures as well as neuronal hyperexcitability in the dentate gyrus (Gehman et al., 2011). Relatively few splicing and expression changes were detected in the *Rbfox1*$^{-/-}$ whole brain, presumably due to redundancy of RBFOX2 and RBFOX3 function (Gehman et al., 2011; Lovci et al., 2013). However, these splicing changes affect transcripts encoding ion channels, neurotransmitter receptors, structural proteins and Ca^{2+} signaling molecules, many of which are associated with seizure disorders in human or mouse, such as *Gabrg2*, *Grin1 (GluN1)*, *Scn8a ($Na_V1.6$)*, and *Snap25* (Chapman et al., 1996; Corradini et al., 2009; Mulley et al., 2003; Papale et al., 2009; Zapata et al., 1997) (Figures 1-3B and 1-7A). Changes in the isoform ratios for these proteins may increase action potential firing or disrupt excitation/inhibition balance

in neuronal circuits. For example, the gene for the SNARE protein SNAP25 uses a pair of mutually exclusive exons (5a and 5b) to produce two alternative isoforms that exhibit differences in the kinetics of synaptic vesicle release (Bark et al., 2004; Sørensen et al., 2003). The *Rbfox1*$^{-/-}$ brains exhibit decreased 5b and increased 5a inclusion. The *Rbfox1*$^{-/-}$ seizure phenotype is thus consistent with studies showing that mice carrying genetic substitution of the 5b exon with 5a also exhibit seizures (Johansson et al., 2008).

The *Rbfox1*$^{-/-}$, *ELavl3*$^{-/-}$ and CELF4 *null* mice present interesting animal models for the study of human epileptogenesis and mechanisms controlling neuronal excitability. It will be interesting to compare their molecular targets and mutant physiology to understand whether they impact a common regulatory program or perhaps drive different splicing changes that have similar physiological outcomes.

SRRM4 regulation of synaptic transmission and neuronal excitability

A recent analysis of a mouse model of SRRM4 haploinsufficiency found that reduced levels of this RBP leads to autistic features in social behavior (Quesnel-Vallières et al., 2016). In a 3-chamber apparatus behavioral test, heterozygous animals preferred interacting with an inanimate object over social interaction with another animal. Interestingly, while both male and female haploinsufficient animals displayed reduced socialization, the effect was more pronounced in males, echoing observations in human ASD patients (Christensen et al., 2016). In the SSRM4 heterozygotes, these behavior defects may stem from alterations in both excitatory and inhibitory synaptic transmission. Genome-wide analyses show that microexons altered in autistic patient samples are enriched in UGC motifs (Nakano et al., 2012; Raj et al., 2014) and are likely SRRM4 targets.

RBFOX proteins control Purkinje cell pacemaking

In addition to affecting Purkinje cell migration, RBFOX2, in conjunction with RBFOX1, also regulates mature Purkinje cell function. *Rbfox2*$^{-/-}$ Purkinje cells eventually form a proper layer, but exhibit decreased dendritic arborization in the molecular layer, as well as irregular and less frequent spontaneous action potentials. This pacemaking defect becomes more severe in *Rbfox1* heterozygous, *Rbfox2* null brains (*Rbfox1*$^{+/-}$; *Rbfox2*$^{-/-}$) (Gehman et al., 2012). Specific depletion of *Rbfox1* and *Rbfox2* from mature Purkinje cells after completion of migration and development, using the L7(Pcp1)-Cre strain (L7-DKO), results in similar pacemaking phenotype and motor defects (Gehman et al., 2012) (Figure 1-6). The early and late phenotypes of *Rbfox* mutation demonstrate roles for these proteins in both cerebellar development and mature function.

The pacemaking defect in the L7-DKO mice is highly reminiscent of mice lacking the voltage-gated sodium channel subunit *Scn8a* (*$Na_V1.6$*) (Levin et al., 2006; Meisler et al., 2001; Raman et al., 1997). SCN8A functions in part to maintain a resurgent sodium current that enables regular, spontaneous firing. Several alternatively spliced exons in *Scn8a* contribute to the resurgent sodium current (Grieco et al., 2005; Raman and Bean, 1997). Mutually exclusive exons 5A and 5N alter voltage-dependent gating and/or interactions with a blocking subunit (Grieco et al., 2005). Another pair of mutually exclusive exons, 18A and 18N, determine whether a functional 18A+ *Scn8a* mRNA is produced. Inclusion of 18N introduces a premature termination codon and leads to nonsense mediated decay, whereas skipping both 18A and 18N produces an isoform lacking large portions of the third and fourth transmembrane domains (O'Brien et al., 2012; Plummer et al., 1997) (Figure 1-7B). While the single *Rbfox1*$^{-/-}$ and *Rbfox2*$^{-/-}$ brains

show modest changes in *Scn8a* splicing, the *Rbfox1*$^{+/-}$; *Rbfox2*$^{-/-}$ brains exhibit dramatic splicing changes at both exons 5 and 18, including a 2-fold decrease in exon18A that decreases the amount of functional SCN8A (Gehman et al., 2012). Thus, the Purkinje cell pacemaking defect in *Rbfox* mutant mice could largely arise from the loss of SCN8A. These results further confirm the partial redundancy of the *Rbfox* family members.

SCNM1 enhances non-consensus splicing of Scn8a

Forward genetic studies have also identified an *Scn8a* splicing mutation that causes severe neurological defects. This mutation, *med*^{J}, causes skipping of both exons 2 and 3 in a majority of *Scn8a* transcripts (Figure 1-7b), and produces a severely truncated, nonfunctional SCN8A protein (Kohrman et al., 1996). The *med*^{J} mice exhibit hindlimb paralysis, muscle atrophy and degeneration of Purkinje cells (SIDMAN et al., 1979). Normally, SCN8A ($Na_v1.6$) replaces the fetal $Na_v1.2$ at nodes of Ranvier during the first few weeks of postnatal development (Caldwell et al., 2000). In *med*^{J} /C3H mice, replacement of fetal $Na_v1.2$ is delayed, and the amount of $Na_v1.6$ at nodes of Ranvier reaches only 10-20% of that seen in wildtype mice. Nerve conduction velocity in *med*^{J} mutants is decreased by half (Kearney et al., 2002), probably as a consequence of insufficient SCN8A expression.

The severity of the *med*^{J} phenotype was found to be affected by genetic background and to correlate with the amount of correctly spliced transcript (Sprunger et al., 1999). In the C3H background, *med*^{J} mice live a normal lifespan with dystonia and ataxia, and with 10% of *Scn8a* transcripts correctly spliced. The same mutation in a C57Bl/6J background produces only 5% correctly spliced transcript, and the mice exhibit progressive paralysis and lethality by one month of age (Kearney et al., 2002). The

phenotypic severity of the *Scn8a*^{medJ} hypomorphic allele was found to be determined by a single gene modifier, sodium channel modifier 1 (*Scnm1*). C67Bl/6J mice have a nonsense mutation in *Scnm1*, and targeted deletion of *Scnm1* in the C3H strain confirmed that SCNM1 affects both the splicing of *Scn8a*^{medJ} transcript and the mouse phenotype (Howell et al., 2008; Sprunger et al., 1999). Finally, a BAC transgene expressing wildtype *Scnm1* can rescue the lethality and paralysis of *Scn8a*^{medJ} in the C57BL/6J (Buchner et al., 2003).

Although the genetic interaction between *Scnm1* and *Scn8a* splicing has been studied in detail, the mechanism of SCNM1 function as a splicing regulator is less clear. The protein has one zinc finger domain, a basic nuclear localization signal and an acidic carboxy terminus. Its overexpression in heterologous cells can enhance correct splicing of an *Scn8a* minigene, possibly via interactions with the spliceosomal proteins U1-70k and LUC7L2 (Howell et al., 2008). The studies of *Scnm1* indicate that splicing regulators can be an important class of phenotypic modifiers. Given the many human disease-causing mutations that affect pre-mRNA splicing, polymorphisms in splicing regulatory genes may play a large role in modifying disease severity across individuals.

Splicing regulators and neurodegeneration

Splicing mis-regulation is increasingly implicated in neurodegenerative disorders. Dysfunction of TDP-43 and FUS lead to phenotypes characteristic of amyotrophic lateral sclerosis (ALS) and frontal temporal lobar disease (FTLD), while mutation of a core spliceosomal component, the U2 snRNA (*Rnu2-8*), leads to specific neurodegeneration in the cerebellum.

TDP-43 and FUS in amyotrophic lateral sclerosis

Errors of splicing regulation are increasingly implicated in a variety of neurodegenerative disorders, including amyotrophic lateral sclerosis (ALS) and frontal temporal lobar disease (FTLD) (Da Cruz and Cleveland, 2011; Ling et al., 2013). Familial and sporadic forms of ALS and some cases of FTLD have been associated with mutations in TDP-43, Fus /TLS (Da Cruz and Cleveland, 2011; Ling et al., 2013), hnRNPA1, hnRNPA2B1 (Kim et al., 2013), and Matrin3 (Johnson et al., 2014) – all of which are regulators of splicing. Disruption of TDP-43 and FUS function through protein aggregation or mislocalization is a characteristic of ALS and FTLD derived from many different mutations (Buratti and Baralle, 2012; Mackenzie et al., 2010; Polymenidou et al., 2012), and neurogenetic analyses of TDP-43 and Fus have been the most extensive.

Transactivating response DNA binding protein (TDP-43, or TARDBP) is a major component of cytoplasmic inclusions found in 95% cases of sporadic ALS and FTLD (Ling et al., 2013). Widely expressed in many tissues and predominantly nuclear, TDP-43 affects multiple steps of RNA metabolism including transcription, splicing, decay, transport and translation (Lagier-Tourenne et al., 2010). One hypothesis for TDP-43's pathogenic role is that the formation of TDP-43 cytoplasmic inclusions leads to its depletion from the nucleus and a loss of splicing function (Da Cruz and Cleveland, 2011; Ling et al., 2013). Consistent with this, ALS-like phenotypes are seen in mice with partial depletion of TDP-43 by RNAi, or with targeted deletion of *Tdp-43* in motor neurons, while germline *Tdp-43* null mice are embryonic lethal (Kraemer et al., 2010; Sephton et al., 2010; Wu et al., 2010). Dominant missense mutations are sufficient to cause familial disease in humans (Lee et al., 2012), and transgenic rodents expressing either wildtype or disease-associated mutants also show neurodegeneration. These phenotypes could

be indicative of a toxic gain-of-functions (Johnson et al., 2008; 2009; Zhang et al., 2009), or, alternatively, the mutations and overexpression could somehow both promote cytoplasmic inclusion formation with a loss-of-function (Budini et al., 2015; Lee et al., 2012; Polymenidou et al., 2011; Vanden Broeck et al., 2014; Yang et al., 2014).

Both the ALS-associated mutations and the changes in wildtype TDP-43 expression alter a large program of alternative exons in mutant mice (Arnold et al., 2013; Polymenidou et al., 2011; Tollervey et al., 2011). However, less than a quarter of affected exons are shared between the transgenic and RNAi depletion mouse models. Motor neurons may be particularly sensitive to aberrant splicing changes, or some of the common TDP-43 dependent splicing events might be sufficient to cause the phenotype. The many models will allow rich comparisons in identifying potentially causative splicing changes.

Another ALS and FTLD gene, fused in sarcoma/translocated in liposarcoma (FUS/TLS) (Ling et al., 2013) is a widely expressed, predominantly nuclear RRM domain RNA binding protein (Iko et al., 2004; Zinszner et al., 1997) that, like TDP-43, plays multiple roles in RNA processing, including splicing regulation (Lagier-Tourenne et al., 2010; Rogelj et al., 2012). *Fus* null mice die soon after birth (Hicks et al., 2000), whereas a transgenic rat model of mutant *Fus* exhibits a variety of ALS-like phenotypes (Huang et al., 2011). Interestingly, TDP-43 and FUS regulate distinct groups of alternative exons and target different sets of mRNAs in the cytoplasm (Fujioka et al., 2013; Rogelj et al., 2012), suggesting different roles for the wildtype proteins. It will be interesting to compare the targets of these two proteins to the targets of other RNA binding proteins implicated

in ALS including hnRNPA1, hnRNPA2 and Matrin3, and assess how their mutation might converge on similar disease pathologies.

Rnu2-8 is required for cerebellar granule neuron survival

A forward genetic screen recently uncovered a novel form of neurodegeneration caused by mutation of a core component of the spliceosome. The mouse mutant (*NMF291*) contains a functionally compromised allele of *Rnu2-8* (Jia et al., 2012), one of multiple genes encoding the U2 snRNA (Wahl et al., 2009). U2 snRNA binds to the branch point during spliceosome assembly and then forms base pairs with the U6 snRNA to become a key portion of the spliceosome catalytic center for all major class introns (Black, 2003; Lee and Rio, 2015; Matera and Wang, 2014; Wahl et al., 2009) (Figure 1-2), and its dysfunction might be expected to be lethal for all cell growth. Mammalian genomes contain multiple clustered copies of the U2 snRNA gene that allow production of the extremely high levels of U2 snRNA found in cells, and which were previously thought to be equally expressed across tissues. Thus, the highly tissue specific phenotype of *NMF291* was unanticipated. The *NMF291* mutation is a 5nt deletion that removes the first 2nt of the branch site recognition sequence (BSRS) within the U2 snRNA, as well as a 3nt linker between the BSRS and the U2/U6 helix IA. When highly expressed, the mutant U2 snRNA decreases overall splicing efficiency and affects alternative splicing patterns. In particular, about 3,000 annotated introns showed higher levels of retention in the *NMF291* cerebellum (see Figure 1-1 and Figure 1-4A). These results are reminiscent of recent data on myelodysplastic syndromes, where mutations in several components of the core splicing apparatus such as U2AF65, SF3B1 and other proteins were found to cause very specific splicing defects in particular transcripts and to lead to a highly tissue

specific phenotype (Lindsley and Ebert, 2013; Yoshida and Ogawa, 2014; Yoshida et al., 2011). These studies open the possibility for other neurological disorders being caused by mutation of general splicing factors.

NMF291 mice exhibit progressive and severe degeneration of the cerebellum due to loss of cerebellar granule neurons beginning at postnatal week 4 (Figure 1-6), and develop tremors at 8 weeks progressing to truncal ataxia by 12 weeks. Consistent with the phenotype, both wildtype and mutant *Rnu2-8* RNA are selectively expressed in the cerebellum and increase in expression after granule neuron maturation. A transgenic mouse expressing the mutant *Rnu2-8* in the wild-type background displays a similar course of granule neuron loss and ataxia. Conversely, increasing the dose of the wild-type RNA in the *NMF291* mutant decreases neurodegeneration in the granule layer. These data nicely demonstrate that not all U2 genes are the same, but individual genes within a cluster can exhibit temporal and cell type specific patterns of expression. Their mutation can thus lead to a highly cell-specific phenotype.

Discussion

The analysis of RBP mutations is challenged by their highly pleiotropic phenotypes. Mutations are often lethal or lead to developmental abnormalities that obscure additional later functions. Several studies have overcome these obstacles using ever more precise Cre expression to ablate a regulatory gene in particular cell types at particular times. RNAseq and CLIPseq now allow the relatively simple identification of posttranscriptional targets potentially determining the mutant phenotype. These genome-wide analyses indicate that individual RBPs affect coherent sets of transcripts that can be involved in common biological pathways (Calarco et al., 2011; Jangi and Sharp, 2014).

However, the large number of targets makes it difficult to link a phenotype to a particular posttranscriptional event. As described above, phenotypes can be connected to particular events using transgenes expressing single spliced isoforms to rescue particular functions. This strategy will need to be applied to more refined populations of cells and circuits, perhaps through *in utero* electroporation, viral transduction or CRISPR-mediated genetic engineering. One challenge will be to match the expression from the rescuing gene to that of an endogenous locus in time and quantity. Developmental phenotypes may be reverted by an overexpressed transgene, but the rescue of physiological defects will likely need precise control of isoform ratios, perhaps through genome editing of endogenous loci.

The obverse problem to the many targets of RBPs is that these regulators frequently occur in highly related gene families. Groups of paralogous regulators that exhibit partially redundant functions can mute the effect of single gene mutations. In cells where they are co-expressed, double mutation will often lead to new splicing changes not seen in either single mutant and reveal new phenotypes. However, regulators are rarely entirely redundant and usually exhibit differences in their range of expression, as seen with the NOVA, nELAVL and RBFOX proteins.

It is important to keep in mind that many RNA binding proteins controlling splicing choices also affect the choice of poly-A site, and can also be found in the cytoplasm where they control the translation or stability of target transcripts through binding in 3' UTRs (Lee et al., 2016b) (Figure 1-4B). The consequences of their mutation will include the loss of these functions in addition to splicing changes. Cytoplasmic functions can be examined by measuring overall expression changes by RNAseq, rather than splicing changes, and

by identifying 3' UTR targets in CLIPseq datasets. The relationships between the nuclear and cytoplasmic regulatory programs controlled by RNA binding proteins are only beginning to be examined. It will also be important to define those effects that arise from the direct regulation of a transcript rather than an indirect consequence of splicing factor loss. Splicing regulators extensively modulate each other's activity, as well as controlling the activity of transcriptional regulators (Figure 1-3). Thus, gene expression changes in mutant mice may derive in part from extensive secondary effects downstream of the protein being examined.

Recent human genetic studies have clearly implicated RBPs in neurodegenerative diseases such as ALS. Other work has connected RNA binding proteins to mis-splicing in neuropsychiatric disorders ranging from epilepsy, ASD, inherited ataxias, and schizophrenia. Splicing programs provide a highly interconnected layer of regulation that can alter protein activity without easily discernible changes in overall expression. Perturbations of these programs have potential to alter neuronal connectivity and firing properties in a manner that has dramatic consequences for overall circuit function and behavior. The mouse mutations described above provide the first glimpses of these regulatory programs. In the RNA binding protein knockouts so far analyzed, the heterozygous mice develop largely normally, but some splicing targets are still altered by the reduction in regulatory protein dose. It will be particularly interesting to assess these heterozygous mice for behavioral defects. Future work in these genetic systems will provide potential new models for a variety of disorders.

In addition to relating splicing regulation to neurological disease, there are many questions to be addressed. Although many alternative splicing events are conserved

across mammalian or vertebrate species, the effect of these splicing changes on protein activity is usually unknown. It will be important to characterize the set of protein isoforms expressed from each gene and understand their different roles in cell biology. This will be a particular challenge for physiology, but such analyses are needed to relate changes in synaptic and membrane protein structure to changes in synaptic activity and firing. Another issue is how the programs controlled by different regulators interact (Figure 1-3A). RNA binding proteins can antagonize each other or synergize in RNA binding. The complex overlap between their regulatory programs allows for a high degree of specificity in where and when particular splicing events occur. It will be very interesting to assess how the expression of spliced isoforms or the posttranscriptional regulation of mRNA levels contributes to defining specific neuronal subtypes. Future application of mouse genetics to the characterization of RBP regulatory programs should allow some of these questions to be answered.

Chapter 2: RBFOX1 REGULATION OF VAMP1 EXPRESSION

Introduction

The Rbfox family of brain-enriched RBPs have been most widely studied as regulators of alternative splicing. In mammals there are three Rbfox family members – Rbfox1, Rbfox2 and Rbfox3 – each having a highly conserved RNA recognition motif (RRM) that binds the sequence (U)GCAUG (Conboy, 2017; Jin et al., 2003; Kuroyanagi, 2009; Ponthier et al., 2006). In regulating splicing, Rbfox proteins function in complex with a Large Assembly of Splicing Regulators (Damianov et al., 2016; Ying et al., 2017). These proteins exhibit a position-dependent effect, where Rbfox binding in the intron upstream of an alternative exon represses it, while binding in the downstream intron promotes exon inclusion in the final mRNA (Conboy, 2017; Kuroyanagi, 2009). While all three proteins function to regulate splicing in the nucleus, the proteins are also alternatively spliced to create cytoplasmic isoforms (Lee et al., 2009; Nakahata and Kawamoto, 2005) that bind within 3' UTR sequences to regulate translation (Carreira-Rosario et al., 2016; Lee et al., 2016b). The ratio of nuclear to cytoplasmic Rbfox varies between cells and can be dynamically regulated by membrane depolarization (Lee et al., 2009).

Previous work from our group characterizing pan-neuronal *Rbfox1*$^{loxP/loxP}$ *; Nestin-Cre*$^{+/-}$ knockout mice (*Rbfox1 Nes-cKO*) found that loss of Rbfox1 from neurons led to infrequent, spontaneous seizures (Gehman et al., 2011). When challenged with kainic acid, *Rbfox1 Nes-cKO* mice displayed significantly increased susceptibility to seizure compared to wildtype littermates or *Rbfox2* knockouts. Electrophysiological analyses of the synaptic input/output relationship using field recordings in the dentate gyrus found that low intensity presynaptic fiber stimulation elicited larger fEPSPs in cKO granule cells compared to wildtype. Spine density was only modestly decreased in cKO dendrites, and

expression levels of the synaptic markers Synapsin-I and PSD-95 remained unchanged. These results suggested that a change in synaptic function rather than synapse number was responsible for the neuronal hyperexcitability in the *Rbfox1 Nes-cKO* brain. Interestingly, many of the splicing changes observed in the cKO brain were in transcripts previously implicated in synaptic function and seizure disorders. However, most work on Rbfox1 has focused on alternative splicing changes in whole mouse brain and not specifically the hippocampus (Gehman et al., 2011; Lovci et al., 2013). In addition, the loss of cytoplasmic Rbfox1 presumably also contributes to the pathophysiology of the *Rbfox1 Nes-cKO* in parallel with the splicing changes controlled by the nuclear protein. The contribution of the cytoplasmic protein to Rbfox1 function remains unexplored.

Recent work demonstrated a role for cytoplasmic Rbfox1 in promoting transcript stability and/or translation by binding the 3'UTRs of target transcripts (Carreira-Rosario et al., 2016; Lee et al., 2016b). This cytoplasmic portion of the Rbfox1 regulatory program was enriched for many key neuronal functions such as the calcium signaling pathway, as well as regulatory modules controlling cortical development and modules altered in ASD (Lee et al., 2016b). Interestingly, this cytoplasmic program largely affected transcripts different from those regulated by the splicing program. Thus, the neuronal hyperexcitability phenotype observed in the adult *Rbfox1 Nes-cKO* mice is likely to involve both changes in splicing and changes in mRNA abundance. Here we examine the changes in gene expression and electrophysiology controlled by Rbfox1, specifically in the hippocampus. We identify *Vamp1* as a major target of cytoplasmic Rbfox1 that plays a critical role in inhibitory synaptic transmission. Our work demonstrates how regulation of Vamp1 mRNA abundance by cytoplasmic Rbfox1 controls synaptic function in a

specific neuronal cell type and contributes to the greater network defects in the *Rbfox1 Nes-cKO* brain.

Results

Vamp1 is a direct Rbfox1 target

Previous electrophysiological analysis of Rbfox1 Nes-cKOs was performed in the hippocampus, where cFos staining indicated enhanced neuronal activity after spontaneous seizure. Subsequent whole transcriptome profiling of gene expression and alternative splicing by ex-on-junction microarray and RNAseq assayed the whole brain of the Rbfox1 Nes-cKO and was difficult to relate to the electrophysiological results (Gehman et al., 2011; Lovci et al., 2013). A recent RNAseq study of cultured hippocampal neurons revealed that the cytoplas-mic Rbfox protein also regulates the expression of genes involved in synaptic transmission and calcium signaling. Thus the effects of the cytoplasmic protein on neurophysiology need to be considered along with the effects of the nuclear protein on splicing (Lee et al., 2016a). However, this study examined gene expression and splicing changes in response to the double knockdown of Rbfox1 and Rbfox3. To obtain a more refined view of posttranscriptional regulation specifically by Rbfox1 and specifically in the hippocampus, we performed RNAseq on adult (P60-70) hippocampi isolated from the Rbfox1 Nes-cKO and from wildtype littermates (n=3, each genotype). Isolated PolyA-plus RNA was converted to cDNA and subjected to 50 nt paired-end sequencing using the standard Illumina platform (Figure 2-1A). An average of 48 million reads were generated per replicate sample, aligned to the mouse genome using TopHat (Trapnell et al., 2012) (with an average mapping rate of 90%), and analyzed

for spliced isoform expression using SpliceTrap (Table S2-1) (Wu et al., 2011) and for overall expression levels using the Cufflinks package (Table S2-2) (Trapnell et al., 2012). Comparing cKO to wild type, we identified significant changes in alternative splicing and in overall mRNA abundance, consistent with the dual role of Rbfox1 in regulation of both alternative splicing and mRNA stability. As seen previously, Rbfox1-dependent gene expression changes did not significantly overlap with splicing changes (19 genes changing in both overall mRNA abun-dance and exon usage, Figure S2-1 and Table S2-3). The gene expression changes identified in the cKO hippocampus (1034 genes) partially overlapped (183 genes) with those previously identified as cytoplasmic Rbfox1 targets in cultured neurons (774 genes) (Lee et al., 2016b). The differences between these two RNAseq datasets are likely due both to gene expression changes between tissue and in vitro culture, to different effects of prolonged versus acute loss of Rbfox and to additional loss of Rbfox3 in the previous study.

Focusing on gene expression changes resulting from loss of Rbfox1 in the adult mouse hippocampus, we examined the overlap of our target transcripts with previously published Rbfox1 iCLIP datasets from the soluble nucleoplasmic fraction of adult mouse forebrain (Damianov et al., 2016) and from the cytoplasmic fraction of cultured primary neurons (Lee et al., 2016b). Examining the 1034 differentially expressed (DE) genes detected in our adult hippocampal samples, we filtered the target list by requiring DE genes to contain 3'UTR CLIP clusters in both the nucleoplasmic and cytoplasmic datasets, and that these clusters contain an Rbfox motif [(U)GCAUG] within ±10

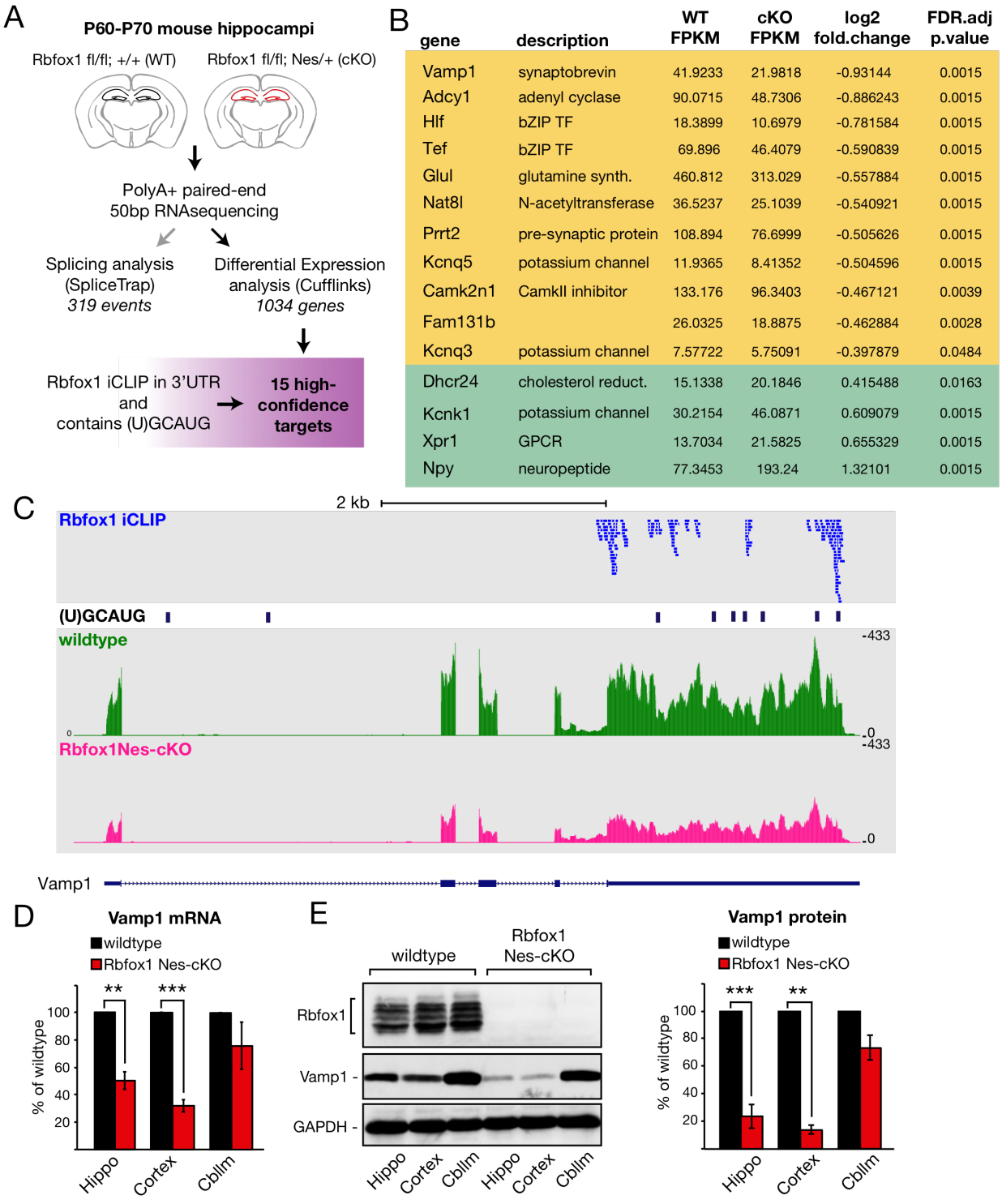

gene	description	WT FPKM	cKO FPKM	log2 fold.change	FDR.adj p.value
Vamp1	synaptobrevin	41.9233	21.9818	-0.93144	0.0015
Adcy1	adenyl cyclase	90.0715	48.7306	-0.886243	0.0015
Hlf	bZIP TF	18.3899	10.6979	-0.781584	0.0015
Tef	bZIP TF	69.896	46.4079	-0.590839	0.0015
Glul	glutamine synth.	460.812	313.029	-0.557884	0.0015
Nat8l	N-acetyltransferase	36.5237	25.1039	-0.540921	0.0015
Prrt2	pre-synaptic protein	108.894	76.6999	-0.505626	0.0015
Kcnq5	potassium channel	11.9365	8.41352	-0.504596	0.0015
Camk2n1	CamkII inhibitor	133.176	96.3403	-0.467121	0.0039
Fam131b		26.0325	18.8875	-0.462884	0.0028
Kcnq3	potassium channel	7.57722	5.75091	-0.397879	0.0484
Dhcr24	cholesterol reduct.	15.1338	20.1846	0.415488	0.0163
Kcnk1	potassium channel	30.2154	46.0871	0.609079	0.0015
Xpr1	GPCR	13.7034	21.5825	0.655329	0.0015
Npy	neuropeptide	77.3453	193.24	1.32101	0.0015

Figure 2-1: Vamp1 is a direct Rbfox1 target.

Figure 2-1 continued.

(A) Schematic of samples used for RNAseq and Rbfox1 target identification. Adult hippocampi were dissected from wildtype and Rbfox1 Nes-cKO littermates for RNA extraction and PolyA+ mRNA sequencing. Splicing changes were analyzed using SpliceTrap and differential gene expression (DE) was detected using the Cufflinks package. Direct Rbfox1 DE targets were identified by iCLIP clusters present in two different iCLIP datasets and a (U)GCAUG within ±10nt.

(B) Table of high confidence direct Rbfox1 DE target genes filtered by the criteria outlined in (A) with down-regulated transcripts in yellow and up-regulated transcripts in green.

(C) UCSC genome browser view of mouse Vamp1 gene expression and Rbfox1 binding. Top, Rbfox1 iCLIP tags (blue) from the nucleoplasmic fraction of adult mouse brain, with Rbfox binding motifs (U)GCAUG indicated as black bars below. Middle, RNAseq reads map-ping to Vamp1 from representative wildtype (green) and Rbfox1 Nes-cKO (pink) hippocampi. The gene structure of Vamp1 is shown at bottom (tall boxes, exons; short boxes, 5' and 3' UTRs; dashed lines, introns; arrow indicate direction of transcription). Genomic scalebar is shown at top.

(D) Vamp1 mRNA levels are reduced in the Rbfox1 Nes-cKO forebrain but not in cerebellum. qPCR analyses of Vamp1 mRNA from adult (P60-P70) hippocampus, cortex and cerebellum of wildtype and Rbfox1 Nes-cKO littermates. Vamp1 was normalized to Hprt expression and shown as a percentage of wildtype in each brain region.

(E) Vamp1 protein levels are reduced in the Rbfox1 Nes-cKO forebrain but not in cerebellum. Left, immunoblot of Rbfox1, Vamp1 and GAPDH in hippocampus, cortex and cerebellum of adult (P60-P70) wildtype and Rbfox1 Nes-cKO littermates. Right,

Figure 2-1 continued.

quantification of Vamp1 protein as a percentage of wildtype expression for each brain region after normalization to GAPDH.

For D,E n=3 littermate pairs; Student's t-test; ** $p \leq 0.01$, *** $p \leq 0.001$; error bars, s.e.m.

See also **Figure S2-1** and **Tables S2-4**.

nucleotides of the edge of the cluster (Figure 2-1A). These stringent filters generated a list of 15 high confidence DE genes directly regulated by Rbfox1 (Figure 2-1B and Table S2-4). This short list of Rbfox1 targets included a number of transcripts playing important roles in neuronal function including adenylyl cyclase, potassium channels, neuropeptide Y and others. Most targets were downregulated upon Rbfox1 loss, as seen previously in cultured cells, but four were upregulated and thus appear to be re-pressed by the protein. Using less stringent filters, many additional transcripts are seen to be regulated by Rbfox1 (Tables S2-2 and S2-4).

Vamp1 (also known as Synaptobrevin1) mRNA exhibited one of the largest changes in expression, decreasing by 50% in the Rbfox1 Nes-cKO hippocampus as measured by RNAseq and by quantitative PCR (qPCR) (Figure 2-1 B,D). Rbfox1 binding on the Vamp1 mRNA is restricted to the 3'UTR and is observed in the nucleoplasmic and cytoplasmic fractions, but not in the high molecular weight, chromatin-associated pellet from the nucleus where the Rbfox1 binds within introns to regulate splicing (Damianov et al., 2016) (Figure 2-1C). The final intron in the Vamp1 transcript was seen to be incompletely spliced in the RNAseq data (Table S2-1 and Figure S2-1C). However, qPCR analyses of the fully spliced Vamp1 transcript and that re-taining the final intron showed that only the spliced transcript was red uced in the Rbfox1 cKO, and this spliced transcript constituted more than 95% of the Vamp1 mRNA pool (Figure S2-1 D,E). To assess Vamp1 protein levels, we performed immunoblotting for Vamp1 in Rbfox1 Nes cKO and wildtype adult brains. We found that Vamp1 protein, like the mRNA, was dramatically depleted by ~80% in the cKO cortex and hippocampus (Figure 2-1E). Interestingly, although sharply reduced in the cKO hippocampus and cortex, there was relatively little

effect on Vamp1 expression in the cerebellum, where its regulation presumably involves additional factors (Figure 2-1D, E). The mRNA and protein levels of the paralog Vamp2 were also unchanged between Rbfox1 Nes cKO and wildtype (Figure S2-1 F,G). In the forebrain, the reduced Vamp1 mRNA and protein levels and the direct binding of Rbfox1 to the Vamp1 3'UTR all suggest a role for cytoplasmic Rbfox1 in regulating Vamp1 expression by promoting its mRNA stability and/or translation.

The Vamp1 3'UTR confers Rbfox1-dependent expression

Although we observed Rbfox1 binding to the Vamp1 3'UTR by iCLIP (Figure 2-1C), it was possible that the decreased Vamp1 expression in the cKO forebrain resulted from loss of the nu-clear Rbfox1 function or from indirect effects of Rbfox1 loss. To assess the mechanisms of Rbfox mediated regulation, we examined whether and how cytoplasmic Rbfox1 regulates Vamp1 expression. We cultured primary hippocampal neurons from Rbfox1 Nes-cKO embryos that lack both the nuclear and cytoplasmic isoforms. We then assayed Vamp1 expression before and after re-expression of just the cytoplasmic Rbfox1 isoform. Using qPCR, we found that *Vamp1* mRNA was reduced ~40% in cultured cKO neurons compared to the wildtype (Figure 2-2A), similar to the 50% reduction observed in the adult cKO hippocampus by RNAseq (Figure 2-1 B,D). Vamp1 protein levels were reduced by ~60% in the cultured cKO neurons, a similar although somewhat smaller reduction to that seen in the adult cKO hippocampus (Figure 2-1E). We used adeno-associated virus (AAV) to re-express cytoplasmic Rbfox1 under the control of the human *SynapsinI* (*hSyn*) promoter in the cKO neurons (C rescue). We found that the cytoplasmic isoform of Rbfox1 alone can indeed rescue both Vamp1 mRNA and VAMP1 protein to levels comparable to that of wildtype neurons (Figure 2-2A). These

results demonstrate that cytoplasmic Rbfox1 is sufficient to promote Vamp1 expression. Given the observed binding in the *Vamp1* 3'UTR (Figure 2-1C), Rbfox1 may enhance *Vamp1* mRNA stability or translation.

To examine the role of the *Vamp1* 3' UTR in Rbfox1 regulation, we used the luciferase re-porter system in primary hippocampal neurons. We cultured neurons from Rbfox1$^{fl/fl}$ embryos and infected them at DIV3 with AAV expressing hSyn-driven eGFP or Cre-eGFP to create wildtype or Rbfox1 cKO neurons, respectively. Loss of Rbfox1 was confirmed by immunoblot (Figure 2-2B). At DIV5, we transfected a reporter containing the luciferase coding region fused to the full length *Vamp1* 3'UTR (FL; Figure 2-2C) along with a Renilla control reporter and as-sayed luciferase activity at DIV14, after synapses had been established. The loss of Rbfox1 from neurons decreased reporter expression by ~50% (FL, Figure 2-2C-D), indicating that expression from transcripts containing the *Vamp1* 3'UTR is strongly Rbfox1-dependent. The residual expression seen upon loss of Rbfox1 may be due to the presence of cytoplasmic Rbfox3 in these cells ((Lee et al., 2016a); and see below).

Using the luciferase assay, we tested the roles of the multiple Rbfox binding motifs (U)GCAUG in stimulating expression by mutating them to (U)GACGU. The Vamp1 3'UTR contains seven Rbfox motifs. Mutation of the first six sites significantly reduced reporter expression (FLm1-6, Figure 2-2C-D). Mutation of all seven sites virtually abolished reporter expression (FLm1-7, Figure 2-2C-D). Most notably, mutation of only the 3'-most Rbfox binding site reduced reporter expression as strongly as mutation of all six upstream sites (FLm7, Figure 2-2C-D). These results indicate that the 3'most (U)GCAUG plays a major role in Rbfox1-dependent stimulation of Vamp1 expression, though the upstream

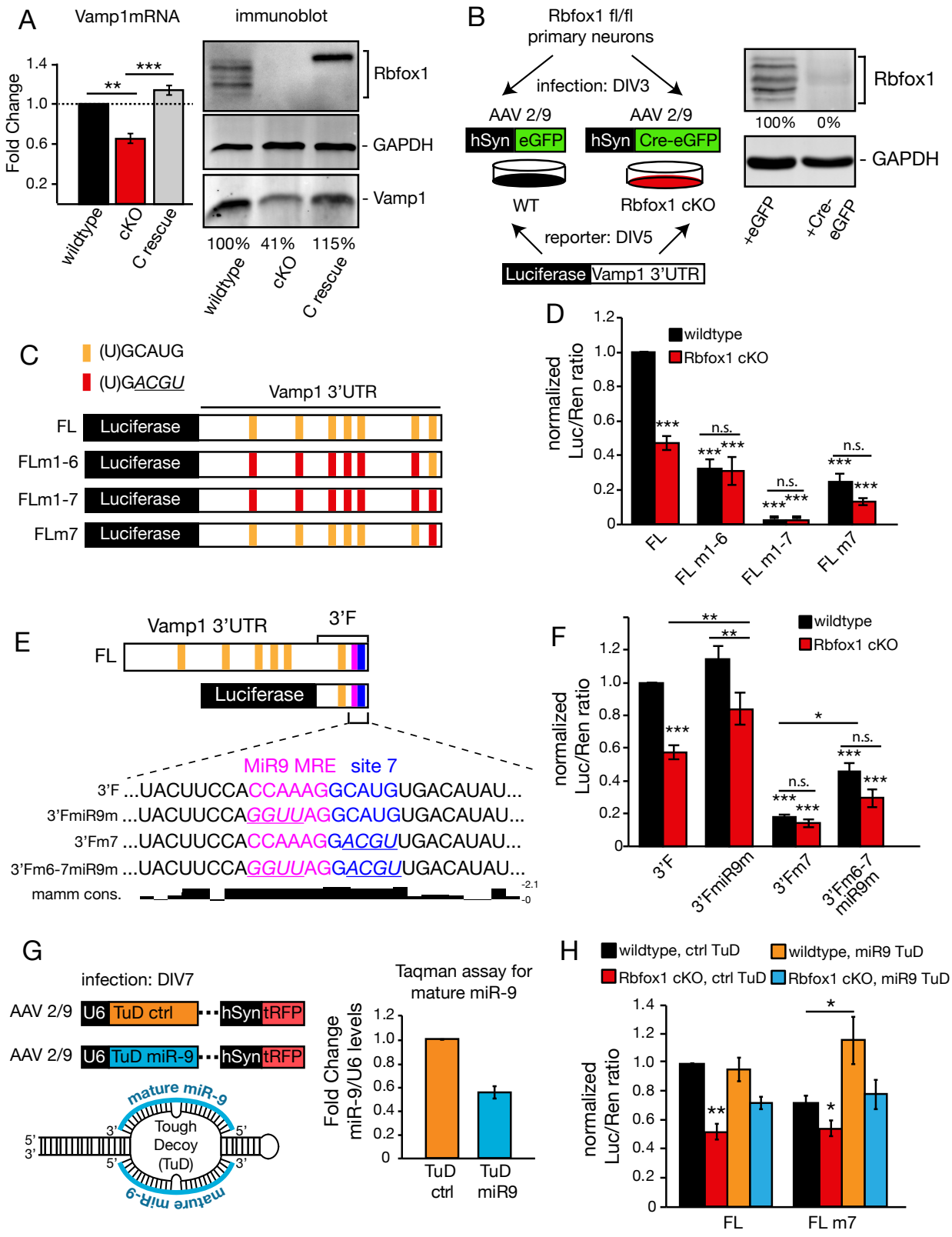

Figure 2-2: The Vamp1 3'UTR confers Rbfox1-dependent expression.

Figure 2-2 continued.

(A) Cytoplasmic Rbfox1 rescues Vamp1 expression levels. Left, qPCR quantification of Vamp1 mRNA in wildtype (black), Rbfox1 Nes-cKO (red, cKO) and cKO primary hippocampal neurons tra¬nsduced with AAV2/9 hSyn-Rbfox1 (C rescue; gray). Vamp1 was normalized to Hprt expression levels and shown as fold-change relative to wildtype. Right, immunoblot of Rbfox1, Vamp1 and GAPDH. Average levels of Vamp1 expression normalized to GAPDH and relative to wildtype are given below Vamp1 panel. n=3 cultures (biological replicates); ANOVA with Bonferroni correction; ** $p \leq 0.01$, *** $p \leq 0.001$; error bars, s.e.m.

(B) Left, schematic of luciferase experiment. Right, immunoblot of Rbfox1 and GAPDH in DIV14 neurons transduced with hSyn-eGFP and hSyn-Cre-eGFP. Average Rbfox1 expression normalized to GAPDH and relative to hSyn-eGFP condition given below Rbfox1 panel. n=3 cultures (biological replicates).

(C) Schematic of full length Vamp1 3'UTR luciferase reporters. Vertical bars in 3'UTR represent the wildtype Rbfox binding motif (U)GCAUG (yellow) or mutated motif (U)GACGU (red).

(D) Quantification of full length luciferase reporter expression. Luciferase reporter expression was normalized to Renilla and the Luc/Ren ratio for each condition was then normalized to that of the wildtype full length (FL) reporter in hSyn-eGFP transduced cells (first black bar). The significance for each comparison to the FL reporter in wildtype cells are noted by asterisks directly above respective bars. Comparisons between other conditions are noted by horizontal bars. Wildtype, black; Rbfox1 cKO, red. Luciferase assays were performed at DIV14. n=6 cultures (biological replicates)

Figure 2-2 continued.

(E) Schematic of Vamp1 3'F luciferase reporters. Top, the full length Vamp1 3'UTR is shown with the indicated 3'F reporters. Vertical bars represent the Rbfox binding motif (U)GCAUG (yellow), 3'-most motif (blue) and 3'-most miR9 microRNA recognition element (magenta). In-set, sequence surrounding the 3'-most miR9 site and Rbfox motif in 3'F reporters. Bottom, mammalian conservation track for inset sequence from the UCSC Genome Browser.

(F) Quantification of 3'F luciferase reporter expression. Luciferase expression was normalized to Renilla expression, and the Luc/Ren ratio for each condition then was normalized to the wildtype 3'F reporter in hSyn-eGFP neurons (first black bar). Significance for these comparisons are noted by asterisks directly above respective bars. Comparisons between other conditions are noted by horizontal bars. Wildtype, black; Rbfox1 cKO, red. Luciferase assays were performed at DIV14. n=3 cultures

(G) Left, schematic of Tough Decoy microRNA inhibitors. Right, quantification of mature miR9 levels by Taqman assay in neurons infected with the TuD-miR9 or -control virus. miR9 levels were normalized to the total U6 RNA levels in each sample.

(H) Quantification of luciferase reporter expression with or without miR9 inhibition. Luciferase expression was normalized to Renilla, and the Luc/Ren ratio for each condition was normalized to the wildtype FL reporter in wildtype neurons (FL, first black bar). Comparisons be-tween other conditions are noted by horizontal bars. n=9 cultures

Luciferase assays were performed at DIV14. ANOVA with Bonferonni correction; * $p \leq 0.05$, ** $p \leq 0.01$; *** $p \leq 0.001$; error bars, s.e.m.

Rbfox motifs also contribute to this upregulation. We did not observe a significant change in expression of the FLm1-6 mutant upon loss of Rbfox1 (n.s. comparing WT and cKO). In contrast, there was a visible, though not statistically significant, decrease in FLm7 reporter expression with loss of Rbfox1. This difference in response to the loss of Rbfox1 by the mutant 3' UTRs may indicate differences in their responses to cytoplasmic Rbfox3 (Lee et al., 2016b). Overall, these results indicate that binding of Rbfox1 to the Vamp1 3'UTR strongly stimulates its expression and that the 3'-most Rbfox binding site plays a major role in this regulation.

Opposing regulation by Rbfox1 and microRNA-9

RNA-binding proteins can regulate translation and mRNA stability directly or by antagonizing microRNA binding in 3'UTRs. We noted that the 3'-most Rbfox binding site immediately abuts a microRNA response element (MRE) identified by the TargetScan (Friedman et al., 2009; Grimson et al., 2007; Lewis et al., 2005) program as a binding site for microRNA-9 (MiR-9 MRE, magenta; Figure 2-2E). MiR-9 plays an important role in early neuronal commitment and development (Coolen et al., 2013; Delaloy et al., 2010; Sun et al., 2013a; Yoo et al., 2011; Zhao et al., 2009) and continues to be highly expressed in mature neurons (Liu et al., 2012). The Vamp1 3'UTR sequence encompassing these two regulatory elements shows a high degree of mammalian conservation (Figure 2-2E), indicating a likely regulatory function. We hypothesized that Rbfox1 binding to the 3'-most GCAUG contributes to stabilization of the Vamp1 transcript by blocking miR-9 binding. To dissect the roles of this GCAUG and the adjacent miR-9 site, we created a luciferase reporter containing a small 3' fragment of the Vamp1 3'UTR that includes the last two Rbfox binding sites and the miR-9 site (3'F; Figure 2-2E).

Luciferase expression from this 3'F reporter was again dependent on Rbfox1, with a 40% reduction observed in the cKO neurons compared to wildtype (3'F, red bar; Figure 2-2F). Similar to the full-length 3'UTR, mutating the final GCAUG in this fragment dramatically de-creased reporter expression in wildtype and mutant neurons (3'Fm7, black bar; Figure 2-2F). Conversely, mutation of the miR-9 binding site increased expression in wildtype neurons (3'F vs 3'FmiR9m, black bars; Figure 2-2F) and significantly reduced the effect of Rbfox1 loss in the cKO neurons (3'F vs. 3'FmiR9m, red bars; Figure 2-2F). A compound mutation eliminating the miR-9 MRE and both GCAUG elements (3'Fm6-7miR9m; Figure 2-2F) increased reporter ex-pression relative to mutation of only the 3'-most Rbfox site, again indicating a repressive role of the miRNA and an enhancing effect of Rbfox1 (3'Fm7 vs 3'Fm6-7miR9m, black bars; Figure 2-2F). These results indicate that miR-9 is repressive of Vamp1 expression and that this repression is overcome by Rbfox1 binding. The enhancing effect of the upstream sites indicate that Rbfox binding can also stimulate expression on its own.

To test whether inhibition of miR-9 could affect expression through the Vamp1 3'UTR, we used AAV-mediated delivery of a U6-driven Tough Decoy (TuD) (Bak et al., 2013; Haraguchi et al., 2009; Xie et al., 2012), containing sequence complementary to the mature miR-9 or a control sequence encompassed within a stable hairpin (Figure 2-2G). Applying the Taqman assay 7 days post-infection of the TuD virus (DIV14), we observed ~50% reduction of mature miR-9 levels in neurons infected with the miR-9 inhibitor (TuD-miR9) compared to control (TuD-ctrl) (Figure 2-2G). Using this system, we tested the effect of miR-9 inhibition on the ex-pression of the full length (FL) 3'UTR reporter and the full length 3' UTR containing a mutation of the 3'-most Rbfox binding site

(FLm7). Suppressing miR-9 in the presence of Rbfox1 did not significantly change expression of the FL reporter, indicating that binding of Rbfox1 at the 3' end of the UTR efficiently blocks miR-9 activity (Figure 2-2H; FL, black vs orange bars). In the Rbfox1 knockout neurons with this luciferase reporter, inhibition of *miR-9* resulted in a visible, though not statistically significant, increase in expression compared to the control TuD (Figure 2-2H; FL, red vs blue bars). Notably, the results were different with the reporter lacking the Rbfox binding site adjacent to the *miR-9* element (FLm7). For this construct, inhibition of *miR-9* significantly increased expression of the reporter in the presence of Rbfox1, indicating that loss of the 3'most Rbfox binding site causes the reporter to become responsive to miR-9 (Figure 2-2H; FLm7, orange vs black bars). A similar increase in expression of FLm7 with *miR-9* inhibition was seen in the cKO neurons (Figure 2-2H; FLm7, blue bar), but this was not statistically significant. Overall, these results indicate that Rbfox1 binding to the upstream sites promotes expression independently of *miR-9*, while the 3'-most Rbfox site is blocking the effect of *miR-9*.

Discussion

Through binding within the 3' UTR's of mRNAs, cytoplasmic Rbfox1 can increase target mRNA levels by promoting mRNA stability, antagonizing microRNA action or directly stimulating translation (Carreira-Rosario et al., 2016; Lee et al., 2016b). We find that in the regulation of Vamp1, Rbfox1 appears to both antagonize microRNA action and directly increase expression. In binding to the final GCAUG element in the 3'UTR, Rbfox1 counteracts inhibition of Vamp1 expression by *miR-9*. However, upstream Rbfox binding elements whose relationship to miRNA binding sites is less apparent also promote expression, possibly through increasing mRNA stability or enhancing translational

efficiency. It will be interesting to dissect these two activities of Rbfox1. *MicroRNA-9* has largely been studied in the context of progenitor cell commitment to the neuronal lineage (Coolen et al., 2013; Delaloy et al., 2010; Sun et al., 2013a; Yoo et al., 2011; Zhao et al., 2009). However, *miR-9* continues to be expressed in the adult brain (Liu et al., 2012), and recent work indicates that it plays important roles in mature neuronal function including dendritic arborization, and learning and memory (Dajas-Bailador et al., 2012; Giusti et al., 2014; Malmevik et al., 2016; Shi et al., 2013; Sim et al., 2016; Xue et al., 2016). Although both are broadly expressed across multiple neuronal cell types and brain regions, our work defines roles for Rbfox1 and miR-9 in modulating the expression of Vamp1 specifically in inhibitory neurons. It will be interesting to further characterize the overlap in the Rbfox1 and *miR-9* regulatory networks and to understand the role of these opposing regulators in the function of other neuronal cell types and circuits.

Chapter 3: RBFOX1 REGULATION OF INHIBITORY SYNAPTIC TRANSMISSION

Introduction

The high degree of conservation between the Rbfox proteins, their identical RRMs and their broadly overlapping expression in neurons would suggest that their functions are largely redundant. However, pan-neuronal loss of Rbfox1 or Rbfox2 in conditional mutant mice revealed very different phenotypes that could be traced to different neuronal populations affected by loss of each RBP. While loss of Rbfox2 caused marked alterations in Purkinje cell development and function (Gehman et al., 2012), loss of Rbfox1 led to increased seizure susceptibility but did not dramatically affect the function of cerebellar neuronal populations (Gehman et al., 2011). These results reveal that while an RBP affects mRNA regulation in many neuronal populations, specific cell types can be more susceptible to the loss of a particular regulator than others. One particular neuronal population whose function is differentially affected by Rbfox1 loss are inhibitory neurons. To better understand the impact of Rbfox1 loss on inhibitory neuron function, a brief overview of their roles in cortical and hippocampal circuits, and the molecular and cellular specializations underlying interneuron function are presented below.

Though inhibitory neurons make up only between 10-20% of the total neurons in the mammalian brain, the sheer variety of inhibitory subtypes is indicative of the important role inhibition plays in brain function. The diversity of interneuron types has made their classification less than straightforward (Tremblay et al., 2016). Unlike excitatory principal cells, interneurons are not usually organized into easily definable lamina or nuclei, though a closer examination using multiple criteria reveals the logic of their positioning within various brain structures. As such, classification of inhibitory subtypes uses molecular markers (such as Parvalbumin, Somatostatin, VIP or Reelin) in combination with dendritic

and axonal morphology, and electrophysiological properties such as spiking or action potential firing patterns, intrinsic excitability and synaptic plasticity among others (Tremblay et al., 2016; Wamsley and Fishell, 2017). Classification reveals that inhibitory neurons are finely tuned to sculpting the flow of information through circuits. For example, different subtypes target different anatomical compartments of principal cells to exert control over specific portions of action potential generation. Parvalbumin-positive (PV+) basket cells synapse onto the soma of principal neurons, while PV+ chandelier cells specifically target the axon initial segment, both providing powerful inhibition of spike (action potential) output by synapsing near or at the site of action potential generation. Other subtypes such as the Somatostatin-positive (SST+) interneurons target the dendrites and can regulate the excitatory input coming from specific sources as well as the threshold of spike generation. Some inhibitory subtypes such as PV cells target both excitatory and other inhibitory neurons. VIP+ interneurons while others only target excitatory neurons (Figure 3-1). In the cortex, the axonal arbors of some inhibitory subtypes span several vertical layers, while that of others spread laterally, indicating different functions (Tremblay et al., 2016; Wamsley and Fishell, 2017).

Parvalbumin expressing (PV) interneurons make up ~40% of inhibitory neurons and comprise the largest portion of the inhibitory population (Tremblay et al., 2016). Fast spiking PV interneurons are designed for speed and precision in seemingly every aspect of their function. Extensive work characterizing PV neurons has elicited multiple mechanisms driving the speed and precision of PV+, fast spiking (PV FS) basket cells. On the post-synaptic end, PV FS cells express fast Ca^{2+} permeable AMPA receptors that contain the GluR1 flip subunit and lack GluR2 subunits. The low input resistance of PV

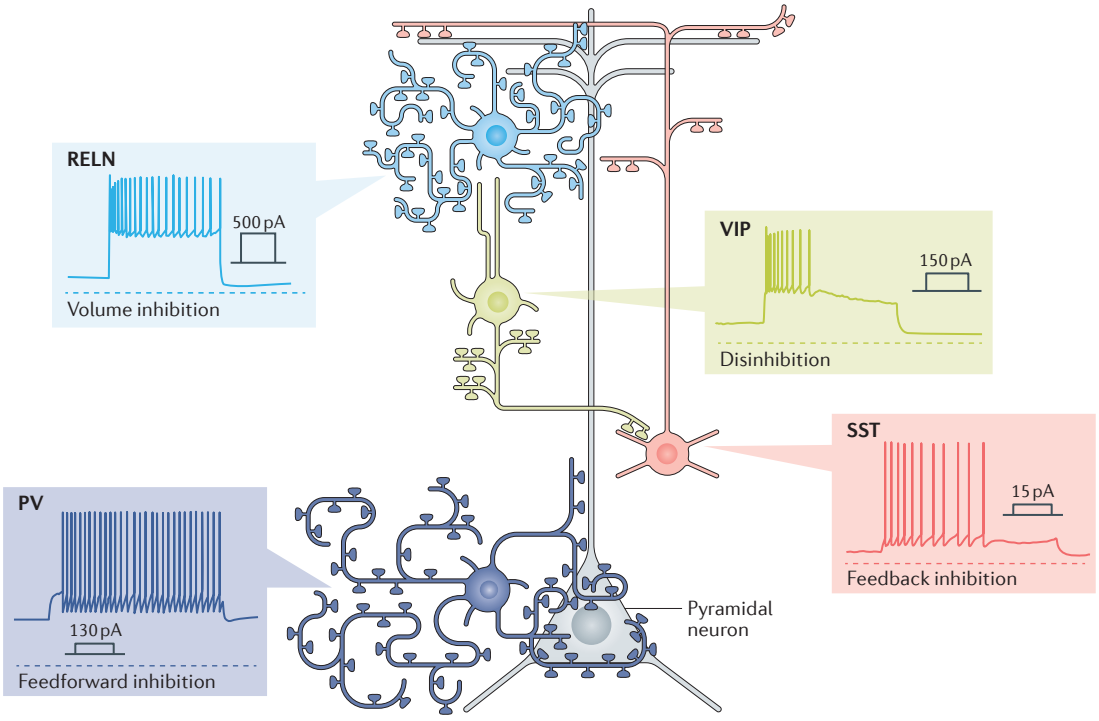

Figure 3-1: Connectivity of the four main classes of cortical interneurons.

The four main classes of cortical interneurons have distinct synaptic targeting biases onto neighbouring excitatory pyramidal neurons and engage in common circuit motifs. Parvalbumin (PV)-expressing basket cells are fast spiking and target the somatic compartment, engaging in feedforward inhibition from the thalamus onto the pyramidal cell. Somatostatin (SST)-expressing Martinotti cells can be burst spiking, target the distal dendrites and engage in feedback inhibition. Reelin (RELN)-expressing (RELN+SST–) cells are late spiking and either directly or by proximity target the distal dendrites. Vasoactive intestinal peptide (VIP)-expressing neurons can be irregular spiking, target the dendrites of SST+ cells and thus participate in disinhibition.
Used with permission from (Wamsley and Fishell, 2017).

FS dendrites and expression of high activation, fast activating/deactivating voltage-gated K_v3 channels function in combination to shorten the time period of excitatory input (EPSPs), allowing these cells both to sample multiple principal cell inputs without as well as acting as accurate coincidence detectors. Generation of action potentials in PV FS cells is fast and reliable due to a high density of Na^+ channels clustered at the axon initial segment. Finally, at the PV FS output synapse, exclusive expression of fast P/Q-type Ca^{2+} channels and Synaptotagmin2, which has the fastest Ca^{2+} binding kinetics of the Synaptotagmin family, increases the efficiency of coupling between Ca^{2+} influx and neurotransmitter release (Hu et al., 2014). Thus, fast spiking PV neurons have developed multiple specializations to be fast and accurate in both detection and in output.

Neuronal excitability, while regulated in part by intrinsic mechanisms such as the expression of specific ion channels, is also a consequence of circuit layout and composition. The coordinated activity of excitatory and inhibitory neurons directs the flow and determines the processing of information through any given circuit. Thus, inhibitory neurons play important roles in cognition, sensory processing, and learning and memory. This coordination of signaling between inhibitory and excitatory neurons can also be thought of as a balance of excitation and inhibition (E/I balance) which shapes the input into the circuit and its response to stimuli (Isaacson and Scanziani, 2011). Indeed, the timing of excitation and inhibition within a circuit can be crucial for proper processing of sensory stimuli in the cortex. For example, in sensory processing, thalamic input into the cortex activates both the excitatory principal cells and the local inhibitory neurons in a feedforward inhibitory circuit (Figure 3-2B). As a result of this circuit layout, the inhibitory input to the principal cell lags behind the excitatory input by one synapse, providing a

window of integration wherein strong or synchronous input could elicit a response in the excitatory principal cell before it is shut down by the inhibitory response. This feedforward circuit motif is used many times over in the cortex to represent the timing of sensory input as well as to distinguish between different types of stimuli, such as velocity or direction. Feedforward inhibition also coordinately recruits inhibitory neurons in proportion to excitatory cells as a mechanism to modulate gain, allowing for a wide range of inputs, where the circuit can be made sensitive to weak stimuli as well as responsive to strong stimuli without becoming saturated (Hu et al., 2014; Isaacson and Scanziani, 2011; Tremblay et al., 2016).

E/I balance can, on the other hand, be thought of as a mechanism to prevent runaway excitation. This can be observed in feedback inhibitory circuits, where the target principal (excitatory) cell of a local interneuron (inhibitory) also synapses back onto the inhibitory neuron (Figure 3-2A). Thus, excitation of the principal cell is accompanied by a commensurate amount of inhibition (Xue et al., 2014). In lateral feedback inhibition, inhibitory neurons can also target excitatory cells surrounding the principal cell providing the stimulus, limiting the number of excitatory cells recruited by a stimulus. This serves both to prevent uncontrolled, hyper-synchronous recruitment of excitation and to promote specificity of response to the stimulus at the level of neuronal populations. Thus, in feedforward circuits E/I balance works to gate the timing and the signal to noise ratio of incoming information, while in feedback circuits inhibition functions to select the responsive principal cell population.

E/I imbalance has been implicated in neuropsychiatric diseases including schizophrenia (Lewis et al., 2012; Uhlhaas and Singer, 2010), epilepsy and autism

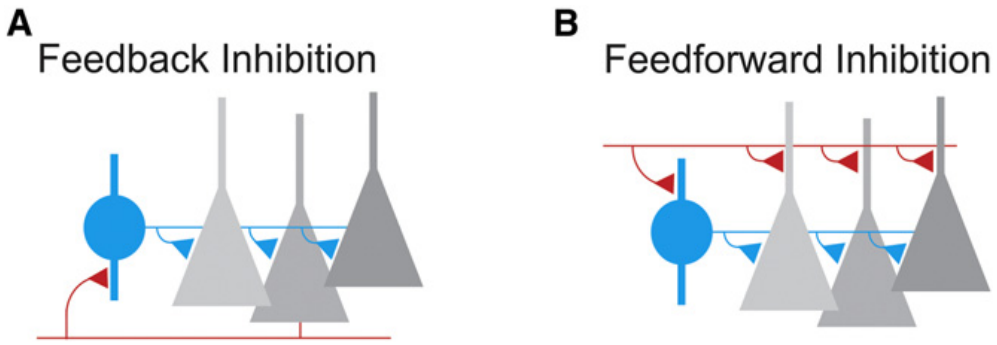

Figure 3-2: Feedback and feedforward circuits are fundamental building blocks of cortical inhibition.

(A) Feedback inhibition arises when cortical principal cells (gray) make excit- atory synaptic contacts (red) on local interneurons (blue) that in turn form inhibitory synaptic contacts (blue triangles) on the principal cell population**. (B)** Feedforward inhibition is generated when long-range excitatory afferent inputs (red) diverge onto both principal cells and local interneurons.

Used with permission from (Isaacson and Scanziani, 2011).

spectrum disorders (ASD) (Hunt et al., 2017; Marín, 2012). Abnormal inhibitory function is postulated to cause cognitive deficits in schizophrenia, in particular by disrupting working memory (Barr et al., 2010; Haenschel et al., 2009; Radhu et al., 2015). In mouse models, reducing excitatory drive to PV neurons by blocking the excitatory NMDA receptors or by genetic deletion of the NR1 subunit critical for constitution of NMDA receptors leads to asynchronous activity, schizophrenia-like symptoms (Belforte et al., 2010) and working memory deficits (Carlén et al., 2012; Korotkova et al., 2010). Though the genetic causes leading to epilepsy are diverse, E/I imbalance due to inhibitory dysfunction is a common thread in the various mechanistic changes leading to seizure. Indeed, mouse models of mutations affecting the generation and development of interneuron types as well as those altering mature inhibitory function commonly result in seizure phenotypes (Jiang et al., 2016).

Inhibitory neuron dysfunction and E/I imbalance are also shared features in multiple ASDs including Rhett and Asperger's syndromes (Tremblay et al., 2016). Mouse mutants of genes associated with these syndromes, such as Shank3, Mecp2 and Cntnap2, display reduced inhibitory neurotransmitter levels (Chao et al., 2010) and altered inhibitory synaptic connectivity (Peça et al., 2011; Peñagarikano et al., 2011). Dysfunction or mutation of Rbfox1 has also been implicated in epilepsy and ASD, though the underlying molecular mechanism of how Rbfox1 loss could contribute to ASD has not been explored. The neuronal hyperexcitability phenotype and seizure susceptibility of the Rbfox1 Nes-cKO indicate that E/I imbalance or inhibitory neuron dysfunction perhaps play a role. In addition, recent work found that transcripts stabilized by cytoplasmic Rbfox1, including Vamp1, significantly overlap with those affected in ASD. However, whether

Vamp1 plays a role in inhibitory function and can affect the Rbfox1 cKO phenotype remains unexplored.

Results

Vamp1 is specifically expressed in inhibitory neurons

Vamp1 (*Synaptobrevin1/Syb1*) is a paralog of the well-studied vSNARE *Vamp2* (*Synaptobrevin2/Syb2*), which is found in both excitatory and inhibitory neurons and is critical for synaptic vesicle docking and neurotransmitter release (Deák et al., 2006; Schoch et al., 2001). Although much less characterized, Vamp1 is highly homologous to Vamp2 in protein sequence and domain structure (Figure 3-3A), and several studies have demonstrated that Vamp1 functions similarly to Vamp2 in regulating synaptic vesicle release. Vamp1 loss in motor neurons leads to decreased probability of neurotransmitter release at the neuromuscu-lar junction (Liu et al., 2011). Other work found that re-expression of Vamp1 in primary neurons lacking Vamp2 could restore synaptic transmission (Zimmermann et al., 2014). We observed that both proteins are expressed in the adult mouse brain, although the onset of Vamp1 expression occurs quite late during development (P15; Figure 3-3B), well after the induction of Vamp2 (E18; Figure 3-3B). In primary hippocampal neurons, anti-Vamp1 antibodies yielded the punctate staining pattern expected from a pre-synaptic protein. Virtually all Vamp1+ puncta also contained Vamp2, though only a subset of Vamp2 puncta were also positive for Vamp1 (~20% Vamp2+ puncta are also Vamp1+; Figure 3-3C). The late induction of Vamp1 expression in vivo at P15, and its restricted expression in immunocytochemistry of cultured neurons

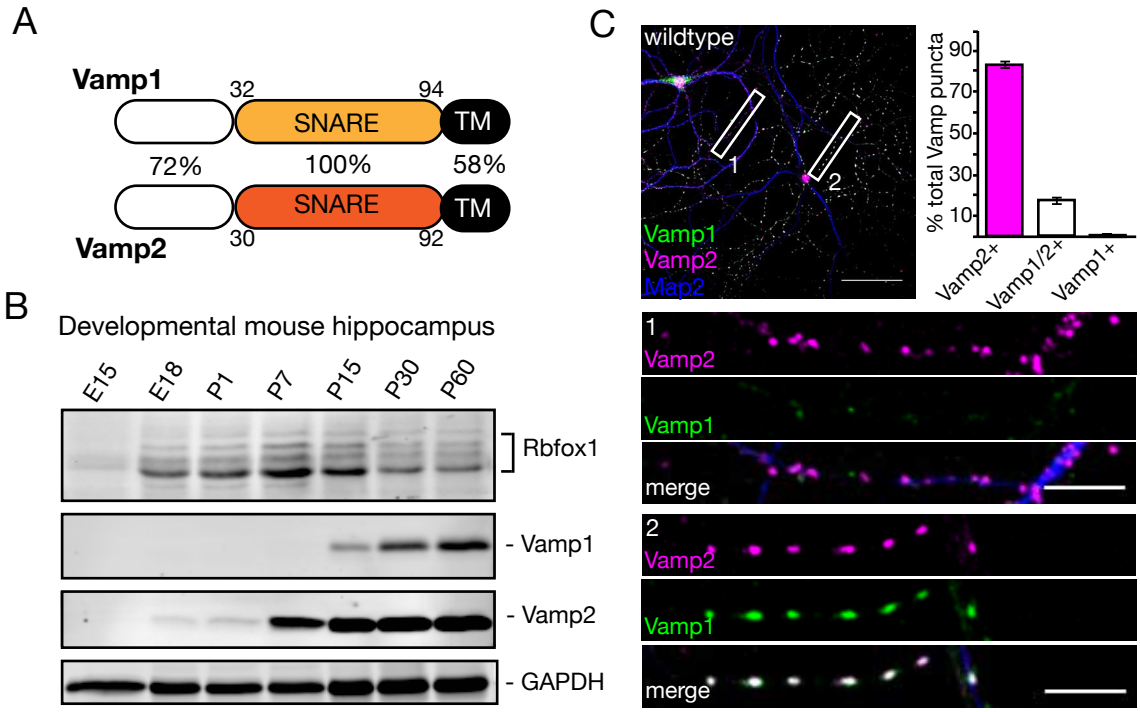

Figure 3-3: Overlapping and distinct expression patterns of Vamp1 and Vamp2.

(A) Schematic of VAMP1 and VAMP2 protein domains. Percentages indicate level of amino acid sequence identity of VAMP1 compared to VAMP2. Numbers indicate amino acid position. SNARE, Soluble NSF Attachment Protein Receptor domain; TM, transmembrane domain.

(B) Vamp1 expression is induced late during brain development compared to Vamp2. Immunoblot of Rbfox1, Vamp1, Vamp2 and GAPDH in mouse hippocampus from E15 to P60.

(C) Left and bottom, immunofluorescence of Vamp1 (green) and Vamp2 (magenta) in wildtype DIV18 primary hippocampal neurons. MAP2, marking dendrites, in blue. Right, quantification of puncta overlap. Right, quantification of Vamp1+ and Vamp2+ puncta over-lap. n=3 cultures; puncta were counted in 50um2 areas, at least 3 areas per image,

Figure 3-3 continued.

in 9 images per replicate; error bars are s.e.m.; panel scalebar, 50um; inset scalebar, 10um; 63x magnification.

See also **Figure S3-1.**

suggested that Vamp1 might be specifically expressed in a particular neuronal cell type. Indeed, Vamp1 has been reported to be preferentially expressed at inhibitory synapses (Ferecskó et al., 2015).

To determine whether Vamp1 was expressed in all neurons or only in certain neuronal subtypes, we first performed double-label immunocytochemistry of Vamp1 and general markers of excitatory and inhibitory neurons in primary hippocampal cultures. Using Gad67 as a marker for inhibitory neurons, we counted all puncta that were Vamp1+, Gad67+ or Vamp1+/Gad67+ to obtain the total number of puncta. We found that over 80% of the total puncta counted were Vamp1+/Gad67+. In a parallel analysis, Vamp1 had virtually no overlap with the excitatory markers Vglut1 and Vglut2 (Figure 3-4 A,B). Of the total puncta counted containing one or both markers, 30% were Vamp1+ only, 70% were Vglut1/2+ and Vamp1-, while none were double positive. We observed a similar co-localization of Vamp1 with inhibitory markers in sections of adult mouse hippocampi. Vamp1 puncta were enriched perisomatically in the CA1 and CA3 pyramidal layers, and in the dentate granule (DG) layer. Vamp1+ puncta were also detected more sparsely in stratum oriens and radiatum of CA1 and CA3, as well as the molecular layer and hilus of the DG (Figure 3-4 C-F, Figure S4 B-E, and data not shown). Determining the total of Vamp1+, Gad67+ and Vamp1+/Gad67+ puncta, over 85% of puncta within the CA1 pyramidal layer were Vamp1+/Gad67+ (s.p., Figure 3-4 C,D). Notably, this co-localization was significantly reduced in the *Rbfox1 Nes-cKO*, where only ~50% of puncta were Gad67+/ Vamp1-. Vamp1 similarly co-localized with Gad67 in strata oriens and radiatum (s.o. and s.r., ~80% co-localization), with a similar reduction in the *Rbfox1 Nes-cKO* (~30% co-localization) (Figure 3-4D). Rbfox1 loss lead to a significant reduction in the

number of detectable Vamp1+ puncta in all hippocampal regions assayed (Figure S3-2A). The reduced Vamp1 levels observed by immunoblot indicated that the loss of Vamp1 co-localization with Gad67 in the cKO hippocampus is due to a loss of Vamp1+ puncta rather than to mis-localization of the protein. The high level of co-localization between Vamp1+ and Gad67+ puncta confirmed our initial immunocytochemical observation that Vamp1 is expressed specifically in GABAergic inhibitory neurons. Vamp1 co-localization with Gad67 is also consistent with the perisomatic enrichment of Vamp1+ puncta in the pyramidal layers, an innervation pattern typical of Parvalbumin-expressing (Pv+) basket cells (Tremblay et al., 2016). Although Rbfox1 is broadly expressed across the brain (Gehman et al., 2011; Underwood et al., 2005), its expression in the Vamp1+ inhibitory neurons has not been described. We found that in addition to expression in excitatory neurons, Rbfox1 is also present in the Pv+ neurons that constitute the major inhibitory subtype in the hippocampus (Figure S3-1A-D). Rbfox1+, Pv- cells can also be found in strata radiatum, oriens and lacunosum moleculare, where SST+ and VIP+ inhibitory neurons are typically found (Figure S3-1D, arrows). Thus, Rbfox1 might directly regulate Vamp1 in these inhibitory neuronal populations.

Parvalbumin-positive (Pv+) interneurons make up the majority of inhibitory neurons in the mouse hippocampus (Tremblay et al., 2016). We found that Vamp1 co-localized with both Parvalbumin (data not shown) and Synaptotagmin2 (Syt2), a marker of Pv+ interneuron pre-synaptic terminals (Sommeijer and Levelt, 2012) (Figure 3-4E,F). Comparable to our results with Vamp1 and Gad67, we observed a high degree of Vamp1 and Syt2 co-localization in the CA1 pyramidal layer (over 85% of the total puncta in Vamp1, Syt2 co-stained sections were double positive), stratum oriens and stratum

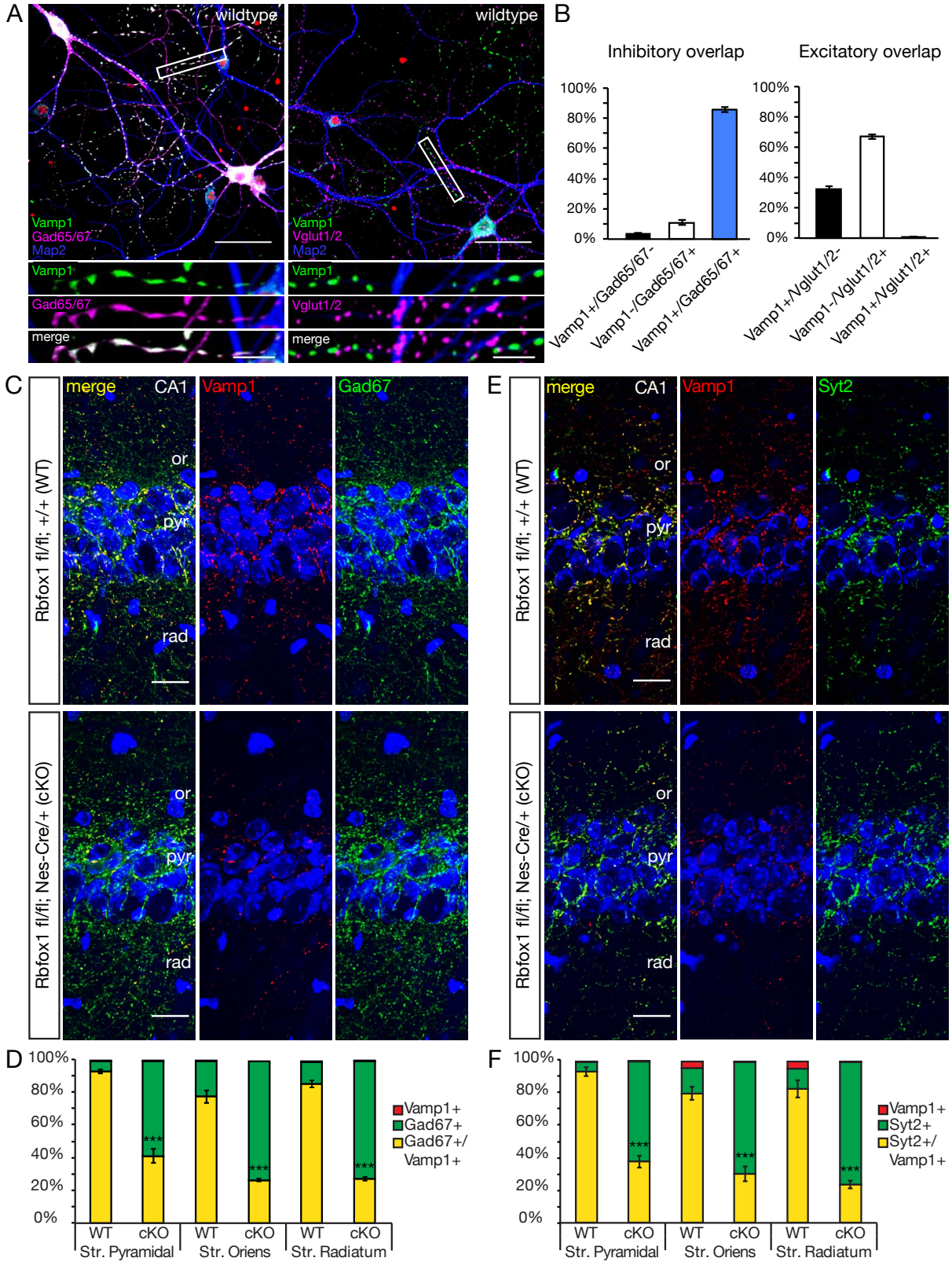

Figure 3-4: Vamp1 is enriched in Parvalbumin+ hippocampal interneurons.

Figure 3-4 continued.

(A-B) Vamp1 co-localizes with inhibitory markers but has no overlap with excitatory markers. **(A)** Immunocytochemistry of Vamp1 (green) and inhibitory pre-synaptic makers Gad65/67 (magenta, left panels) or excitatory pre-synaptic markers Vglut1 and Vglut2 (magenta, right panels) in wildtype DIV18 primary hippocampal neurons. Panel scalebar, 50um; inset scale-bar, 10um; 63x magnification. **(B)** Quantification of Vamp1 overlap with inhibitory and excitatory markers. Puncta were quantified from one 100um^2 field per image; n=15 images from 1 culture; error bars, s.e.m.

(C-D) Vamp1 co-localizes with Gad67 in the adult mouse hippocampus.

(C) Immunohistochemistry of Vamp1 (red) and Gad67 (green) in P60-P70 CA1 of wildtype and Rbfox1 Nes-cKO hippocampus. **(D)** Quantification of Vamp1+ and Gad67+ puncta in CA1. Co-localized or lone puncta are shown as a percent of all the Vamp1+ and Gad67+ puncta counted in each indicated area. Puncta were quantified from at least (3) 50um^2 fields/image, from 3 images per biological replicate.

(E-F) Vamp1 is enriched in Parvalbumin+ interneuron pre-synaptic terminals.

(E) Immunohistochemistry of Vamp1 (red) and Synaptotagmin2 (Syt2, green) in P60-P70 CA1 of wildtype and Rbfox1 Nes-cKO hippocampal sections. **(F)** Quantification of Vamp1+ and Syt2+ puncta in CA1. Co-localized or lone puncta are shown as a percent of all the Vamp1+ and Syt2+ puncta counted in each indicated area. Note that in contrast to the Gad67 IHC, in stratum oriens and radiatum a small portion (~4%) of puncta are Vamp1+/Syt2-. Puncta were quantified from at least (3) 50um^2 fields/image, from 3 images per biological replicate.

Figure 3-4 continued.

For C-F, n=3 littermate pairs; ANOVA with Bonferonni correction; *** $p \leq 0.001$; error bars, s.e.m. scalebar, 20um; 40x magnification. Labels: or, stratum oriens; pyr, stratum pyramidale; rad, stratum radiatum.

See also **Figure S3-2.**

radiatum (s.o. and s.r., ~80% co-localization; Figure 3-4F). The Rbfox1 Nes-cKO hippocampus again showed a significant loss of Vamp1 immunoreactivity in Syt2+ puncta (~40%, s.p. and ~30%, s.o. and s.r.; Figure 3-4F). The loss of Vamp1+/Syt2+ puncta was again due to a reduction in the number of Vamp1+ puncta rather than a change in Vamp1 localization (Figure S3-2A). The high level of Vamp1 co-localization with Syt2 in the wildtype hippocampus is consistent with the enrichment of Vamp1 in Pv+ pre-synaptic terminals, which predominantly form synapses onto the soma of principal cells (Tremblay et al., 2016). The presence of Vamp1+ puncta in stratum radiatum and oriens, where VIP+ and SST+ interneurons are known to synapse indicates that Vamp1 is likely also expressed in these cells. This is also consistent with the small number of Vamp1+/ Syt2- puncta observed in strata oriens and radiatum of CA1, and in the DG hilus. Additional co-localization of Vamp1 with Syt2 in the hippocampus, cortex, and thalamus is presented in Figures S3-2 B-M).

One potential explanation for the reduction in Vamp1+ puncta is a loss of inhibitory pre-synaptic sites. To address this possibility, we quantified the number of total Syt2+ puncta per square micron in adult hippocampal sections to obtain an average Syt2 density. We found no significant difference in Syt2 puncta density in the pyramidal layer, the stratum oriens or the stratum radiatum of CA1 between wildtype and Rbfox1 Nes-cKO hippocampi (Figure S3-3A), suggesting that the number of PV pre-synaptic sites was not changed. This result indicated that the loss of Vamp1+ puncta was due to a loss of Vamp1 expression rather than that of inhibitory pre-synaptic sites (Figure 3-3E). We also assessed whether the excitatory or inhibitory synapse density was altered with loss of Rbfox1. We cultured primary hippocampal neurons from Rbfox1 Nes-cKO and wildtype

embryos and performed immunocytochemistry for markers of excitatory and inhibitory synapses at DIV18, after synapse formation has been established. Using co-localization of the respective pre- and post-synaptic excitatory markers Synaptophysin and PSD-95, we found no significant difference in excitatory synapse density between Rbfox1 Nes-cKO and wildtype (Figure S3-3B). Similarly, using co-localization of pre-synaptic Gad65/67 and post-synaptic Gephyrin, we observed that inhibitory synapse density was also unchanged between the two genotypes (Figure S3-3C). Overall, our immunohistochemical results demonstrate that Vamp1 is expressed specifically in GABAergic inhibitory neurons, including at Pv+ pre-synaptic terminals in the hippocampus and likely also SST+ and VIP+ neurons. In the Rbfox1 Nes-cKO hippocampus, we observed significant reduction in the number of Vamp1+ puncta at Pv+ pre-synaptic terminals, but found no significant changes in total excitatory or inhibitory synapse density between wildtype and cKO hippocampal primary neurons. Thus, the decreased Vamp1 expression in the Rbfox1 Nes-cKO mice is expected to impair inhibitory synaptic transmission and in turn contribute to the hy-perexcitation phenotype.

The Rbfox1 Nes-cKO hippocampus exhibits altered synaptic transmission

To examine whether inhibitory synaptic transmission is affected in the Rbfox1 Nes-cKO brain, we recorded miniature inhibitory (mIPSCs) and excitatory (mEPSCs) post-synaptic currents from CA1 and the DG in acute hippocampal slices from adult (P60-70) Rbfox1 Nes-cKO and wildtype littermates. The average mIPSC and mEPSC peak amplitudes were not significantly different between the two genotypes (Figure 3-5 B,E and 3-3 H,K). There was an increase in the variability of mEPSC amplitudes in the cKO CA1 compared to WT (Figure 3-5A traces), but this difference did not reach statistical

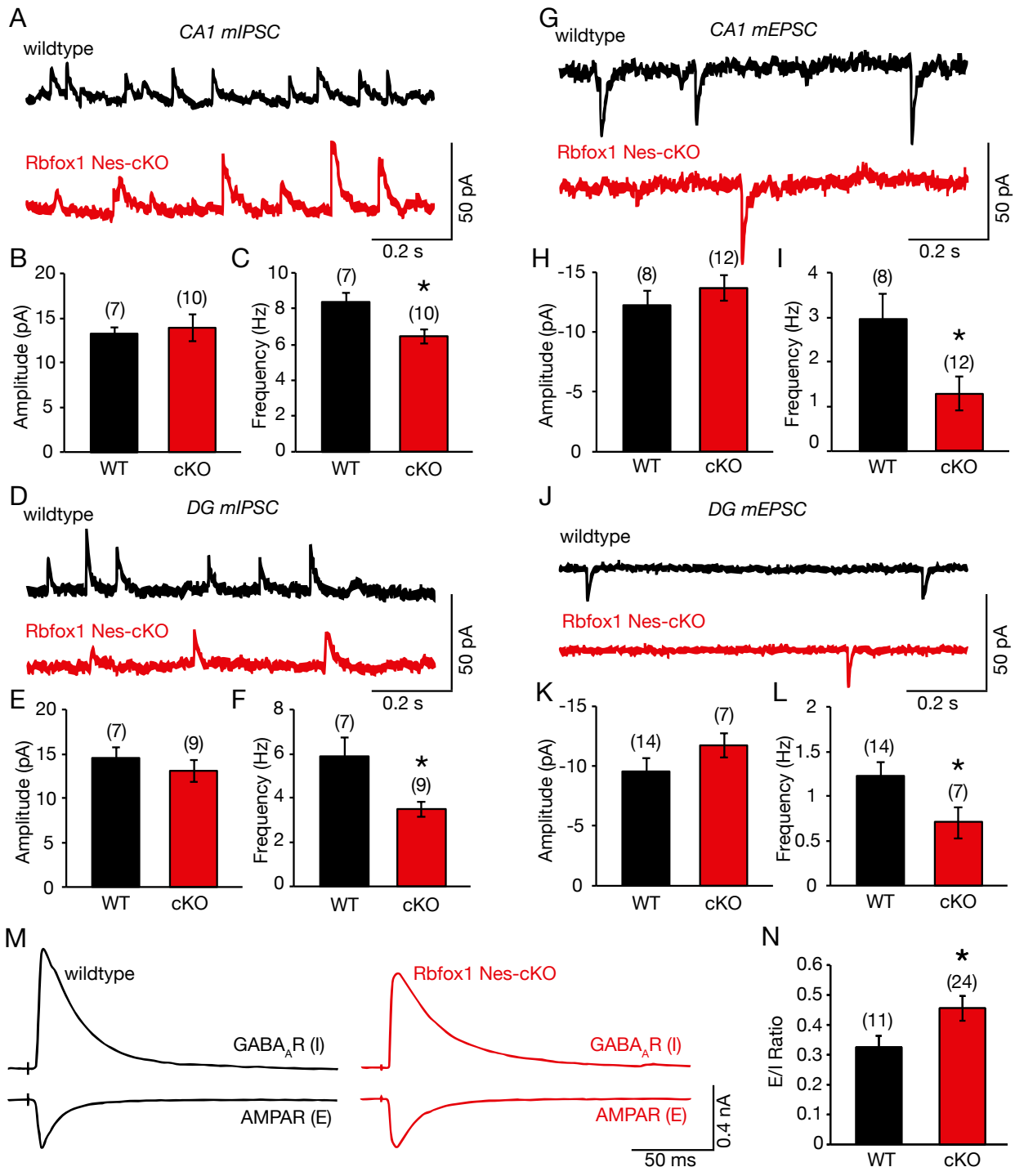

Figure 3-5: Inhibitory synaptic transmission is reduced in the Rbfox1 Nes-cKO.

Figure 3-5 continued.

(A-F) Decreased mIPSC frequency in the Rbfox1 Nes-cKO hippocampus. Pan-neuronal loss of Rbfox1 leads to significantly reduced average mIPSC frequency (C,F), while average mIPSC amplitude is unaffected (B,E), in CA1 and the dentate gyrus (DG).

(G-L) Average mEPSC frequency is also reduced in the cKO CA1 (I) and DG (L); average mEPSC amplitude is not significantly affected (H,K).

Sample traces are shown above quantifications.

(M-N) The E/I ratio is skewed towards increased excitation in the Rbfox1 Nes-cKO. Representative traces of the inhibitory GABAAR current (top trace) and excitatory AMPAR current (bottom trace) in wildtype (black) and cKO (red) are shown in (M) with quantification in (N). The E/I ratio was measured as the ratio of the peak amplitude of each component. (N) Quantification of the E/I ratio shows that it is significantly increased in the cKO compared to wildtype. E/I currents were measured in CA1.

Number of cells recorded per condition across 3 littermate pairs is shown above bars. Wildtype, black; cKO, red. Student's t-test; * $p \leq 0.05$; error bars, s.e.m.

See also **Figure S3-3**.

significance. Interestingly, we found that the frequency of both mIPSC and mEPSC was significantly reduced in both CA1 and the DG (Figure 3-5 C,F and 3-3 I,L). The reduced mIPSC frequency is in concordance with a change in inhibitory synaptic transmission resulting from loss of Vamp1. The decrease in excitatory synaptic transmission is likely due in part to dysregulation of other Rbfox1 targets in excitatory cells (Gehman et al., 2011; Lee et al., 2016b). However, the reduction in mESPC frequency may also result from a compensatory, homeostatic response to the depletion in Vamp1 (see below). The observed reduction in mIPSC frequency coupled with our finding that inhibitory synaptic density is unaffected in the cKO (Figure S3-3) are consistent with Vamp1 being an inhibitory-specific pre-synaptic protein with known roles in regulating release probability.

We next examined how the reduced frequency of both mIPSCs and mEPSCs might account for the neuronal hyperexcitability and seizure phenotype previously observed in the Rbfox1 Nes-cKO brain. To assess the excitation/inhibition (E/I) ratio of synaptic responses elicted by Schaffer collateral stimulation, we recorded synaptic currents in CA1 pyramidal cells voltage-clamped at -68mV and +10mV to isolate the respective excitatory AMPAR-mediated and the inhibitory $GABA_AR$-mediated currents. We recorded the evoked responses and compared the peak amplitudes of each component to obtain an E/I ratio (Figure 3-5M). We found that while both mIPSC and mEPSC frequency are reduced in the Rbfox1 Nes-cKO hippocampus, the E/I ratio of cKO neurons is increased relative to the wildtype (Figure 3-5N). Together, the results indicate that changes in synaptic transmission, rather than differences in excitatory or inhibitory synapse number, result in skewing of the E/I ratio towards increased excitation in the Rbfox1 Nes-cKO hippocampus, possibly due to the loss of Vamp1 in inhibitory cells.

Vamp1 knockdown reduces inhibitory synaptic transmission

The selective expression of Vamp1 at inhibitory pre-synaptic terminals suggests that its loss contributes to the altered inhibitory synaptic transmission seen in the Rbfox1 Nes-cKO hippocampus. To assay functional changes resulting from the depletion of Vamp1 specifically, we used shRNA to knock down Vamp1 in primary hippocampal neurons. Wildtype primary neurons were infected at DIV8 with AAV2/9 expressing CMV-driven GFP and a U6-driven shRNA against Vamp1 or, as a control, against Luciferase (Figure 3-6A). We confirmed the knockdown efficiency by immunoblot (Figure 3-6B and Figure S3-4B). At DIV15-17, when Vamp1 expression normally peaks in cultured neurons (data not shown), we measured the amplitude and frequency of mIPSCs and mEPSCs in Vamp1 shRNA-treated and control cells. Compared to the control (shLuc), the Vamp1 knockdown neurons exhibited decreased mIPSC frequency (~50% decrease in shVamp1 compared to shLuc; Figure 3-6E) but no changes in mIPSC amplitude (Figure 3-6D). Importantly, this change in mIPSC frequency was fully restored in the Vamp1 knockdown by coinfection of a virus expressing an shRNA-resistant Vamp1 driven by the inhibitory neuron specific mDlx enhancer (Dimidschstein et al., 2016) (shVamp1 +mDlx-Vamp1r; Figure 3-6E). This re-expressed Vamp1 localized to axons in discrete puncta, similar to the pattern we observed in wildtype neurons, although the strong expression driven by the mDlx enhancer also led to Vamp1+ puncta in the dendrites (Figure S3-4G). These results con-firmed the specificity of our Vamp1 shRNA and indicated that the loss of Vamp1 leads to reduced mIPSC frequency in concordance with its role in inhibitory synaptic transmission. There was no significant change in mEPSC amplitude with Vamp1 knockdown (Figure 3-6G). Interestingly, we also observed a reduction in mEPSC

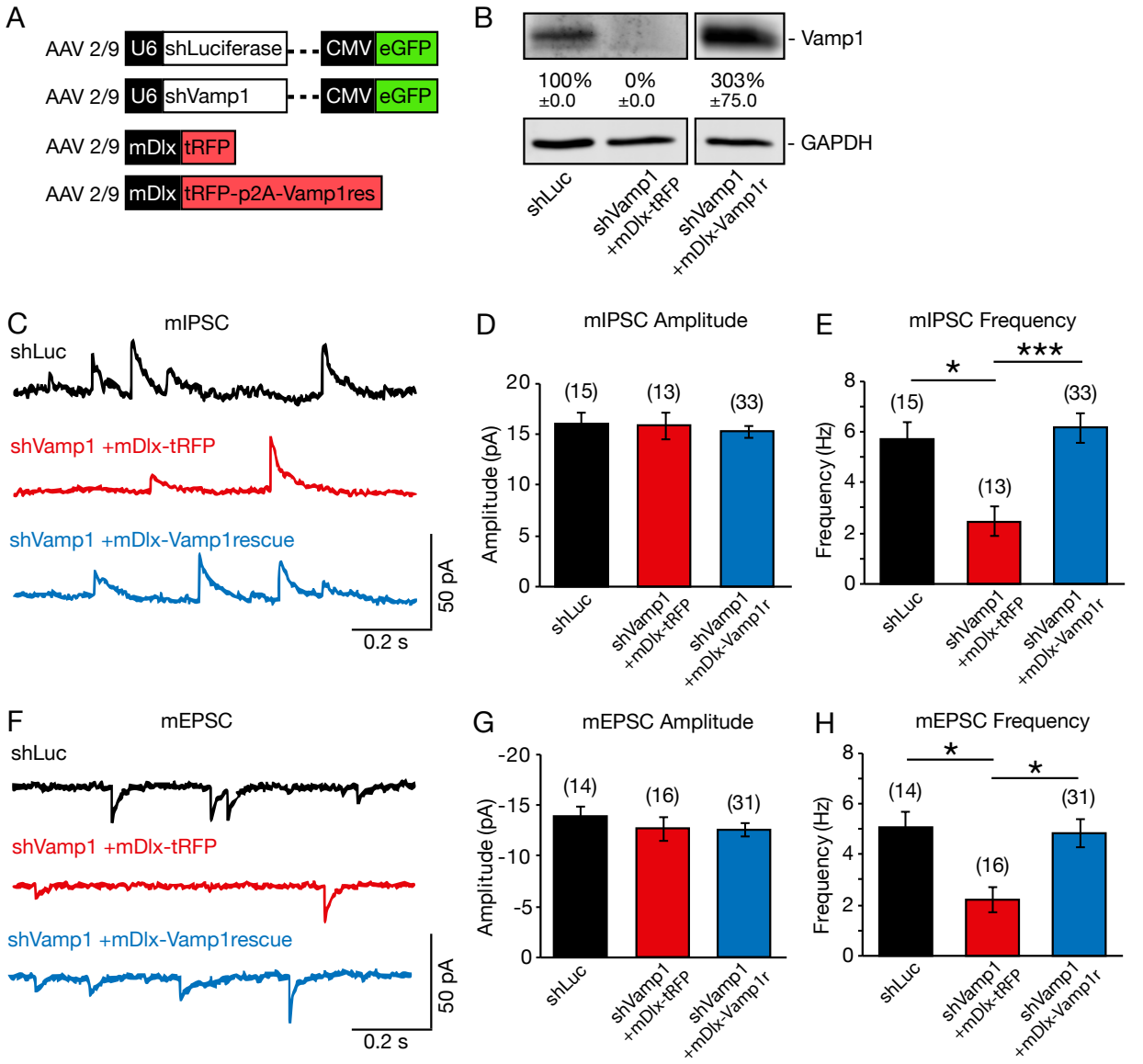

Figure 3-6: Vamp1 knockdown reduces inhibitory synaptic transmission.

(A) Schematic of AAVs used for Vamp1 knockdown.

(B) AAV-mediated Vamp1 knockdown in DIV16 primary hippocampal neurons. Left, immunoblot of Vamp1, Vamp2 and GAPDH neurons transduced with AAV2/9 expressing shRNA against Luciferase (shLuc), Vamp1 (shVamp1) + tRFP control (mDlx-tRFP) or Vamp1 (shVamp1) + Vamp1 rescue (mDlx-Vamp1r). Quantification of average Vamp1

Figure 3-6 continued.

expression normalized to GAPDH shown as a percentage of the control (shLuc) with standard error of the mean below. n=3 cultures (biological replicates)

(C-H) Vamp1 knockdown leads to reduced mIPSC and mEPSC frequency. Representative traces of mIPSCs (C) and mEPSCs (F) in control (shLuc, black), Vamp1 knockdown (shVamp1+mDlx-tRFP, red) and rescue (shVamp1+mDlx-Vamp2rescue, blue) treated primary neurons. Quantification of average mIPSC and mEPSC amplitude (D,G) and frequency (E,H) shown at right.

Number of cells recorded per condition across 3 cultures (biological replicates) is shown above bars. One-way ANOVA with Bonferroni correction; * $p \leq 0.05$, *** $p \leq 0.001$; error bars, s.e.m.

See also **Figure S3-4**.

frequency upon Vamp1 knockdown (~50% reduction in shVamp1 compared to shLuc; Figure 3-6H), and this could also be rescued by the inhibitory neuron specific re-expression of Vamp1 (shVamp1 +mDlx-Vamp1r; Figure 3-6H). This indicates that the initial reduction in mEPSC frequency upon Vamp1 loss likely resulted from a compensatory, homeostatic change in excitatory synaptic transmission in response to decreased inhibition (Fu et al., 2011; Qiu et al., 2012; Turrigiano, 2011). Overall, the Vamp1 knockdown and cell-type specific rescue show that Vamp1 is important for inhibitory synaptic transmission. The similarity of the electrophysiological changes resulting from Vamp1 depletion to those in the Rbfox1 Nes-cKO indicate that loss of Vamp1 expression plays a major role in the altered synaptic transmission observed in the cKO brain.

Vamp1 re-expression rescues synaptic transmission defects in the Rbfox1 cKO

To directly test whether reduced Vamp1 levels contribute to altered inhibitory synaptic trans-mission in the Rbfox1 Nes-cKO brain, we used stereotaxic delivery of AAV2/9 expressing mDlx-driven Vamp1 to adult (P60-70) wildtype and cKO hippocampi and assessed them 3 weeks post-injection. We performed bilateral injections of a control mDlx-tRFP or rescue mDlx-tRFP-p2A-Vamp1 virus into each cKO hippocampus. Wildtype littermates were injected with the tRFP-alone virus in one hippocampus (Figure 3-7A). We observed no changes in synaptic transmission between injected and uninjected wildtype hippocampi (Figure S3-5 C-H). Inhibitory neuron-specific expression by the mDlx enhancer in vivo was previously demonstrated (Dimidschstein et al., 2016), and confirmed in our experiments by immunohistochemistry. We observed that mDlx-driven tRFP+ soma co-localized completely with Gad67+ cells, and that a subset of these

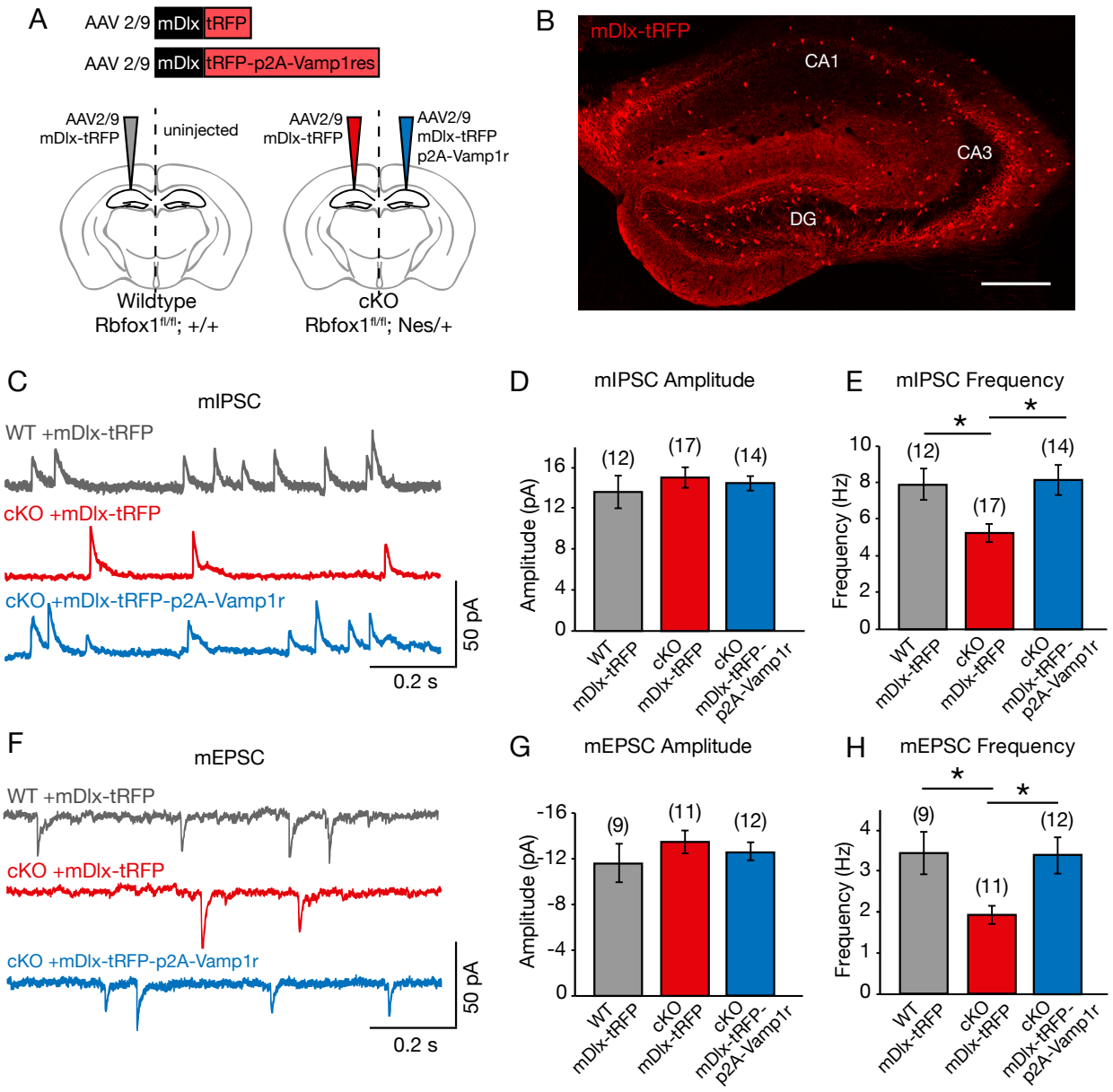

Figure 3-7: Vamp1 re-expression rescues inhibitory synaptic transmission in the Rbfox1 Nes-cKO.

(A) Schematic of the experiment. Adult wildtype and Rbfox1 cKO hippocampi were bilaterally injected with AAV2/9 expressing mDlx-driven transgenes.

Figure 3-7 continued.

(B) Expression of mDlx-driven tRFP in a representative injected hippocampus. Scalebar, 300um; 20x magnification.

(C-E) Reduced ¬mIPSC frequency in the Rbfox1 cKO CA1 is rescued by re-expression of mDlx-Vamp1.

(C) Representative mIPSC traces in the wildtype controls (WT control and +mDlx-tRFP), cKO (cKO +mDlx-tRFP) and rescue (cKO +mDlx-tRFP-p2A-Vamp1r) hippocampi.

(D-E) Quantification of average mIPSC amplitude and frequency shows re-expression of mDlx-driven Vamp1 rescues mIPSC frequency to levels similar to that of wildtype.

(F-H) Reduced mEPSC frequency can also be rescued by re-expression of mDlx-Vamp1.

(F) Representative mEPSC traces of samples as in (C).

(G-H) Quantification of average mEPSC amplitude and frequency shows re-expression of mDlx-driven Vamp1 also rescues mEPSC frequency to levels similar to that of wildtype. Number of cells recorded per condition across 6 littermate pairs is shown above bars. One-way ANOVA with Bonferroni correction; *$p \leq 0.05$; error bars, s.e.m.

See also **Figure S3-5**.

were also positive for Parvalbumin (Figure S3-5A). Generating acute slices of control and experimental hippocampi, we recorded mEPSCs and mIPSCs from CA1 across all three injected conditions. Comparing wildtype and cKO mice infected with control virus, we observed no changes in mEPSC or mIPSC amplitude (Figure 3-7 D,G), but found a significant reduction in both excitatory and inhibitory current frequency (Figure 3-7 E,H), similar to our previous observations (Figure 3-5 A-I). Comparing control and Vamp1 infected cKO samples, we found, remarkably, that re-expression of Vamp1 in Rbfox1 knockout inhibitory neurons could rescue the reduction in mIPSC frequency to levels similar to that of wildtype (Figure 3-7E). Interestingly, we also observed a rescue of mEPSC frequency with re-expression of Vamp1 in inhibitory neurons (Figure 3-7H). Confirming our results in rescuing Vamp1 knock-down in cultured neurons, this indicates that excitation is likely reduced in the Rbfox1 cKO hippocampus as a homeostatic response to loss of inhibition (Figure 3-6). These results demonstrate that simply increasing Vamp1 expression is sufficient to rescue the alterations in synaptic transmission observed in the pan-neuronal Rbfox1 Nestin-cKO hippocampus.

Discussion

We have examined how changes in mRNA metabolism controlled by an RNA binding protein can alter neurophysiology. Synaptic transmission in the Rbfox1 Nes-cKO hippocampus exhibits significantly reduced mIPSC and mEPSC frequency, with skewing of the E/I ratio to-wards increased excitation. Using RNAseq and iCLIPseq we identified a number of high confidence, direct target genes whose overall mRNA expression is dependent upon Rbfox1 and which exhibit binding of cytoplasmic Rbfox1 in their 3' UTR. One prominent Rbfox1 target is the vSNARE protein Vamp1, whose expression is greatly

reduced in the cKO brain. Unlike its close paralog Vamp2, we found that Vamp1 is specifically expressed in inhibitory neurons, with particular enrichment in Pv+ interneurons. Vamp1 loss of function leads to altered inhibitory synaptic transmission and is apparently a major contributor to the electrophysiological phenotypes in the Rbfox1 Nes-cKO brain. Exploring the mechanism of Rbfox1 regulation of Vamp1 expression, we found that Rbfox1 binding in the Vamp1 3'UTR prevents its repression by miR-9. Thus, through its interactions with Vamp1, Rbfox1 can specifically regulate inhibitory synaptic transmission. While Rbfox1 is broadly expressed across many neuronal cell types, inhibitory neuron dependence on Vamp1 expression renders this neuronal population susceptible to Rbfox1 loss. This work demonstrates how the dysregulation of a broadly ex-pressed RNA binding protein can result in defects in specific neuronal subtypes.

The specific expression of Vamp1 in inhibitory neurons of the hippocampus and cortex indicates that these cells maintain a specific machinery for inhibitory synaptic transmission. Unlike excitatory neurons which express only one synaptobrevin, Vamp2, inhibitory neurons express both Vamp1 and Vamp2 (Figure 3-3C). An important role for Vamp1 is indicated by the changes in mIPSC and mEPSC frequency observed upon Vamp1 knockdown. Co-expression of Vamp1 and Vamp2 has also been observed at the neuromuscular junction (NMJ). Work examining NMJ function in a Vamp1 hypomorphic mouse (lew/lew) (Nystuen et al., 2007) showed that loss of Vamp1 in motor neurons reduced the Ca2+ sensitivity and co-operativity of synaptic transmission. Loss of Vamp1 from motor neurons did not abolish neurotransmitter release, but reduced release probability, thus increasing the variability of the post-synaptic response (Liu et al., 2011). Like the NMJ, inhibitory synapses exhibit high neurotransmitter release probability in

response to excitatory signaling (Atallah and Scanziani, 2009; Pouille and Scanziani, 2001). Inhibitory neurons, in particular fast spiking Pv+ basket cells, play a pivotal role in the generation of cortical and hippocampal network oscillations through the precise control of principal cell firing (Bartos et al., 2007; Buzsáki and Wang, 2012; Cardin et al., 2009). These oscillations require the fast and precise conversion of excitatory input into inhibitory neurotransmitter release in Pv+ interneurons (Atallah and Scanziani, 2009; Hu et al., 2014; Jonas et al., 2004; Pouille and Scanziani, 2001). Although not statistically significant, we did observe an increase in mIPSC amplitude variability in the cKO hippocampus that may stem from reduced levels of Vamp1. Similar to its action in motor neurons, Vamp1 may increase release probability in the Pv+ neurons of the central nervous sys-tem and ensure the reliability of inhibitory synaptic transmission. This is consistent with the reduction of inhibitory synaptic transmission we observe in Vamp1 depleted hippocampal neurons, and the rescue of the reduced mIPSC frequency in the Rbfox1 cKO by the re-expression of Vamp1 specifically in inhibitory neurons.

A dynamic interplay between Rbfox1 and *miR-9* may serve to fine tune inhibitory synaptic transmission during physiologically relevant states such as learning and memory. Gamma oscillations in the hippocampus driven by the precisely timed firing of Pv+ interneurons have been proposed to function in working memory, spatial processing and coordination across brain structures (Buzsáki and Wang, 2012; Colgin and Moser, 2010; Lisman and Jensen, 2013; Yamamoto et al., 2014). Vamp1 regulation may also be important in the cortical processing of sensory input, which relies on fast spiking Pv+ cells to distinguish preferred stimuli, recruit specific principal cell populations and modulate sensitivity to stimuli (Hu et al., 2014; Isaacson and Scanziani, 2011; Tremblay et al., 2016;

Xue et al., 2014). Dynamic changes in Vamp1 levels could alter the window of input integration in feedforward circuits, or change the population of excitatory neurons recruited in response to different stimuli.

Rbfox1 regulation of E/I balance and implications in neurologic disease

Mutation and/or dysregulation of Rbfox1 has been implicated in epilepsy and autism spectrum disorders (ASD). Rbfox1/RBFOX1 was identified as a candidate ASD susceptibility gene (Bhalla et al., 2004; Bill et al., 2013; Martin et al., 2007; Sebat et al., 2007; Voineagu et al., 2011), and changes in both Rbfox1-mediated gene expression (Lee et al., 2016b) and alter-native splicing (Parikshak et al., 2016; Voineagu et al., 2011; Weyn-Vanhentenryck et al., 2014a) have been observed in ASD patient brains. Recent work focusing on the regulation of mRNA levels by cytoplasmic Rbfox1 found that its set of target transcripts, including Vamp1, showed significant overlap with genes involved in ASD (Lee et al., 2016b). Mutations in RBFOX1 and RBFOX3 are also potential risk factors in a range of epileptic disorders including idiopathic generalized epilepsy, childhood focal epilepsy, Rolandic epilepsy and sporadic focal epilepsy (Lal et al., 2015b; 2013b; 2013c). E/I balance and altered network oscillations are thought to be dysregulated in ASD (Gogolla et al., 2009; Hammer et al., 2015; Jurgensen and Castillo, 2015; Lee et al., 2015; Nakamura et al., 2015; Yizhar et al., 2011) and epilepsy (Fritschy, 2008; Peñagarikano et al., 2011). In one study for example, opto-genetic increase of the E/I ratio led to ASD-like impairments in social and cognitive function in mice and to changes in baseline gamma oscillations (Yizhar et al., 2011). Our finding that Vamp1 expression in inhibitory neurons rescues not only inhibitory but also excitatory synaptic transmission indicates that the reduced Vamp1 is a major component of the E/I imbalance seen in response to

the Rbfox1 mutation. Changes in Rbfox1 function may thus underlie the changes in inhibitory signaling and E/I balance associated with these diseases (Marín, 2012).

Individual neuronal cell-types exhibit specific susceptibilities to Rbfox1 loss

Although the Rbfox proteins are co-expressed in many neuronal cell types, their functions are not redundant. The proteins are highly homologous and exhibit similar binding activities *in vivo* (Damianov et al., 2016; Weyn-Vanhentenryck et al., 2014a) and similar splicing regulatory activities in *in vitro* assays (Tang et al., 2009; Underwood et al., 2005). However, the different phenotypes of the Rbfox1 and Rbfox2 knockout mice reveal the particular susceptibility of neuronal subpopulations to the loss of individual Rbfox paralogs. Whole transcriptome profiling of alternative splicing and gene expression in the Rbfox1 Nes-cKO hippocampus revealed targets affecting both excitatory and inhibitory synapses, consistent with the observed changes in both excitatory and inhibitory synaptic transmission. For example, we observed changes in alternative splicing of Homer1 and Grip1 (see Table S2-1), two scaffolding proteins of the post-synaptic density that affect excitatory function. However, the shift in E/I ratio to-wards increased excitation, and the similarity of the Vamp1 depletion phenotype to that of the Rbfox1 Nes-cKO, indicate a greater effect on inhibitory signaling. Interestingly, we found that the transcript set down-regulated by Rbfox1 loss was enriched for genes whose expression correlates with the expression of inhibitory neuron markers, while transcripts that increase in the cKO were enriched for genes associated with excitatory neuron marker expression (Kang et al., 2011) (Figure S2-1B). Similar to our findings that Vamp1 is specific to inhibitory neurons and is strongly down regulated by Rbfox1 loss, this analysis further emphasizes how RBP's can function in distinct ways in different cell types. Rather than a general Rbfox

regulatory program common to all neurons, neuronal subtypes have their own programs of posttranscriptional regulation leading to cell type specific patterns of gene expression.

Differences in Rbfox expression between neuronal populations is not limited to the broad categories of excitatory and inhibitory neurons. Within the hippocampus, some cells in layers typically occupied by non-Pv+ interneurons express Rbfox1 but not NeuN/Rbfox3, or vice versa (Figure S3-1D). In the cortex, excitatory neurons of layer 4 display markedly lower Rbfox1 expression than seen in other layers. Indeed, the regulation of Vamp1 by Rbfox1 can differ between different regions of the forebrain. Although Vamp1 expression is enriched in Pv+ neurons of the cortex (Figure S3-2 F,G) and thalamus (Figure S3-2 J,K), similar to the hippocampus, loss of Rbfox1 leads to a larger reduction of Vamp1 in layer 4 than in layer 5 (Figure S3-2 H,I) and does not seem to be affected in the thalamus (Figure S3-2 L,M). These differences in the dependence of Vamp1 on Rbfox1 may stem from differences in the cytoplasmic levels of the other Rbfox paralogs (Lee et al., 2016b), or from differences in expression of microRNAs or other RBPs.

The regulation of inhibitory neuron-specific Vamp1 by Rbfox1 provides a paradigm for how other broadly expressed RBPs may perform crucial functions in defined neuronal populations. There are many families of RNA-binding proteins that are expressed across multiple neuronal populations, and the consequences of RBP loss have mostly been studied after pan-neuronal or germline deletion. Similarly, RNAseq and CLIPseq analyses of these RBPs have identified their targets in whole-brain or mixed tissue samples. Our results indicate that examination of these other RNA regulators in specific cell types (Hwang et al., 2017) should yield important new understanding of their functions.

Chapter 4: MATERIALS AND METHODS

Experimental model and subject details

Mouse models

All breeding and experimental procedures were conducted in accordance with the National Institutes of Health guidelines and approved by the Institutional Animal Care and Use Committee of the University of California, Los Angeles. Generation of and genotyping protocols for Rbfox1$^{fl/fl}$ [Rbfox1tm1.1Dblk; JAX strain 014078] and Nestin-Cre [Tg(Nes-cre)1Kln; JAX strain 003771] mice have been previously described (Gehman et al., 2011; Tronche et al., 1999) and further information can be found at http://www.jax.org/. Rbfox1fl/fl mice were originally generated in the 129S2/Sv strain and backcrossed 10 generations to C57BL/6J (Gehman et al., 2011). Both Rbfox1fl/fl and Nestin-Cre mice were maintained on a C57BL/6J background and group housed under standard conditions. Rbfox1fl/fl animals were crossed to Nes-Cre$^{+/-}$ to generate heterozygous Rbfox1$^{fl/+;}$Nes-Cre$^{+/-}$. Heterozygous animals were crossed to Rbfox1$^{fl/fl}$ to generate litters containing wildtype (Rbfox1$^{fl/fl}$; Nes-Cre$^{+/+}$) and cKO (Rbfox$^{fl/fl}$;Nes-Cre$^{+/-}$) animals.

For RNAseq, qPCR and immunoblot experiments, male littermates were sacrificed between P60 and P70 by CO_2 overdose followed by cervical dislocation. For immunohistochemistry, P60-P70 male littermates were anesthetized with a mixture of 100mg/kg Ketamine and 10mg/kg Xylazine, followed by transcardial perfusion with ice-cold 1x PBS and 4% paraform-aldehyde in 1xPBS. For electrophysiology experiments, male littermates were deeply anesthetized with isoflurane and sacrificed by decapitation between P60-P70. Stereotaxic injections were performed on P60-P70 male littermates.

Primary neuronal culture

Embryonic day 16-18 C57BL/6J pregnant dams were sacrificed by CO_2 overdose followed by cervical dislocation. Embryos were decapitated with sharp scissors, and hippocampi from males and females were dissected out into ice-cold Hank's Balanced Salt Solution (HBSS, Ca^{2+}- and Mg^{2+}- free) and randomly pooled. Hippocampi were trypsinized at 37C for 10 minutes and mechanically dissociated, and cells were plated at a density of ~790 cells/mm^2 (for RNA or protein isolation) or 395 cells/mm^2 (for immunocytochemistry) on plates or nitric-acid treated glass coverslips coated with 0.1mg/mL poly-DL-lysine (Sigma-Aldrich) in 0.1M boric acid, pH8.5. Cells were initially plated in Neurobasal (Gibco) based Plating Media containing B27 (Gibco), Glutamax (Gibco), 25uM glutamate and 25uM B-mercaptoethanol and subsequently fed with Neurobasal based Feeding Media containing B27 and Glutamax every 3 days beginning at 3 days in vitro (DIV3). Primary cultures were maintained in a 37C incubator supplemented with 5% CO_2.

Heterologous cell culture

293T cells were grown in Dulbecco's Modification of Eagle's Medium (DMEM, Corning MT-10-017-CV) with L-glutamine and 4.5g/L glucose, supplemented with 10% fetal bovine serum and penicillin-streptomycin, and maintained in a 37C incubator with 5% CO_2. For transfection, cells were plated on poly-ornithine coated plates, grown to 60-70% confluency and transfected with indicated plasmids using Lipofectamine 2000 (Invitrogen) for 6 hours. Live cells were visualized on a Nikon TE2000-S inverted microscope and imaged using a SPOT RT-KE 7.4 slider CCD camera (Diagnostic instruments), or lysed in RIPA buffer for protein isolation 48 hours post-transfection.

Method Details

Electrophysiology

Slice Preparation. Mice were deeply anesthetized with isoflurane and following decapitation the brain was rapidly removed and placed into ice-cold N-Methyl-D-Glucamine (NMDG)-based cutting solution containing (in mM): 135 NMDG, 10 D-glucose, 4 $MgCl_2$, 0.5 $CaCl_2$, 1 KCl, 1.2 KH_2PO_4, and 26 HEPES (pH = 7.3–7.4, 290–300 mOsm/L), bubbled with 100% O_2. Coronal slices (320 μm) were prepared using a Campden 7000SMZ-2 Vibratome and then maintained in an interface-slice type chamber continuously perfused (2-3 ml/min) with a warm (30C), oxygenated (95% O2/5% CO_2) artificial cerebrospinal fluid (ACSF) containing (in mM): 124 NaCl, 2.4 KCl, 25 NaHCO3, 1 NaH_2PO_4, 2 CaCl2, 1.2 $MgSO_4$, and 10 glucose (pH 7.4, 290–300 mOsm). Slices were allowed to recover for at least 1 hour prior to recordings. All experimental techniques were approved by the Institutional Care and Use Commit-tee at the University of California, Los Angeles.

Patch-clamp recordings in brain slices and cultured neurons. Slices were transferred to a submerged-slice recording chamber continuously perfused (3 ml/min) with ACSF and whole-cell voltage-clamp techniques were used to record both evoked and miniature EPSCs and IPSCs. CA1 pyramidal cells and dentate gyrus granule cells were visualized using an IR-DIC upright microscope (Zeiss Examiner D1) and whole-cell recordings were performed using borosilicate patch electrodes (4–6 MΩ), containing (in mM): 120 $CsMeSO_4$, 10 CsCl, 5 TEA-Cl, 1.5 $MgCl_2$, 10 HEPES, 0.1 EGTA, 2 Na-ATP, 0.5 Na-GTP, and 5 QX-314, pH 7.25–7.30 with CsOH, 275–285 mOsm. Recordings were obtained

using a MultiClamp 700B amplifier with Digidata 1440A and pClamp 10 (Molecular Devices). Series resistance and whole-cell capacitance were automatically compensated and recordings were discontinued if series resistance increased by >20%. A bipolar, tungsten wire stimulating electrode placed in stratum radiatum proximal to the CA3 region was used to activate Schaffer collateral/commissural fibers and elicit EPSCs and IPSCs in CA1 pyramidal cells (stimulation rate = 0.05 Hz). In these experiments, we isolated the excitatory and inhibitory components of the evoked responses by recording synaptic currents at holding potentials (V_{hold}) of -68 and +10 mV, respectively. Bath application of 20 μM CNQX and 50 μM APV blocked synaptic currents at V_{hold} = -68 mV while application of 100 μM picrotoxin blocked synaptic currents at V_{hold} = +10 mV, confirming that EPSCs and IPSCs are isolated at these membrane potentials (data not shown). The intensity of presynaptic fiber stimulation was adjusted to elicit EPSCs with a peak amplitude of 100–300 pA at V_{hold} = −68 mV, and with the same stimulating intensity to record IPSCs at V_{hold} = +10 mV. Miniature EPSCs and IPSCs were recorded in the presence of 1 μM TTX. In experiments recording EPSCs and IPSCs in cultured neurons, cells were bathed in an external solution containing (in mM): 140 NaCl, 3 KCl, 2 $CaCl_2$, 1 $MgCl_2$, 10 D-glucose, 26 HEPES, and 1 μM TTX (pH = 7.4, 290–300 mOsm/L).

Data analysis and chemicals. Evoked currents were analyzed in Clampfit 10, and amplitude was measured as the peak of currents. Miniature E/IPSCs were detected and analyzed with custom-written LabView-based software. All results are presented as mean ± SEM. Statistical significance was determined using unpaired t tests. Picrotoxin and TTX were purchased from Tocris Biosciences. All other chemicals were from Sigma-Aldrich.

Stereotaxic injections

Adult (P60-P70) male littermates were anesthetized with 5% isoflurane, 33% N_2O mixed with O_2. Hair on the head was shaved following anesthesia, and animals were given 0.1mg/kg buprenorphine via intraperitoneal injection. Animals were fitted to a stereotaxic frame with blunt ear bars and provided with the same anesthesia mixture for the duration of the surgery. Skin on the head was sterilized with 70% ethanol and 10% povidone iodine, and an incision in the skin was made followed by craniotomies 2-3mm in diameter above the left and right hippocampi at -2.0mm posterior to Bregma and +/-1.5mm lateral to the midline. A glass micropipette driven by a syringe pump was used to deliver 3.9 E+12 genome copies (~1uL) of AAV2/9 mDlx-tRFP or AAV2/9 mDlx-tRFP-p2A-Vamp1m1/5 to CA1 at a depth of -1.6mm relative to the pial surface, at a rate of 0.2uL/minute. The pipette was left in place for 6 minutes after injection and withdrawn slowly over a 5-minute interval. The surgical incision was closed with external nylon sutures. Animals recovered in their home cages and were given intraperitoneal 0.1mg/kg buprenorphine twice daily for 3 days afterward. Animals were sacrificed three weeks post-injection for electrophysiology or transcardially perfused for immunohistochemistry.

RNA sequencing

Three pairs of P60-P70 Rbfox1 Nes-cKO and wildtype male littermates from different litters were sacrificed and hippocampi were dissected out in ice-cold HBSS. Hippocampi were lysed in Trizol (Invitrogen) using a Tissue Tearor and RNA was extracted according to the manufacturer's instructions. 1ug of total RNA was used for polyA selection and library construction using the Tru-Seq mRNA Stranded Library Kit (Illumina). Libraries

were sequenced on a Hi-Seq 2000 (Illumina) using 50bp paired-end reads and mapped at an average rate of 90% to the mouse mm9 genome using TopHat version 2.0.10. Differential gene expression was detected using Cufflinks version 2.2.1, and $q<0.05$ and log2 fold-change ≥1.2 was used to define significant changes. Splicing changes were detected using SpliceTrap version 0.92. Events with changes in percent spliced in |delta PSI| > 10% and read coverage exon 1> 50 and exon 3 > 50 in both samples were considered significant.

Enrichment of Rbfox1-regulated transcripts in specific cell subtypes

Logistic regression was used to assess enrichment of RbFox1-regulated transcripts in inhibitory and excitatory cell subtypes (Figure S2-1B). “Enriched genes” are those with an FDR adjusted $P<0.05$ for the respective cell type. Cell-specific gene lists encompass the top 100 genes correlated to canonical markers of specific subtypes of inhibitory and excitatory cell types in a spatiotemporal atlas of human brain expression (Kang et al., 2011).

Quantitative PCR

Relative gene expression. Trizol-extracted RNA was subjected to DNAse treatment (DNAseI, Roche) and purified by acidic phenol-chloroform extraction. 1ug of total RNA and oligo(dT)18 primers were used for reverse transcription by SSIII (Invitrogen), and equal volumes of cDNA across samples were used for qPCR, using the SensiFAST SYBR Lo-ROX qPCR mix in a QuantStudio6 (Applied Biosystems). All relative fold change quantifications were normalized to expression of the housekeeping gene, Hprt.

Absolute quantitation. DNAse-treated RNA was extracted and reverse transcribed as described as above. For spliced and unspliced Vamp1 transcripts, cDNA from brain samples was quantified against a standard curve of 10-fold dilutions of spliced or unspliced products ranging from 10^3-10^8 nM. For quantitation of AAV titer, an aliquot of the virus was treated with DNAse, followed by DNAse inhibition and Proteinase K treatment to release the viral genome. Viral genomes were quantified against a standard curve of the cognate AAV genome plasmid ranging from $5x10^1$-$5x10^8$ copies/uL to obtain a titer of genome copies (GC) per mL.

Taqman assay. DNAse-treated RNA was extracted as described above, and 10ng of total RNA was used for reverse transcription (RT) using the Multiscribe Reverse Transcriptase (ThermoFisher) and primers specific to the mature *mmu-miR-9* or, as a control, U6 snRNA. The RT product was then amplified using fluorescent Taqman-MGB probes specific for *miR-9* or *U6*. Relative fold changes in *miR-9* levels were normalized to *U6*.

DNA constructs and adeno-associated viruses

Luciferase reporters. pGL3-control (Promega) was used to insert the full length (FL) or a portion (3'F) of the Vamp1 3'UTR following the Luciferase gene using the NdeI and FseI restriction sites. Mutations of Rbfox binding sites in the 3'UTR from (U)GCAUG to (U)GACGU and the *miR9* seed site from CCAAAG to GGUUAG were created using site-directed mutagenesis and subcloned into pGL3-control.

RNAi constructs. The pAAV-U6-shLuc-CMV-GFP plasmid was used as a backbone to insert a hairpin targeting the Vamp1 coding sequence (5'-GAGCAGTGCTGCCAAGCTAAA-3') using the BamHI and EcoRI restriction sites.

Vamp expression constructs. The Vamp1 coding sequence (NM_009496.3) was generated as a gBlock (IDT) along with p2A-tRFP and cloned into pcDNA3.1(+) using BamHI and Eco-RI, or into pAAV-hSyn-Cre-WPRE-hGH (University of Pennsylvania Vector Core Facility #PL-C-PV1969) using AgeI and EcoRI. The Vamp2 construct in pcDNA3.1(+) was similarly created using the Vamp2 coding sequence (NM_009497.3). The tRFP-p2A-Vamp1m1/5 RNAi-resistant construct was created using site-directed mutagenesis and subcloned into pcDNA3.1(+) and pAAV-hSyn-Cre-WPRE-hGH to create rescue constructs. The pAAV-mDlx-GFP-Fishell-1 plasmid (Addgene #83900) was used as a backbone to insert either tRFP or tRFP-p2A-Vamp1m1/5 using the SpeI and AscI restriction sites to create pAAV-mDlx-tRFP and pAAV-mDlx-tRFP-p2A-Vamp1m1/5.

Tough Decoy constructs. Tough decoy sequences were designed according to ((Haraguchi et al., 2009); Figure 2). The mature *miR-9* targeting sequence is 5'- CTCATA-CAGCTAATCTGATAACCAAAGA-3', and the control sequence is 5'-CGCGACTATACGATCTCGCAATATGGT-3', where the ATCT is not complementary to the mature miR sequence and produces a bulge. The control sequence was obtained from a negative control sequence as validated by IDT (IDT© miRNA Inhibitors). Synthetic oligos of TuD stem loops containing the mature miR-9 or control sequence were annealed and insert-ed into pAAV-U6-shLuc-CMV-eGFP-SV40 (University of Pennsylvania Vector Core Facility # PL-C-PV1867) using the BamHI and EcoRI sites. CMV-eGFP was replaced with hSyn-tRFP using XbaI and NotI.

Adeno-associated viruses. All AAV were packaged with capsid serotype 9. AAV2/9 mDlx-tRFP, mDlx-tRFP-p2A-Vamp1m1/5, U6-TuDctrl-hSyn-tRFP and U6-TuDmiR9-hSyn-

tRFP were produced by co-transfection of the AAV2 genomic plasmid, pHelper and an AAV9 enve-lope plasmid into 293T cells. Viral particles were obtained from the cell pellet and media by PEG precipitation, purified using an ioxodianol gradient and concentrated using an Amicon centrifugal filter with a 100kDa membrane. Viral titer was determined by qPCR using a standard curve of the genome plasmid. AAV2/9 hSyn-Rbfox1-cytoplasmic was previously de-scribed [hSyn.Flag-Rbfox1_c_siMt] (Lee et al., 2016a), and U6-Vamp1sh#5-CMV-GFP and U6-shLuc-CMV-GFP viruses were generated at the University of Pennsylvania Vector Core Facility. AAV2/9 hSyn-eGFP and AAV2/9 hSyn-Cre-eGFP viruses were purchased from the University of Pennsylvania Vector Core Facility.

Luciferase Assays

Primary hippocampal neurons were isolated from E16-18 Rbfox1fl/fl embryos and plated at a density of ~790 cells/mm2 on poly-DL-lysine coated 96-well plates. Cells were infected at DIV3 with AAV2/9 hSyn-eGFP or AAV2/9 hSyn-Cre-eGFP and co-transfected at DIV5 with pRL-TK Renilla and pGL3 Luciferase reporters using Lipofectamine 2000. For experiments using Tough Decoys, cells were infected again at DIV7 with AAV2/9 U6-TuDctrl-hSyn-tRFP or AAV2/9 U6-TuDmiR9-hSyn-tRFP. Cells were collected at DIV14 for luciferase assay using the Dual-Glo Luciferase Kit (Promega) and analysed using a Synergy2 Multi-Mode Reader (Biotek).

Immunoblotting

P60-P70 mice were sacrificed and brain tissue was dissected out in ice-cold HBSS. Tissue was lysed in RIPA buffer with protease and phosphatase inhibitors (Roche) and benzonase using a Tissue Tearor. Lysates were cleared and boiled in SDS loading buffer, separated on 10% or 12% Tris-glycine gels and transferred to 0.45um PVDF membranes (GE Amersham). Membranes were imaged on a Typhoon Variable Mode Imager 9410 (GE Amersham Biosci-ence) and quantified using ImageQuantTL software version 8.1. The following primary anti-bodies were used: ms α-Rbfox1 clone 1D10 (EMD Millipore), 1:2000; rb α-Vamp1, 1:1000 (Synaptic Systems); gp α-Vamp2, 1:1000 (Synaptic Systems); ms α-GAPDH clone C65, 1:4000 (Ambion). Cy3- or Cy5- conjugated secondary antibodies against –ms, -rb or –gp were used at 1:2500 (GE Healthcare).

Immunocytochemistry and immunohistochemistry

Immunocytochemistry. Primary hippocampal neurons grown on nitric-acid treated coverslips were fixed at DIV18 in 4% paraformaldehyde/PBS. Fixed cells were permeablized with 0.1% Triton/PBS and blocked with 10% goat serum/PBS. Primary antibodies were incubated over-night at 4C, followed by 3 washes and secondary antibody incubation for 2hrs at room temperature. Antibodies were diluted in 3% BSA with 0.02% sodium azide in PBS. Coverslips were mounted using ProLong Gold (Invitrogen) and imaged on Zeiss LSM 510 Meta and LSM 780 confocal microscopes using 40x or 63x oil objectives as indicated in each figure legend.

Immunohistochemistry. Adult Rbfox1 Nes-cKO and wildtype littermates were transcardially perfused with ice-cold PBS followed by ice-cold 4%

paraformaldehyde/PBS. Brains were further fixed in 4% paraformaldehyde/PBS overnight at 4C, then cryoprotected in 30% sucrose and embedded in OCT compound (Tissue-Tek). 40um frozen sections were cut in coronal orientation using a Leica Microm HM505E cryostat onto SuperFrost Plus (VWR) glass slides. Sections were rehydrated in PBS, permeablized with 0.5% Triton/PBS and blocked with 10% goat serum in 0.5% Triton/PBS for 1 hour at room temperature. Sections were incubated with primary antibodies overnight at 4C, followed by 3 washes and secondary antibody incubation for 2hrs at room temperature. Antibodies were diluted in 3% BSA with 0.02% sodium azide in PBS. Sections were mounted in ProLong Gold and imaged using 10x, 20x air or 40x, 63x oil objectives as indicated in each figure legend on Zeiss LSM 510 Meta and LSM 780 confocal microscopes.

The following antibodies were used: ms α-Rbfox1 clone 1D10 (EMD Millipore), 1:2000; rb α-Vamp1, 1:1000 (Synaptic Systems); gp α-Vamp2, 1:1000 (Synaptic Systems); ms α-Gad67 clone 1G10.2, 1:1000 (EMD-Millipore); rb α-Gephyrin, 1:1000 (Synaptic Systems); ch α-Map2, 1:2000 (Abcam); ms α-PSD-95, 1:1000 (Antibodies Incorporated); gp α-Synaptophysin, 1:1000 (Synaptic Systems); ms α-znp-1 (Synaptotagmin2), 1:1000 (ZIRC); gp α-Parvalbumin, 1:1000 (Synaptic Systems). Alexa Fluor 488-, 568- or 647-conjugated goat α –mouse, -rabbit, -chicken or –guinea pig secondary antibodies (Thermo Fisher) were used at a dilution of 1:1000 for 488 and 568, and 1:500 for 647.

Quantification of pre-synaptic puncta

All quantification was done by hand. Cultured neurons used for quantification were imaged at 63x magnification. For Vamp1 co-localization with excitatory or inhibitory

markers (Figure 3-4 A,B), puncta were counted within 100um^2 areas in a total of 15 images from 1 culture (biological replicate). For co-localization of excitatory or inhibitory pre- and post-synaptic puncta (Figure S3-3 B,C), puncta were counted along 3-4 50um dendritic sections per image, from 5-6 images per culture, in 3-4 cultures (biological replicates).

Tissue sections used for quantification were imaged at 40x magnification. For Vamp1 puncta co-localization with Gad67 or Syt2 in CA1 (Figure 3-4 C-F), puncta were counted within at least (3) 50um^2 areas/image, in a total of 3 images per animal (n=3 animals). For Vamp1 puncta co-localization with Gad67 or Syt2 in DG (Figure S3-2 B-E), puncta were counted within at least 2 (DG hilus) or 3 (DG sp and ip) 50um^2 fields/image, in a total of 1 (DG hilus) or 2 (DG sp and ip) images per animal (n=3 animals).

Accession Numbers

The accession number for the RNAseq data reported in this paper is GEO: GSE96722.

CONCLUDING REMARKS

APPENDICES

Chapter 2 Supplemental Figures

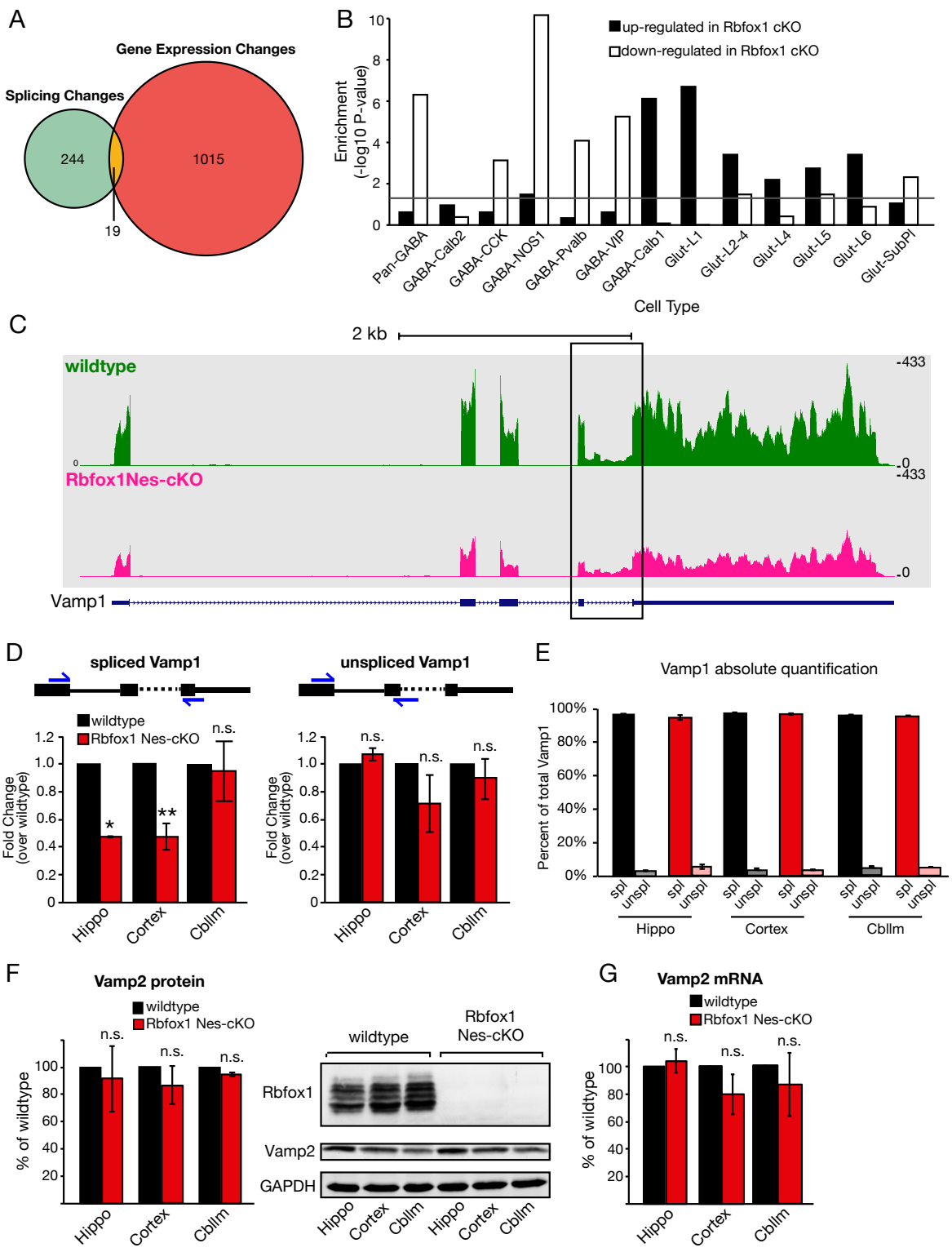

Figure S2- 1: Splicing and gene expression analyses.

Figure S2-1 continued.

Related to **Figure 2-1** and **Table S2-3.**

(A) Venn diagram of overlap between genes changing in splicing and mRNA expression levels.

(B) Enrichment plot showing DE genes significantly downregulated in the cKO are enriched for genes associated with inhibitory neuron subtypes, while those upregulated are associated mainly with excitatory subtypes.

(C-E) Rbfox1 does not affect intron retention in the Vamp1 transcript.

(C) UCSC Genome Browser view of Vamp1 as in Figure 1-1C. The box highlights the last intron, identified as an alternatively retained intron by SpliceTrap.

(D) qPCR analyses of spliced (left) and unspliced (right) Vamp1, using primers flanking or within the last intron, respectively. Vamp1 was normalized to Hprt expression and shown as a percentage of wildtype expression in each brain region.

(E) Absolute quantification of spliced and unspliced Vamp1 transcript. n=3 littermate pairs; Student's t-test; * $p \leq 0.05$, ** $p \leq 0.01$; n.s., not significant; error bars, s.e.m.

(F,G) Vamp2 protein and mRNA levels are unchanged between wildtype and cKO.

(F) Left, immunoblot of Rbfox1, Vamp2 and GAPDH in hippocampus, cortex and cerebellum of adult (P60-P70) wildtype and *Rbfox1 Nes-cKO* littermates. Right, quantification of Vamp2 protein as a percentage of wildtype expression for each brain region after normalization to GAPDH is shown at right.

(G) qPCR analyses of Vamp2 mRNA. Expression was normalized to Hprt expression and expressed as a percentage of wildtype expression in each brain region. n=3 littermate pairs; Student's t-test; n.s., not significant; error bars, s.e.m.

Chapter 3 Supplemental Figures

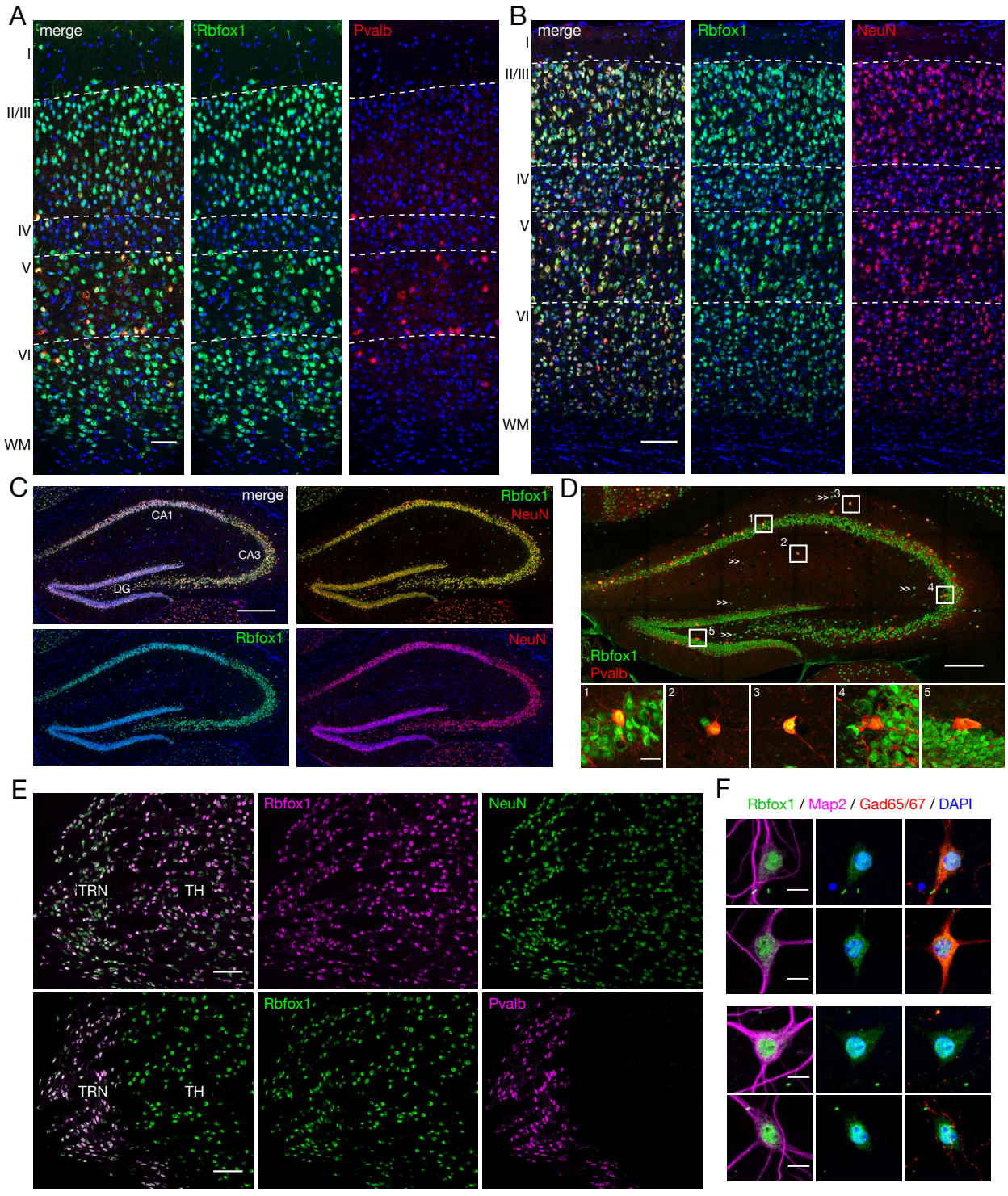

Figure S3- 1: Rbfox1 expression in the forebrain.

Figure 3-1 continued.

Related to **Figure 3-3.**

(A-B) Rbfox1 expression in the adult (P60) mouse cortex. Rbfox1 (green) co-staining with Parvalbumin (red) shows that Rbfox1 is expressed in Pv+ neurons in all cortical layers (A). Co-staining of Rbfox1 (green) with the pan-neuronal marker NeuN/Rbfox3 (red) shows Rbfox1 is expressed in all cortical neurons (B). Note that Rbfox1 expression is markedly lower in layer 4. Scalebar, 100um; 20x magnification.

(C-D) Rbfox1 expression in adult (P60) mouse hippocampus. **(C)** Rbfox1 (green) co-staining with NeuN/Rbfox3 (red) shows that Rbfox1 is expressed in the excitatory pyramidal layers of CA1 and CA3 and in the dentate gyrus (DG). **(D)** Rbfox1 is expressed in Parvalbumin+ inhibitory neurons (red) throughout the hippocampus (insets 1-5), as well as in non-Pv+ cells that are likely SST+ or VIP+ interneurons based on their location in the stratum radiatum and oriens (arrows). Scalebar, 300um; 20x magnification.

(E) Rbfox1 expression in the thalamus. Rbfox1 (magenta) and Rbfox3/NeuN (green) are expressed in the excitatory relay neurons of thalamus (TH, top panels) and the Pv+ interneurons of the reticular nucleus (TRN, bottom panels). Though Rbfox1 expression is relatively similar between the TRN and the TH, Rbfox3/NeuN is more highly expressed in the TRN. Scalebar, 100um; 20x magnification.

(F) Rbfox1 is expressed in both excitatory and inhibitory neurons in vitro. Example images of Rbfox1 (green) co-staining with the inhibitory marker Gad 65/67 (red) and the pan-neuronal dendritic marker Map2 (magenta) shows Rbfox1 is expressed in all neurons, including inhibitory neurons. Cultured hippocampal neurons, DIV19. Scalebar, 10um; 40x magnification.

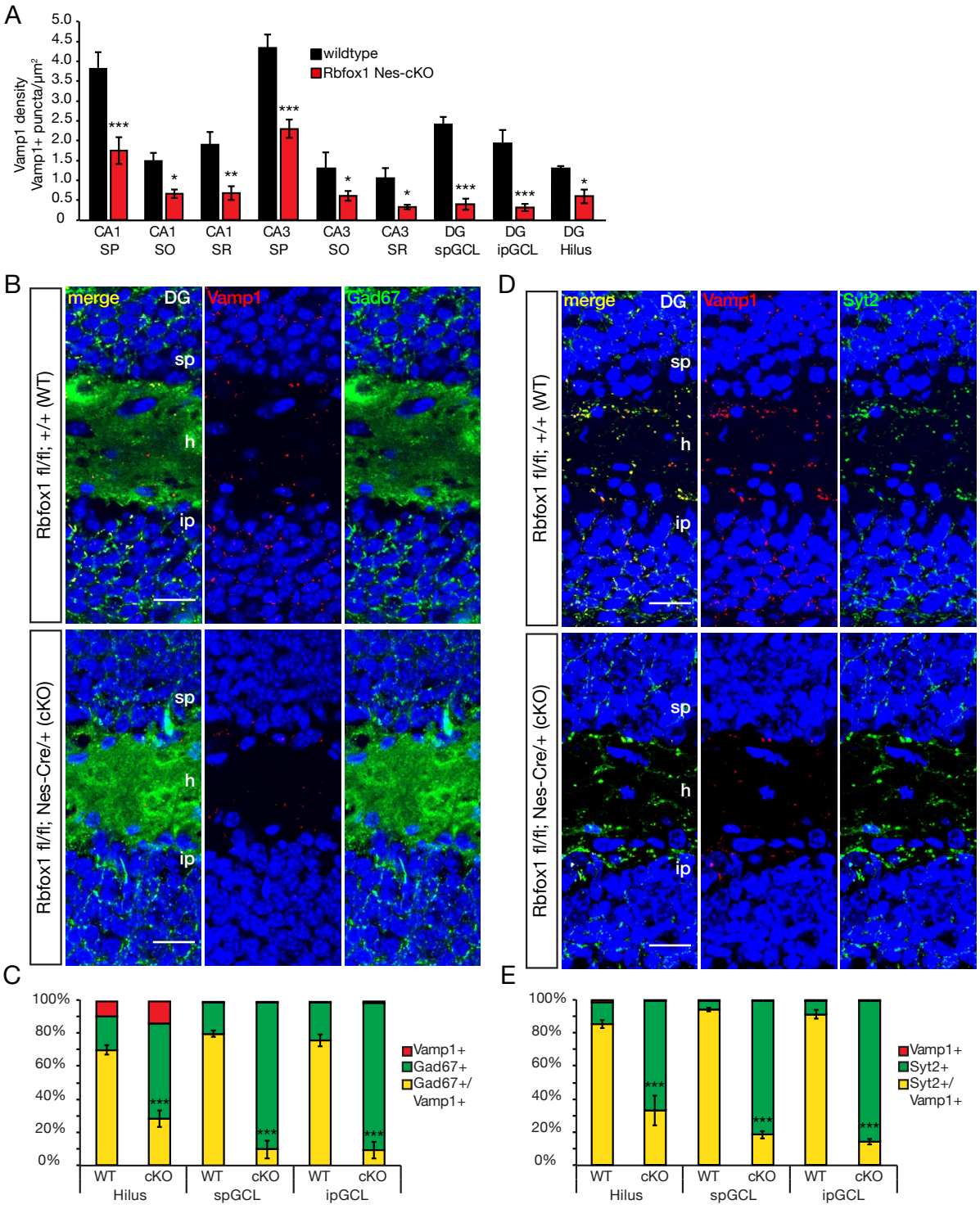

Figure S3- 2: Vamp1 enrichment in Parvalbumin+ interneurons.

Figure S3-2 continued

Related to **Figure 3-4.**

(A) Vamp1 density is significantly reduced by Rbfox1 loss in all hippocampal areas. Vamp1 density was assayed by counting the number of VAMP1+ puncta within 50um^2 fields and the average density is shown as VAMP1+ puncta/um^2. Puncta were quantified from at least 2 (DG hilus) or 3 (DG sp and ip) fields of 50um^2 per biological replicate.

(B-C) Vamp1 co-localizes with Gad67 in adult mouse dentate gyrus (DG). Immunohistochemistry of Vamp1 (red) and Gad67 (green) in P60-P70 DG of wildtype and Rbfox1 Nes-cKO hippocampal sections. In the wildtype DG hilus, ~70% of puncta counted contained both Vamp1 and Gad67, ~20% were Gad67+ only and ~10% were Vamp1+ only. In the Nes-cKO ~30% of puncta were Vamp1+ and Gad67+, while ~55% were Gad67+ only. Vamp1 and Gad67 puncta overlap was slightly higher in the suprapyramidal granule cell layer (spGCL) and infrapyramidal GCL (ipGCL) (~85%) with noticeably increased loss of co-localized puncta (~10% spGCL and ipGCL) and concomitant increase in Gad67+ only puncta (~90%). Note that in the hilus a portion (~10%) of puncta are Vamp1+ and Syt2-.

(D-E) Vamp1 is enriched in Parvalbumin+ interneuron pre-synaptic terminals in the DG. Immunohistochemistry of Vamp1 (red) and Synaptotagmin2 (Syt2, green) in P60-P70 DG of wildtype and Rbfox1 Nes-cKO hippocampal sections. Over 80% of puncta counted contained both Vamp1 and Syt2 in the DG hilus and ~90% in both ipGCL and spGCL. In the Nes-cKO, only ~30% of puncta were Vamp1+ and Syt2+ in the hilus, ~20% in spGCL and ~15% in ipGCL. n=3 littermate pairs; puncta were quantified from at least 2 (DG hilus)

Figure S3-2 continued.

or 3 (DG sp and ip) 50um^2 fields/image, from 1 (DG hilus) or 2 (DG sp and ip) images per biological replicate.

For A, Student's t-test; for B-E, ANOVA with Bonferonni correction;

For A-E, n=3 littermate pairs;* $p \leq 0.05$, ** $p \leq 0.01$, *** $p \leq 0.001$; error bars, s.e.m. Labels: **or**, stratum oriens; **pyr**, stratum pyramidal; **rad**, stratum radiatum; **sp**, suprapyramidal GCL; **ip**, infrapyramidal GCL; **h**, hilus.

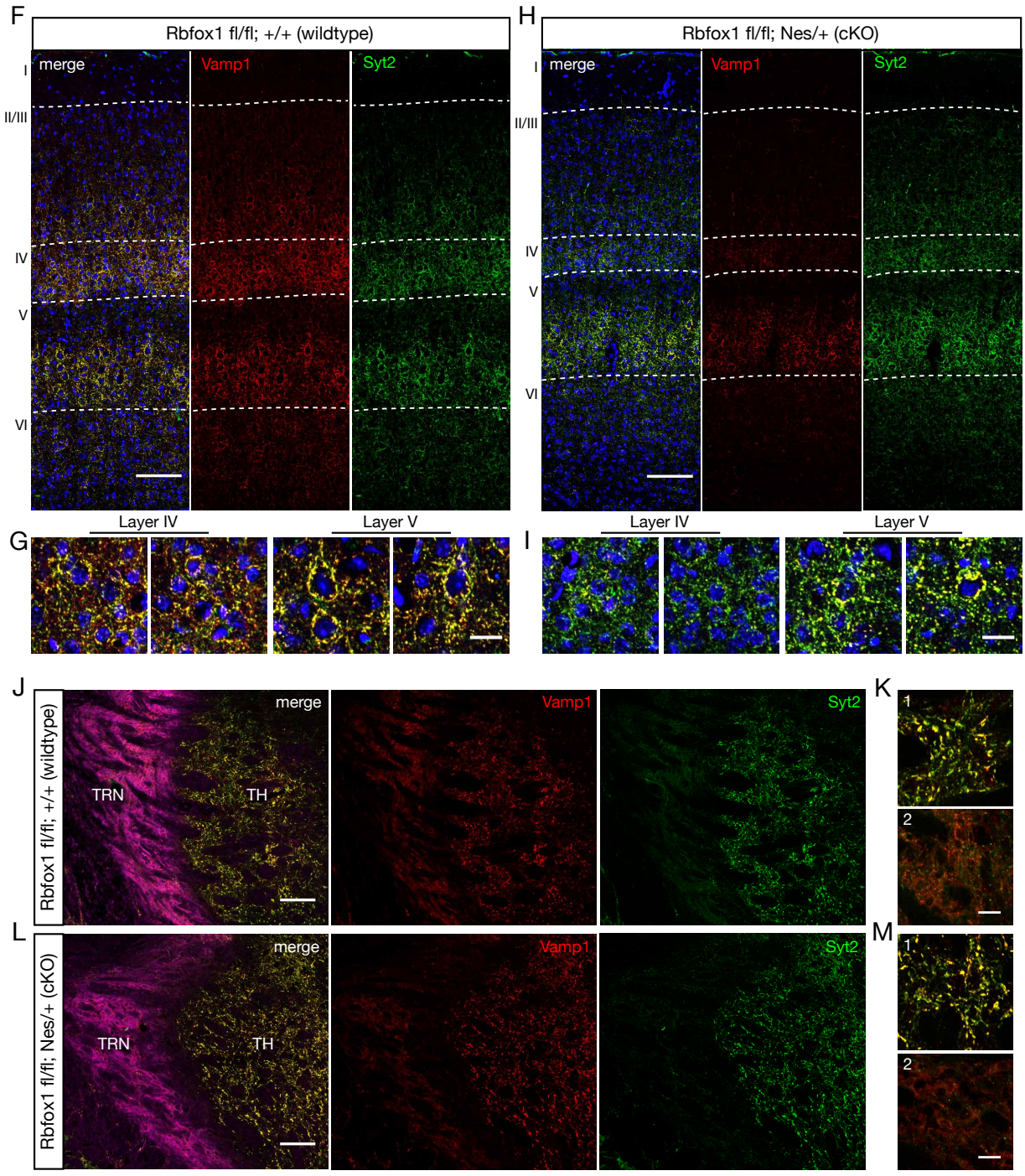

Figure S3-2 continued: Vamp1 expression in the cortex and thalamus.

Related to **Figure 3-4.**

(F-I) Vamp1 co-localizes with Syt2 in the cortex and is enriched in layers 4 and 5.

Figure S3-2 continued.

(F) Immunohistochemistry of Vamp1 (red) and Syt2 (green) in wildtype and cKO cortex. Note that Vamp1 expression is enriched in layers 4 and 5, though there is also co-localization in layers 2/3 and layer 6.

(G) Insets show Vamp1+/Syt2+ puncta localized around DAPI+ cell bodies in layers 4 and 5. **(H)** In the Rbfox1 cKO cortex, Vamp1 expression is markedly reduced in layer 4 compared to wildtype, though reduction is also visible in layer 5. Overall Syt2 expression does not seem to be affected in the cKO cortex.

(I) Insets in show markedly reduced Vamp1+/Syt2+ puncta in cKO layers 4 and 5.

(J-M) Vamp1 co-localizes with Syt2 in the thalamus (TH) and the reticular nucleus (TRN). Some Vamp1 (red) is present in the TRN, as identified by wisteria floribundin agglutin (WFA) staining (magenta). Vamp1+ puncta are much more strongly expressed in the thalamus and co-localize with Syt2 (green). Though Vamp1 expression is somewhat reduced in the cKO TRN compared to wildtype (K, M inset 1), expression is not markedly altered in the thalamus (K, M inset 2).

Panel scalebars, 100um; inset scalebars 20um; 20x magnification.

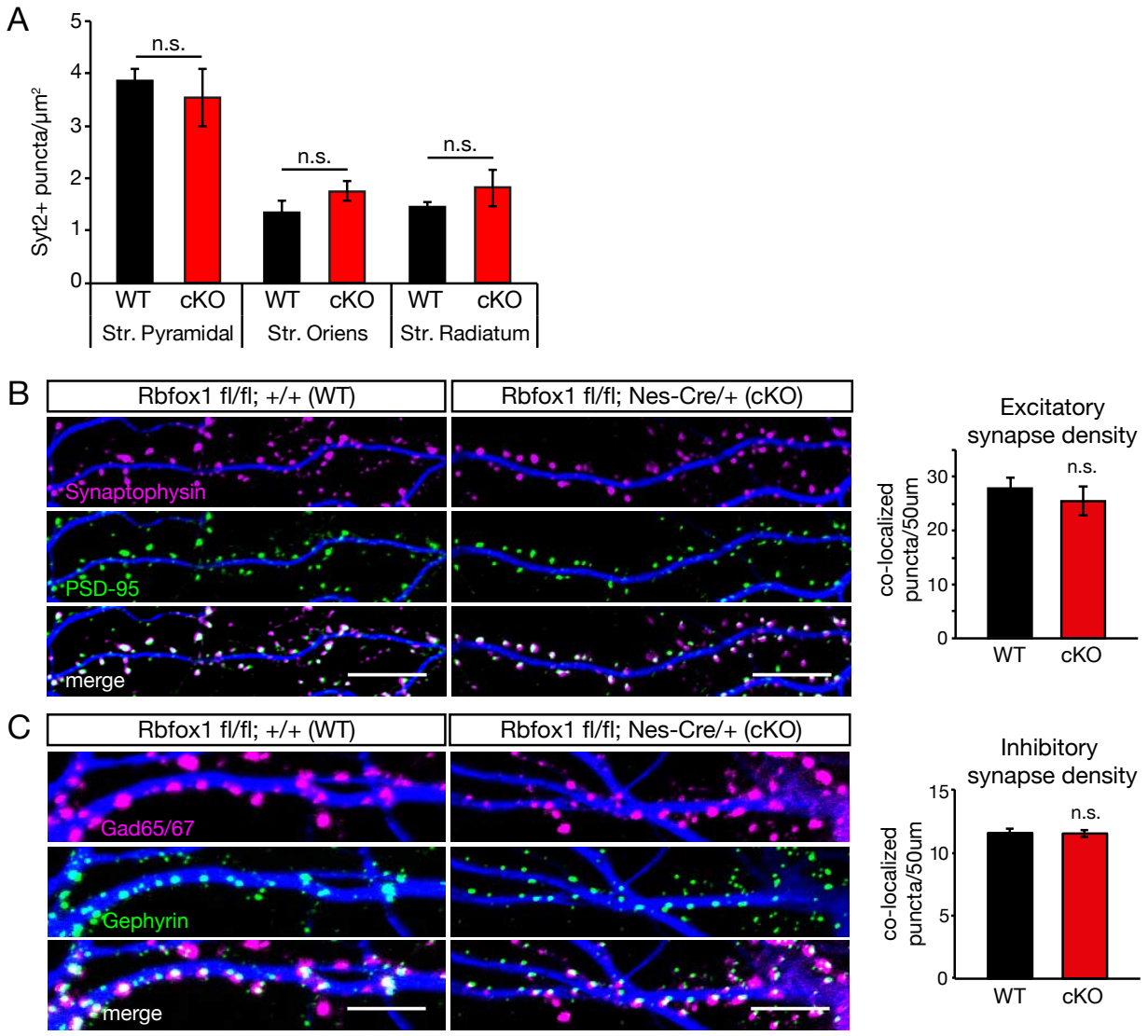

Figure S3- 3: Rbfox1 loss does not affect excitatory or inhibitory synapse density.

Related to **Figure 3-5.**

(A) Synaptotagmin2+ puncta density is similar between wildtype (black bars) and *Rbfox1 Nes-cKO* (red bars) in adult (P60-70) mouse CA1. The number of Syt2+ puncta were counted within 50um^2 fields to obtain an average density per um^2.

n=3 littermate pairs; puncta were quantified from at least 10 fields of 50um^2 per biological replicate. ANOVA with Bonferonni correction; n.s., not significant; error bars, s.e.m.

Figure S3-3 continued.

(B-C) Representative images of excitatory pre-synaptic marker Synaptophysin (magenta) and post-synaptic marker PSD-95 (green) co-localization (B) and inhibitory pre-synaptic markers Gad65/67 (magenta) and post-synaptic marker Gephyrin (green) co-localization (C). Co-localized puncta (white) were counted over 50um lengths of dendrite and quantified at right. Neither excitatory nor inhibitory synapse density are significantly different between wildtype and cKO.

n=3 cultures of littermate pairs (biological replicates); for (A) puncta were counted along four 50um dendritic segments per image, in at least 5 images per replicate; for (C) puncta were counted along 3 50um dendritic segments proximal to the soma per image, in at least 6 images per replicate. n=3 cultures; Student's t-test; n.s., not significant. Error bars, s.e.m. scalebar, 10um; 63x magnification.

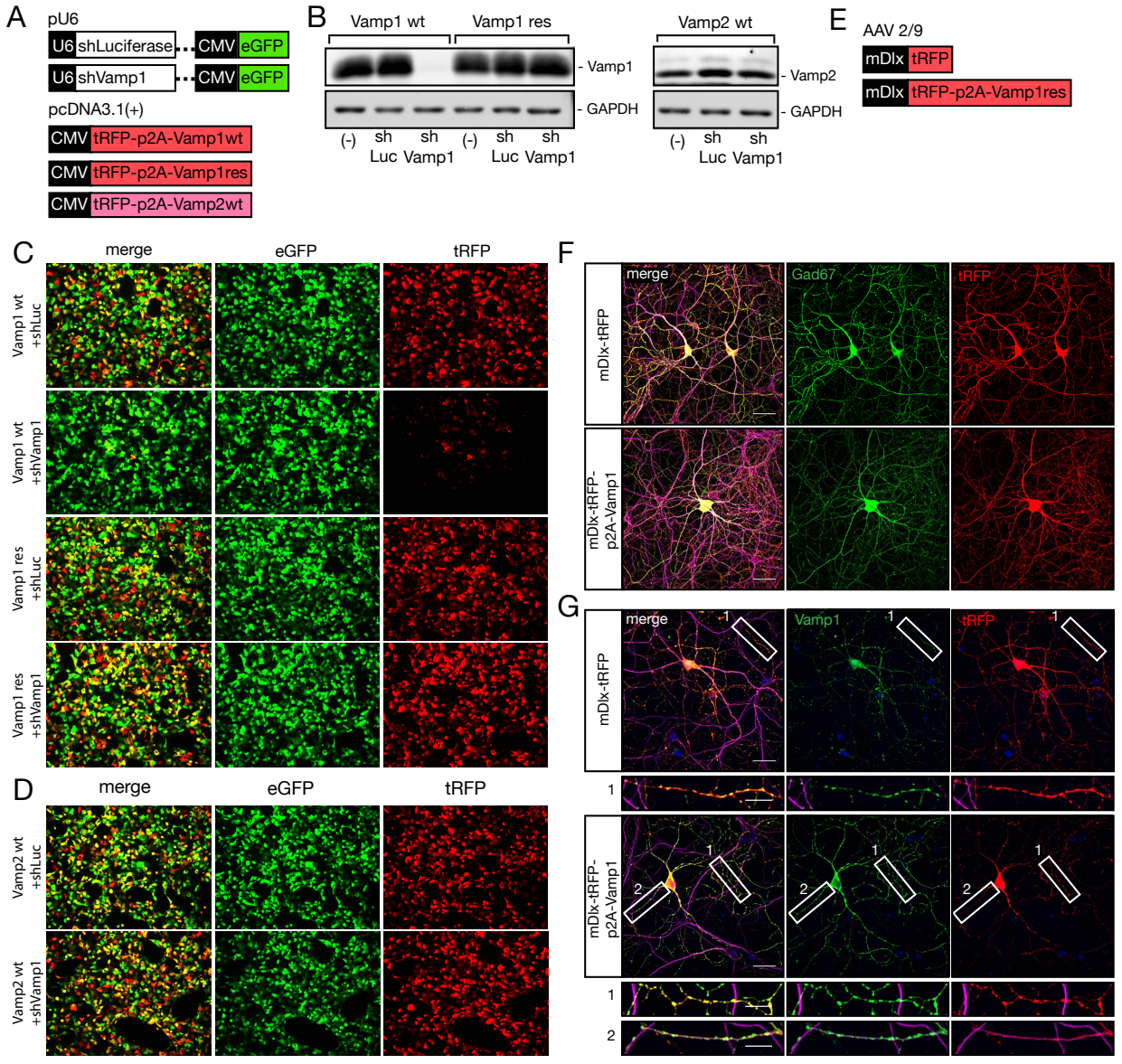

Figure S3- 4: Vamp1 shRNA knockdown and rescue.

Related to **Figure 3-6.**

(A) Schematic of plasmids used to assay Vamp1 knockdown in heterologous cells.

(B-D) Vamp1 shRNA efficiently knocks down Vamp1 in heterologous cells but does not affect Vamp2.

(B) Left, immunoblot of Vamp1 and GAPDH in 293T cells transfected with pCDNA3.1(+) *CMV*-driven wildtype Vamp1 cDNA (Vamp1wt) or RNAi-resistant Vamp1 cDNA

Figure S3-4 continued.

(Vamp1res). Vamp1 plasmids were co-transfected with either empty vector (-), *U6*-driven shRNA against Luciferase (shLuc) or shRNA against Vamp1 (shVamp1). Vamp1 protein expression is efficiently reduced when co-expressed with Vamp1 shRNA, while the control RNAi (shLuc) has no effect. The Vamp1 rescue construct is unaffected by both the control and Vamp1 shRNAs. Right, immunoblot of Vamp2 and GAPDH in 293T cells transfected with pcDNA3.1(+) *CMV*-driven wildtype Vamp2 cDNA (Vamp2wt) and either empty vector (-), *U6*-driven shRNA against Luciferase (shLuc) or shRNA against Vamp1 (shVamp1). Vamp2 expression is unaffected by control and Vamp1 shRNAs.

(C-D) Epifluorescence images of live 293T cells co-transfected with the indicated Vamp1, Vamp2 and shRNA plasmids.

(E-G) Expression of *mDlx*-Vamp1 constructs in vitro.

(E) Schematic of AAV constructs used.

(F) Co-staining of the inhibitory neuron marker Gad67 (green) with tRFP (red) in cultures infected with the control virus (mDlx-tRFP) and rescue virus (mDlx-tRFP-p2A-Vamp1).

(G) Representative co-staining of Vamp1 (green) in cultures infected with control and rescue viruses. Top, with control virus infection, endogenous Vamp1 expression is limited to axonal (Map2-) segments in infected (tRFP+) neurons (top inset 1). Bottom, with rescue virus, exogenous Vamp1 is punctal and found in both axonal (Map2-) segments (bottom inset 1) and dendritic (Map2+) segments (bottom inset 2).

Wildtype primary hippocampal neurons were infected at DIV8 and fixed and stained at DIV14.

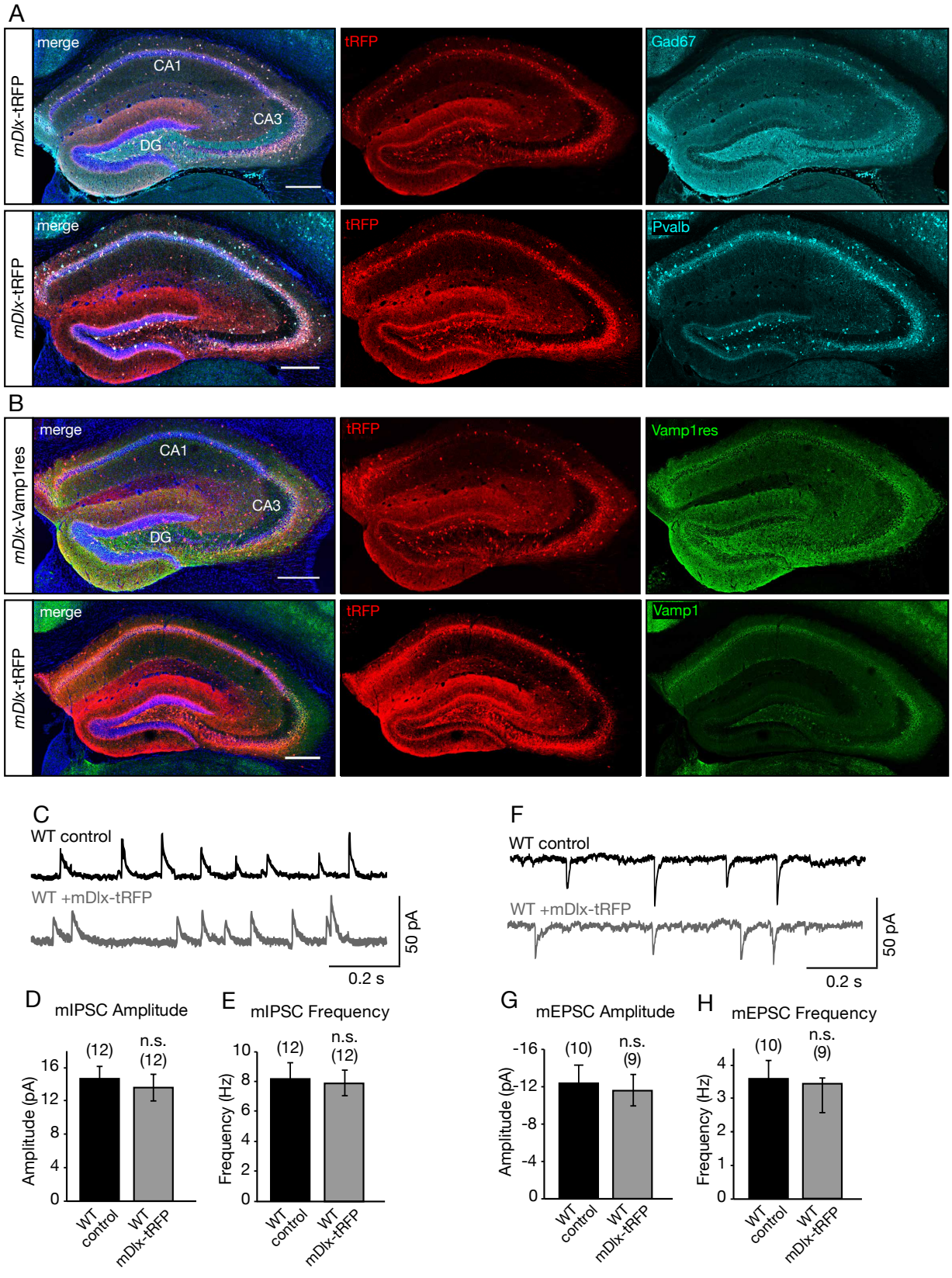

Figure S3- 5: Expression of mDlx rescue constructs in vivo.

Figure S3-5 continued.

Related to **Figure 3-7.**

(A-B) Immunohistochemistry of control AAV2/9 *mDlx*-tRFP and *mDlx*-tRFP-Vamp1 (*mDlx*-Vamp1res) in stereotaxically injected adult mouse hippocampi. **(A)** Top, tRFP expression driven by the *mDlx* enhancer co-localizes with the inhibitory neuron marker Gad67 (cyan) and does not show non-specific expression. Bottom, *mDlx*-driven tRFP also co-localizes with Parvalbumin (cyan).

(B) Top, immunohistochemistry of Vamp1 expression in a cKO hippocampus injected with rescue virus. Overexpressed Vamp1 (green) is enriched around the CA1 and CA3 pyramidal cell layers, and in the DG. This perisomatic expression in the pyramidal layers is similar to that observed of endogenous Vamp1 (green) in a wildtype hippocampus injected with control virus, bottom. Scalebar, 300um; 10x magnification.

(C,F) Representative CA1 mIPSC and mEPSC traces in the wildtype controls (WT control and +mDlx-tRFP), cKO (cKO +mDlx-tRFP) hippocampi.

(D-E) Average mIPSC amplitude and frequency are not significantly different between injected and uninjected wildtype samples.

(G-H) Average mEPSC amplitude and frequency are not significantly different between injected and uninjected wildtype samples.

Number of cells recorded per condition across 6 littermate pairs is shown above bars.

One-way ANOVA with Bonferroni correction; n.s., not significant; error bars, s.e.m.

REFERENCES

Aberg, K., Saetre, P., Jareborg, N., and Jazin, E. (2006). Human QKI, a potential regulator of mRNA expression of human oligodendrocyte-related genes involved in schizophrenia. Proc. Natl. Acad. Sci. U.S.a. *103*, 7482–7487.

Akamatsu, W., Fujihara, H., Mitsuhashi, T., Yano, M., Shibata, S., Hayakawa, Y., Okano, H.J., Sakakibara, S.-I., Takano, H., Takano, T., et al. (2005). The RNA-binding protein HuD regulates neuronal cell identity and maturation. Proc. Natl. Acad. Sci. U.S.a. *102*, 4625–4630.

Arnaud, L., Ballif, B.A., and Cooper, J.A. (2003). Regulation of protein tyrosine kinase signaling by substrate degradation during brain development. Molecular and Cellular Biology *23*, 9293–9302.

Arnold, E.S., Ling, S.-C., Huelga, S.C., Lagier-Tourenne, C., Polymenidou, M., Ditsworth, D., Kordasiewicz, H.B., McAlonis-Downes, M., Platoshyn, O., Parone, P.A., et al. (2013). ALS-linked TDP-43 mutations produce aberrant RNA splicing and adult-onset motor neuron disease without aggregation or loss of nuclear TDP-43. Proceedings of the National Academy of Sciences *110*, E736–E745.

Atallah, B.V., and Scanziani, M. (2009). Instantaneous modulation of gamma oscillation frequency by balancing excitation with inhibition. Neuron *62*, 566–577.

Ayala, R., Shu, T., and Tsai, L.-H. (2007). Trekking across the brain: the journey of neuronal migration. Cell *128*, 29–43.

Backx, L., Fryns, J.-P., Marcelis, C., Devriendt, K., Vermeesch, J., and Van Esch, H. (2010). Haploinsufficiency of the gene Quaking (QKI) is associated with the 6q terminal deletion syndrome. Am. J. Med. Genet. A *152A*, 319–326.

Bak, R.O., Hollensen, A.K., Primo, M.N., Sørensen, C.D., and Mikkelsen, J.G. (2013). Potent microRNA suppression by RNA Pol II-transcribed “Tough Decoy” inhibitors. Rna *19*, 280–293.

Ballas, N., Grunseich, C., Lu, D.D., Speh, J.C., and Mandel, G. (2005). REST and its corepressors mediate plasticity of neuronal gene chromatin throughout neurogenesis. Cell *121*, 645–657.

Barbosa-Morais, N.L., Irimia, M., Pan, Q., Xiong, H.Y., Gueroussov, S., Lee, L.J., Slobodeniuc, V., Kutter, C., Watt, S., Colak, R., et al. (2012). The evolutionary landscape of alternative splicing in vertebrate species. Science *338*, 1587–1593.

Bark, C., Bellinger, F.P., Kaushal, A., Mathews, J.R., Partridge, L.D., and Wilson, M.C. (2004). Developmentally regulated switch in alternatively spliced SNAP-25 isoforms alters facilitation of synaptic transmission. Journal of Neuroscience *24*, 8796–8805.

Barr, M.S., Farzan, F., Tran, L.C., Chen, R., Fitzgerald, P.B., and Daskalakis, Z.J. (2010). Evidence for excessive frontal evoked gamma oscillatory activity in schizophrenia during working memory. Schizophr. Res. *121*, 146–152.

Barry, G., Briggs, J.A., Vanichkina, D.P., Poth, E.M., Beveridge, N.J., Ratnu, V.S., Nayler, S.P., Nones, K., Hu, J., Bredy, T.W., et al. (2014). The long non-coding RNA Gomafu is acutely regulated in response to neuronal activation and involved in schizophrenia-associated alternative splicing. Mol. Psychiatry *19*, 486–494.

Bartos, M., Vida, I., and Jonas, P. (2007). Synaptic mechanisms of synchronized gamma oscillations in inhibitory interneuron networks. Nat. Rev. Neurosci. *8*, 45–56.

Batra, R., Charizanis, K., Manchanda, M., Mohan, A., Li, M., Finn, D.J., Goodwin, M., Zhang, C., Sobczak, K., Thornton, C.A., et al. (2014). Loss of MBNL leads to disruption of developmentally regulated alternative polyadenylation in RNA-mediated disease. Mol. Cell *56*, 311–322.

Baudouin, S., and Scheiffele, P. (2010). SnapShot: Neuroligin-neurexin complexes. Cell *141*, 908–908.e1.

Beffert, U., Weeber, E.J., Durudas, A., Qiu, S., Masiulis, I., Sweatt, J.D., Li, W.-P., Adelmann, G., Frotscher, M., Hammer, R.E., et al. (2005). Modulation of Synaptic Plasticity and Memory by Reelin Involves Differential Splicing of the Lipoprotein Receptor Apoer2. Neuron *47*, 567–579.

Belforte, J.E., Zsiros, V., Sklar, E.R., Jiang, Z., Yu, G., Li, Y., Quinlan, E.M., and Nakazawa, K. (2010). Postnatal NMDA receptor ablation in corticolimbic interneurons confers schizophrenia-like phenotypes. Nat Neurosci *13*, 76–83.

Bhalla, K., Phillips, H.A., Crawford, J., McKenzie, O.L.D., Mulley, J.C., Eyre, H., Gardner, A.E., Kremmidiotis, G., and Callen, D.F. (2004). The de novo chromosome 16 translocations of two patients with abnormal phenotypes (mental retardation and epilepsy) disrupt the A2BP1 gene. J. Hum. Genet. *49*, 308–311.

Bill, B.R., Lowe, J.K., Dybuncio, C.T., and Fogel, B.L. (2013). Orchestration of neurodevelopmental programs by RBFOX1: implications for autism spectrum disorder. Int. Rev. Neurobiol. *113*, 251–267.

Black, D.L. (2003). M ECHANISMS OFA LTERNATIVEP RE-M ESSENGERRNA S PLICING. Annu. Rev. Biochem. *72*, 291–336.

Blencowe, B.J., Ahmad, S., and Lee, L.J. (2009). Current-generation high-throughput sequencing: deepening insights into mammalian transcriptomes. Genes Dev. *23*, 1379–1386.

Bock, H.H., Jossin, Y., May, P., Bergner, O., and Herz, J. (2004). Apolipoprotein E receptors are required for reelin-induced proteasomal degradation of the neuronal adaptor protein Disabled-1. J. Biol. Chem. *279*, 33471–33479.

Boutz, P.L., Stoilov, P., Li, Q., Lin, C.-H., Chawla, G., Ostrow, K., Shiue, L., Ares, M., and Black, D.L. (2007). A post-transcriptional regulatory switch in polypyrimidine tract-binding proteins reprograms alternative splicing in developing neurons. Genes Dev. *21*, 1636–1652.

Brennan, C.M., and Steitz, J.A. (2001). HuR and mRNA stability. Cell. Mol. Life Sci. *58*, 266–277.

Buchner, D.A., Trudeau, M., and Meisler, M.H. (2003). SCNM1, a putative RNA splicing factor that modifies disease severity in mice. Science *301*, 967–969.

Budini, M., Romano, V., Quadri, Z., Buratti, E., and Baralle, F.E. (2015). TDP-43 loss of cellular function through aggregation requires additional structural determinants beyond its C-terminal Q/N prion-like domain. Human Molecular Genetics *24*, 9–20.

Buratti, E., and Baralle, F.E. (2012). TDP-43: gumming up neurons through protein-protein and protein-RNA interactions. Trends Biochem. Sci. *37*, 237–247.

Burgess, R.W., Nguyen, Q.T., Son, Y.J., Lichtman, J.W., and Sanes, J.R. (1999). Alternatively spliced isoforms of nerve- and muscle-derived agrin: their roles at the neuromuscular junction. Neuron *23*, 33–44.

Buzsáki, G., and Wang, X.-J. (2012). Mechanisms of gamma oscillations. Annu. Rev. Neurosci. *35*, 203–225.

Calarco, J.A., Zhen, M., and Blencowe, B.J. (2011). Networking in a global world: Establishing functional connections between neural splicing regulators and their target transcripts. Rna *17*, 775–791.

Caldwell, J.H., Schaller, K.L., Lasher, R.S., Peles, E., and Levinson, S.R. (2000). Sodium channel Na(v)1.6 is localized at nodes of ranvier, dendrites, and synapses. Proc. Natl. Acad. Sci. U.S.a. *97*, 5616–5620.

Cardin, J.A., Carlén, M., Meletis, K., Knoblich, U., Zhang, F., Deisseroth, K., Tsai, L.-H., and Moore, C.I. (2009). Driving fast-spiking cells induces gamma rhythm and controls sensory responses. Nature *459*, 663–667.

Carlén, M., Meletis, K., Siegle, J.H., Cardin, J.A., Futai, K., Vierling-Claassen, D., Rühlmann, C., Jones, S.R., Deisseroth, K., Sheng, M., et al. (2012). A critical role for NMDA receptors in parvalbumin interneurons for gamma rhythm induction and behavior. Mol. Psychiatry *17*, 537–548.

Carreira-Rosario, A., Bhargava, V., Hillebrand, J., Kollipara, R.K., Ramaswami, M., and Buszczak, M. (2016). Repression of Pumilio Protein Expression by Rbfox1 Promotes Germ Cell Differentiation. Dev. Cell *36*, 562–571.

Cayouette, M., and Raff, M. (2002). Asymmetric segregation of Numb: a mechanism for neural specification from Drosophila to mammals. Nat Neurosci *5*, 1265–1269.

Chao, H.-T., Chen, H., Samaco, R.C., Xue, M., Chahrour, M., Yoo, J., Neul, J.L., Gong, S., Lu, H.-C., Heintz, N., et al. (2010). Dysfunction in GABA signalling mediates autism-like stereotypies and Rett syndrome phenotypes. Nature *468*, 263–269.

Chapman, A.G., Woodburn, V.L., Woodruff, G.N., and Meldrum, B.S. (1996). Anticonvulsant effect of reduced NMDA receptor expression in audiogenic DBA/2 mice. Epilepsy Res. *26*, 25–35.

Cheong, M.A., and Steel, K.P. (2002). Early development and degeneration of vestibular hair cells in bronx waltzer mutant mice. Hear. Res. *164*, 179–189.

Chih, B., Gollan, L., and Scheiffele, P. (2006). Alternative splicing controls selective trans-synaptic interactions of the neuroligin-neurexin complex. Neuron *51*, 171–178.

Christensen, D.L., Baio, J., Van Naarden Braun, K., Bilder, D., Charles, J., Constantino, J.N., Daniels, J., Durkin, M.S., Fitzgerald, R.T., Kurzius-Spencer, M., et al. (2016). Prevalence and Characteristics of Autism Spectrum Disorder Among Children Aged 8 Years--Autism and Developmental Disabilities Monitoring Network, 11 Sites, United States, 2012. MMWR Surveill Summ *65*, 1–23.

Colgin, L.L., and Moser, E.I. (2010). Gamma oscillations in the hippocampus. Physiology (Bethesda) *25*, 319–329.

Conaco, C., Otto, S., Han, J.-J., and Mandel, G. (2006). Reciprocal actions of REST and a microRNA promote neuronal identity. Proc. Natl. Acad. Sci. U.S.a. *103*, 2422–2427.

Conboy, J.G. (2017). Developmental regulation of RNA processing by Rbfox proteins. Wiley Interdiscip Rev RNA *8*, e1398.

Coolen, M., Katz, S., and Bally-Cuif, L. (2013). miR-9: a versatile regulator of neurogenesis. Front Cell Neurosci *7*, 220.

Corradini, I., Verderio, C., Sala, M., Wilson, M.C., and Matteoli, M. (2009). SNAP-25 in neuropsychiatric disorders. Ann. N. Y. Acad. Sci. *1152*, 93–99.

Craig, A.M., and Kang, Y. (2007). Neurexin-neuroligin signaling in synapse development. Current Opinion in Neurobiology *17*, 43–52.

Da Cruz, S., and Cleveland, D.W. (2011). Understanding the role of TDP-43 and FUS/TLS in ALS and beyond. Current Opinion in Neurobiology *21*, 904–919.

Dajas-Bailador, F., Bonev, B., Garcez, P., Stanley, P., Guillemot, F., and Papalopulu, N. (2012). microRNA-9 regulates axon extension and branching by targeting Map1b in mouse cortical neurons. Nat Neurosci *15*, 697–699.

Damianov, A., and Black, D.L. (2010). Autoregulation of Fox protein expression to produce dominant negative splicing factors. Rna *16*, 405–416.

Damianov, A., Ying, Y., Lin, C.-H., Lee, J.-A., Tran, D., Vashisht, A.A., Bahrami-Samani, E., Xing, Y., Martin, K.C., Wohlschlegel, J.A., et al. (2016). Rbfox Proteins Regulate Splicing as Part of a Large Multiprotein Complex LASR. Cell *165*, 606–619.

Darbelli, L., Vogel, G., Almazan, G., and Richard, S. (2016). Quaking Regulates Neurofascin 155 Expression for Myelin and Axoglial Junction Maintenance. Journal of Neuroscience *36*, 4106–4120.

Darnell, R.B. (2013a). RNA protein interaction in neurons. Annu. Rev. Neurosci. *36*, 243–270.

Darnell, R.B. (2013b). RNA protein interaction in neurons. Annu. Rev. Neurosci. *36*, 243–270.

Darnell, R.B., and Posner, J.B. (2003). Paraneoplastic syndromes involving the nervous system. N. Engl. J. Med. *349*, 1543–1554.

Deák, F., Shin, O.-H., Kavalali, E.T., and Südhof, T.C. (2006). Structural determinants of synaptobrevin 2 function in synaptic vesicle fusion. Journal of Neuroscience *26*, 6668–6676.

DeBoer, E.M., Azevedo, R., Vega, T.A., Brodkin, J., Akamatsu, W., Okano, H., Wagner, G.C., and Rasin, M.-R. (2014). Prenatal deletion of the RNA-binding protein HuD disrupts postnatal cortical circuit maturation and behavior. Journal of Neuroscience *34*, 3674–3686.

Decker, C.J., and Parker, R. (2012). P-bodies and stress granules: possible roles in the control of translation and mRNA degradation. Cold Spring Harbor Perspectives in Biology *4*, a012286–a012286.

Delaloy, C., Liu, L., Lee, J.-A., Su, H., Shen, F., Yang, G.-Y., Young, W.L., Ivey, K.N., and Gao, F.-B. (2010). MicroRNA-9 coordinates proliferation and migration of human embryonic stem cell-derived neural progenitors. Cell Stem Cell *6*, 323–335.

Deol, M.S., and Gluecksohn-Waelsch, S. (1979). The role of inner hair cells in hearing. Nature *278*, 250–252.

Di Fruscio, M., Chen, T., and Richard, S. (1999). Characterization of Sam68-like mammalian proteins SLM-1 and SLM-2: SLM-1 is a Src substrate during mitosis. Proc. Natl. Acad. Sci. U.S.a. *96*, 2710–2715.

Dimidschstein, J., Chen, Q., Tremblay, R., Rogers, S.L., Saldi, G.-A., Guo, L., Xu, Q., Liu, R., Lu, C., Chu, J., et al. (2016). A viral strategy for targeting and manipulating interneurons across vertebrate species. Nat Neurosci *19*, 1743–1749.

Donnelly, C.J., Park, M., Spillane, M., Yoo, S., Pacheco, A., Gomes, C., Vuppalanchi, D., McDonald, M., Kim, H.H., Kim, H.K., et al. (2013). Axonally synthesized β-actin and GAP-43 proteins support distinct modes of axonal growth. Journal of Neuroscience *33*,

3311–3322.

Dredge, B.K., Stefani, G., Engelhard, C.C., and Darnell, R.B. (2005). Nova autoregulation reveals dual functions in neuronal splicing. Embo J *24*, 1608–1620.

Du, H., Cline, M.S., Osborne, R.J., Tuttle, D.L., Clark, T.A., Donohue, J.P., Hall, M.P., Shiue, L., Swanson, M.S., Thornton, C.A., et al. (2010). Aberrant alternative splicing and extracellular matrix gene expression in mouse models of myotonic dystrophy. Nat. Struct. Mol. Biol. *17*, 187–193.

Ehrmann, I., Dalgliesh, C., Liu, Y., Danilenko, M., Crosier, M., Overman, L., Arthur, H.M., Lindsay, S., Clowry, G.J., Venables, J.P., et al. (2013). The tissue-specific RNA binding protein T-STAR controls regional splicing patterns of neurexin pre-mRNAs in the brain. PLoS Genet. *9*, e1003474.

Eom, T., Zhang, C., Wang, H., Lay, K., Fak, J., Noebels, J.L., and Darnell, R.B. (2013). NOVA-dependent regulation of cryptic NMD exons controls synaptic protein levels after seizure. Elife *2*, e00178–e00178.

Fagg, W.S., Liu, N., Fair, J.H., Shiue, L., Katzman, S., Donohue, J.P., and Ares, M. (2017). Autogenous cross-regulation of Quaking mRNA processing and translation balances Quaking functions in splicing and translation. Genes Dev. *31*, 1894–1909.

Feng, L., Allen, N.S., Simo, S., and Cooper, J.A. (2007). Cullin 5 regulates Dab1 protein levels and neuron positioning during cortical development. Genes Dev. *21*, 2717–2730.

Ferecskó, A.S., Jiruska, P., Foss, L., Powell, A.D., Chang, W.-C., Sik, A., and Jefferys, J.G.R. (2015). Structural and functional substrates of tetanus toxin in an animal model of temporal lobe epilepsy. Brain Struct Funct *220*, 1013–1029.

Förster, E., Bock, H.H., Herz, J., Chai, X., Frotscher, M., and Zhao, S. (2010). Emerging topics in Reelin function. Eur. J. Neurosci. *31*, 1511–1518.

Friedman, R.C., Farh, K.K.-H., Burge, C.B., and Bartel, D.P. (2009). Most mammalian mRNAs are conserved targets of microRNAs. Genome Res. *19*, 92–105.

Fritschy, J.-M. (2008). Epilepsy, E/I Balance and GABA(A) Receptor Plasticity. Front Mol Neurosci *1*, 5.

Fu, A.K.Y., Hung, K.-W., Fu, W.-Y., Shen, C., Chen, Y., Xia, J., Lai, K.-O., and Ip, N.Y. (2011). APC(Cdh1) mediates EphA4-dependent downregulation of AMPA receptors in homeostatic plasticity. Nat Neurosci *14*, 181–189.

Fu, X.-D., and Ares, M. (2014). Context-dependent control of alternative splicing by RNA-binding proteins. Nat Rev Genet *15*, 689–701.

Fujioka, Y., Ishigaki, S., Masuda, A., Iguchi, Y., Udagawa, T., Watanabe, H., Katsuno, M., Ohno, K., and Sobue, G. (2013). FUS-regulated region- and cell-type-specific

transcriptome is associated with cell selectivity in ALS/FTLD. Sci Rep *3*, 2388.

Gao, Z., Poon, H.Y., Li, L., Li, X., Palmesino, E., Glubrecht, D.D., Colwill, K., Dutta, I., Kania, A., Pawson, T., et al. (2012). Splice-mediated motif switching regulates disabled-1 phosphorylation and SH2 domain interactions. Molecular and Cellular Biology *32*, 2794–2808.

Gautam, M., Noakes, P.G., Moscoso, L., Rupp, F., Scheller, R.H., Merlie, J.P., and Sanes, J.R. (1996). Defective neuromuscular synaptogenesis in agrin-deficient mutant mice. Cell *85*, 525–535.

Gehman, L.T., Meera, P., Stoilov, P., Shiue, L., O'Brien, J.E., Meisler, M.H., Ares, M., Otis, T.S., and Black, D.L. (2012). The splicing regulator Rbfox2 is required for both cerebellar development and mature motor function. Genes Dev. *26*, 445–460.

Gehman, L.T., Stoilov, P., Maguire, J., Damianov, A., Lin, C.-H., Shiue, L., Ares, M., Mody, I., and Black, D.L. (2011). The splicing regulator Rbfox1 (A2BP1) controls neuronal excitation in the mammalian brain. Nature Publishing Group *43*, 706–711.

Gesemann, M., Denzer, A.J., and Ruegg, M.A. (1995). Acetylcholine receptor-aggregating activity of agrin isoforms and mapping of the active site. The Journal of Cell Biology *128*, 625–636.

Gill, J., Park, Y., McGinnis, J.P., Perez-Sanchez, C., Blanchette, M., and Si, K. (2017). Regulated Intron Removal Integrates Motivational State and Experience. Cell *169*, 836–848.e15.

Giusti, S.A., Vogl, A.M., Brockmann, M.M., Vercelli, C.A., Rein, M.L., Trümbach, D., Wurst, W., Cazalla, D., Stein, V., Deussing, J.M., et al. (2014). MicroRNA-9 controls dendritic development by targeting REST. Elife *3*, 14.

Gogolla, N., Leblanc, J.J., Quast, K.B., Südhof, T.C., Fagiolini, M., and Hensch, T.K. (2009). Common circuit defect of excitatory-inhibitory balance in mouse models of autism. J Neurodev Disord *1*, 172–181.

Goodwin, M., Mohan, A., Batra, R., Lee, K.-Y., Charizanis, K., Gómez, F.J.F., Eddarkaoui, S., Sergeant, N., Buée, L., Kimura, T., et al. (2015). MBNL Sequestration by Toxic RNAs and RNA Misprocessing in the Myotonic Dystrophy Brain. Cell Rep *12*, 1159–1168.

Graf, E.R., Zhang, X., Jin, S.-X., Linhoff, M.W., and Craig, A.M. (2004). Neurexins induce differentiation of GABA and glutamate postsynaptic specializations via neuroligins. Cell *119*, 1013–1026.

Grange, J., Boyer, V., Fabian-Fine, R., Fredj, N.B., Sadoul, R., and Goldberg, Y. (2004). Somatodendritic localization and mRNA association of the splicing regulatory protein Sam68 in the hippocampus and cortex. J. Neurosci. Res. *75*, 654–666.

Grieco, T.M., Malhotra, J.D., Chen, C., Isom, L.L., and Raman, I.M. (2005). Open-channel block by the cytoplasmic tail of sodium channel beta4 as a mechanism for resurgent sodium current. Neuron *45*, 233–244.

Grimson, A., Farh, K.K.-H., Johnston, W.K., Garrett-Engele, P., Lim, L.P., and Bartel, D.P. (2007). MicroRNA targeting specificity in mammals: determinants beyond seed pairing. Mol. Cell *27*, 91–105.

Haenschel, C., Bittner, R.A., Waltz, J., Haertling, F., Wibral, M., Singer, W., Linden, D.E.J., and Rodriguez, E. (2009). Cortical oscillatory activity is critical for working memory as revealed by deficits in early-onset schizophrenia. Journal of Neuroscience *29*, 9481–9489.

Hammer, M., Krueger-Burg, D., Tuffy, L.P., Cooper, B.H., Taschenberger, H., Goswami, S.P., Ehrenreich, H., Jonas, P., Varoqueaux, F., Rhee, J.-S., et al. (2015). Perturbed Hippocampal Synaptic Inhibition and γ-Oscillations in a Neuroligin-4 Knockout Mouse Model of Autism. Cell Rep *13*, 516–523.

Hammock, E.A.D., and Levitt, P. (2011). Developmental Expression Mapping of a Gene Implicated in Multiple Neurodevelopmental Disorders, *A2bp1 (Fox1)*. Dev Neurosci *33*, 64–74.

Haraguchi, T., Ozaki, Y., and Iba, H. (2009). Vectors expressing efficient RNA decoys achieve the long-term suppression of specific microRNA activity in mammalian cells. Nucleic Acids Research *37*, e43–e43.

Hardy, R.J., Loushin, C.L., Friedrich, V.L., Chen, Q., Ebersole, T.A., Lazzarini, R.A., and Artzt, K. (1996). Neural cell type-specific expression of QKI proteins is altered in quakingviable mutant mice. J. Neurosci. *16*, 7941–7949.

Hatten, M.E., and Heintz, N. (1995). Mechanisms of neural patterning and specification in the developing cerebellum. Annu. Rev. Neurosci. *18*, 385–408.

Hicks, G.G., Singh, N., Nashabi, A., Mai, S., Bozek, G., Klewes, L., Arapovic, D., White, E.K., Koury, M.J., Oltz, E.M., et al. (2000). Fus deficiency in mice results in defective B-lymphocyte development and activation, high levels of chromosomal instability and perinatal death. Nat Genet *24*, 175–179.

Hinman, M.N., and Lou, H. (2008). Diverse molecular functions of Hu proteins. Cell. Mol. Life Sci. *65*, 3168–3181.

Howell, V.M., De Haan, G., Bergren, S., Jones, J.M., Culiat, C.T., Michaud, E.J., Frankel, W.N., and Meisler, M.H. (2008). A targeted deleterious allele of the splicing factor SCNM1 in the mouse. Genetics *180*, 1419–1427.

Hu, H., Gan, J., and Jonas, P. (2014). Interneurons. Fast-spiking, parvalbumin^{+} GABAergic interneurons: from cellular design to microcircuit function. Science *345*, 1255263–1255263.

Huang, C., Zhou, H., Tong, J., Chen, H., Liu, Y.-J., Wang, D., Wei, X., and Xia, X.-G. (2011). FUS transgenic rats develop the phenotypes of amyotrophic lateral sclerosis and frontotemporal lobar degeneration. PLoS Genet. *7*, e1002011.

Huang, C.S., Shi, S.-H., Ule, J., Ruggiu, M., Barker, L.A., Darnell, R.B., Jan, Y.N., and Jan, L.Y. (2005). Common molecular pathways mediate long-term potentiation of synaptic excitation and slow synaptic inhibition. Cell *123*, 105–118.

Hunt, M.J., Kopell, N.J., Traub, R.D., and Whittington, M.A. (2017). Aberrant Network Activity in Schizophrenia. Trends in Neurosciences *40*, 371–382.

Hwang, H.-W., Saito, Y., Park, C.Y., Blachère, N.E., Tajima, Y., Fak, J.J., Zucker-Scharff, I., and Darnell, R.B. (2017). cTag-PAPERCLIP Reveals Alternative Polyadenylation Promotes Cell-Type Specific Protein Diversity and Shifts Araf Isoforms with Microglia Activation. Neuron *95*, 1334–1349.e1335.

Iijima, T., Iijima, Y., Witte, H., and Scheiffele, P. (2014). Neuronal cell type-specific alternative splicing is regulated by the KH domain protein SLM1. The Journal of Cell Biology *204*, 331–342.

Iko, Y., Kodama, T.S., Kasai, N., Oyama, T., Morita, E.H., Muto, T., Okumura, M., Fujii, R., Takumi, T., Tate, S.-I., et al. (2004). Domain architectures and characterization of an RNA-binding protein, TLS. J. Biol. Chem. *279*, 44834–44840.

Ince-Dunn, G., Okano, H.J., Jensen, K.B., Park, W.-Y., Zhong, R., Ule, J., Mele, A., Fak, J.J., Yang, C., Zhang, C., et al. (2012). Neuronal Elav-like (Hu) Proteins Regulate RNA Splicing and Abundance to Control Glutamate Levels and Neuronal Excitability. Neuron *75*, 1067–1080.

Irimia, M., and Blencowe, B.J. (2012). Alternative splicing: decoding an expansive regulatory layer. Current Opinion in Cell Biology *24*, 323–332.

Isaacson, J.S., and Scanziani, M. (2011). How inhibition shapes cortical activity. Neuron *72*, 231–243.

Jacque, C., Delassalle, A., Raoul, M., and Baumann, N. (1983). Myelin basic protein deposition in the optic and sciatic nerves of dysmyelinating mutants quaking, jimpy, Trembler, mld, and shiverer during development. Journal of Neurochemistry *41*, 1335–1340.

Jangi, M., and Sharp, P.A. (2014). Building robust transcriptomes with master splicing factors. Cell *159*, 487–498.

Jensen, K.B., Dredge, B.K., Stefani, G., Zhong, R., Buckanovich, R.J., Okano, H.J., Yang, Y.Y., and Darnell, R.B. (2000). Nova-1 regulates neuron-specific alternative splicing and is essential for neuronal viability. Neuron *25*, 359–371.

Jia, Y., Mu, J.C., and Ackerman, S.L. (2012). Mutation of a U2 snRNA gene causes

global disruption of alternative splicing and neurodegeneration. Cell *148*, 296–308.

Jiang, X., Lachance, M., and Rossignol, E. (2016). Involvement of cortical fast-spiking parvalbumin-positive basket cells in epilepsy. Prog. Brain Res. *226*, 81–126.

Jin, Y., Suzuki, H., Maegawa, S., Endo, H., Sugano, S., Hashimoto, K., Yasuda, K., and Inoue, K. (2003). A vertebrate RNA-binding protein Fox-1 regulates tissue-specific splicing via the pentanucleotide GCAUG. Embo J *22*, 905–912.

Johansson, J.U., Ericsson, J., Janson, J., Beraki, S., Stanić, D., Mandic, S.A., Wikström, M.A., Hökfelt, T., Ogren, S.O., Rozell, B., et al. (2008). An ancient duplication of exon 5 in the Snap25 gene is required for complex neuronal development/function. PLoS Genet. *4*, e1000278.

Johnson, B.S., McCaffery, J.M., Lindquist, S., and Gitler, A.D. (2008). A yeast TDP-43 proteinopathy model: Exploring the molecular determinants of TDP-43 aggregation and cellular toxicity. Proceedings of the National Academy of Sciences *105*, 6439–6444.

Johnson, B.S., Snead, D., Lee, J.J., McCaffery, J.M., Shorter, J., and Gitler, A.D. (2009). TDP-43 is intrinsically aggregation-prone, and amyotrophic lateral sclerosis-linked mutations accelerate aggregation and increase toxicity. J. Biol. Chem. *284*, 20329–20339.

Johnson, J.O., Pioro, E.P., Boehringer, A., Chia, R., Feit, H., Renton, A.E., Pliner, H.A., Abramzon, Y., Marangi, G., Winborn, B.J., et al. (2014). Mutations in the Matrin 3 gene cause familial amyotrophic lateral sclerosis. Nat Neurosci *17*, 664–666.

Jonas, P., Bischofberger, J., Fricker, D., and Miles, R. (2004). Interneuron Diversity series: Fast in, fast out--temporal and spatial signal processing in hippocampal interneurons. Trends in Neurosciences *27*, 30–40.

Jurgensen, S., and Castillo, P.E. (2015). Selective Dysregulation of Hippocampal Inhibition in the Mouse Lacking Autism Candidate Gene CNTNAP2. Journal of Neuroscience *35*, 14681–14687.

Kanadia, R.N., Johnstone, K.A., Mankodi, A., Lungu, C., Thornton, C.A., Esson, D., Timmers, A.M., Hauswirth, W.W., and Swanson, M.S. (2003). A muscleblind knockout model for myotonic dystrophy. Science *302*, 1978–1980.

Kang, H.J., Kawasawa, Y.I., Cheng, F., Zhu, Y., Xu, X., Li, M., Sousa, A.M.M., Pletikos, M., Meyer, K.A., Sedmak, G., et al. (2011). Spatio-temporal transcriptome of the human brain. Nature *478*, 483–489.

Kearney, J.A., Buchner, D.A., De Haan, G., Adamska, M., Levin, S.I., Furay, A.R., Albin, R.L., Jones, J.M., Montal, M., Stevens, M.J., et al. (2002). Molecular and pathological effects of a modifier gene on deficiency of the sodium channel Scn8a (Na(v)1.6). Human Molecular Genetics *11*, 2765–2775.

Kim, H.J., Kim, N.C., Wang, Y.-D., Scarborough, E.A., Moore, J., Diaz, Z., MacLea, K.S., Freibaum, B., Li, S., Molliex, A., et al. (2013). Mutations in prion-like domains in hnRNPA2B1 and hnRNPA1 cause multisystem proteinopathy and ALS. Nature *495*, 467–473.

Klein, M.E., Castillo, P.E., and Jordan, B.A. (2015). Coordination between Translation and Degradation Regulates Inducibility of mGluR-LTD. Cell Rep *10*, 1459–1466.

Klein, M.E., Younts, T.J., Castillo, P.E., and Jordan, B.A. (2013). RNA-binding protein Sam68 controls synapse number and local β-actin mRNA metabolism in dendrites. Proceedings of the National Academy of Sciences *110*, 3125–3130.

Knoblich, J.A. (2010). Asymmetric cell division: recent developments and their implications for tumour biology. Nat. Rev. Mol. Cell Biol. *11*, 849–860.

Koch, S., Strasser, V., Hauser, C., Fasching, D., Brandes, C., Bajari, T.M., Schneider, W.J., and Nimpf, J. (2002). A secreted soluble form of ApoE receptor 2 acts as a dominant-negative receptor and inhibits Reelin signaling. Embo J *21*, 5996–6004.

Kohrman, D.C., Harris, J.B., and Meisler, M.H. (1996). Mutation detection in the med and medJ alleles of the sodium channel Scn8a. Unusual splicing due to a minor class AT-AC intron. J. Biol. Chem. *271*, 17576–17581.

Korotkova, T., Fuchs, E.C., Ponomarenko, A., Engelhardt, von, J., and Monyer, H. (2010). NMDA receptor ablation on parvalbumin-positive interneurons impairs hippocampal synchrony, spatial representations, and working memory. Neuron *68*, 557–569.

König, J., Zarnack, K., Luscombe, N.M., and Ule, J. (2011). Protein-RNA interactions: new genomic technologies and perspectives. Nat Rev Genet *13*, 77–83.

Kraemer, B.C., Schuck, T., Wheeler, J.M., Robinson, L.C., Trojanowski, J.Q., Lee, V.M.-Y., and Schellenberg, G.D. (2010). Loss of murine TDP-43 disrupts motor function and plays an essential role in embryogenesis. Acta Neuropathol. *119*, 409–419.

Kriegstein, A.R., and Noctor, S.C. (2004). Patterns of neuronal migration in the embryonic cortex. Trends in Neurosciences *27*, 392–399.

Kuroyanagi, H. (2009). Fox-1 family of RNA-binding proteins. Cell. Mol. Life Sci. *66*, 3895–3907.

Lagier-Tourenne, C., Polymenidou, M., and Cleveland, D.W. (2010). TDP-43 and FUS/TLS: emerging roles in RNA processing and neurodegeneration. Human Molecular Genetics *19*, R46–R64.

Lal, D., Pernhorst, K., Klein, K.M., Reif, P., Tozzi, R., Toliat, M.R., Winterer, G., Neubauer, B., Nürnberg, P., Rosenow, F., et al. (2015a). Extending the phenotypic spectrum of RBFOX1 deletions: Sporadic focal epilepsy. Epilepsia *56*, n/a–n/a.

Lal, D., Pernhorst, K., Klein, K.M., Reif, P., Tozzi, R., Toliat, M.R., Winterer, G., Neubauer, B., Nürnberg, P., Rosenow, F., et al. (2015b). Extending the phenotypic spectrum of RBFOX1 deletions: Sporadic focal epilepsy. Epilepsia *56*, e129–e133.

Lal, D., Reinthaler, E.M., Altmüller, J., Toliat, M.R., Thiele, H., Nürnberg, P., Lerche, H., Hahn, A., Møller, R.S., Muhle, H., et al. (2013a). RBFOX1 and RBFOX3 Mutations in Rolandic Epilepsy. PLoS ONE *8*, e73323.

Lal, D., Reinthaler, E.M., Altmüller, J., Toliat, M.R., Thiele, H., Nürnberg, P., Lerche, H., Hahn, A., Møller, R.S., Muhle, H., et al. (2013b). RBFOX1 and RBFOX3 mutations in rolandic epilepsy. PLoS ONE *8*, e73323.

Lal, D., Trucks, H., Møller, R.S., Hjalgrim, H., Koeleman, B.P.C., de Kovel, C.G.F., Visscher, F., Weber, Y.G., Lerche, H., Becker, F., et al. (2013c). Rare exonic deletions of the RBFOX1 gene increase risk of idiopathic generalized epilepsy. Epilepsia *54*, 265–271.

Larocque, D., Pilotte, J., Chen, T., Cloutier, F., Massie, B., Pedraza, L., Couture, R., Lasko, P., Almazan, G., and Richard, S. (2002). Nuclear retention of MBP mRNAs in the quaking viable mice. Neuron *36*, 815–829.

Larouche, M., Beffert, U., Herz, J., and Hawkes, R. (2008). The Reelin receptors Apoer2 and Vldlr coordinate the patterning of Purkinje cell topography in the developing mouse cerebellum. PLoS ONE *3*, e1653.

Lee, E.B., Lee, V.M.-Y., and Trojanowski, J.Q. (2012). Gains or losses: molecular mechanisms of TDP43-mediated neurodegeneration. Nat. Rev. Neurosci. *13*, 38–50.

Lee, J.A., Tang, Z.Z., and Black, D.L. (2009). An inducible change in Fox-1/A2BP1 splicing modulates the alternative splicing of downstream neuronal target exons. Genes Dev. *23*, 2284–2293.

Lee, J.-A., Damianov, A., Lin, C.-H., Fontes, M., Parikshak, N.N., Anderson, E.S., Geschwind, D.H., Black, D.L., and Martin, K.C. (2016a). Cytoplasmic Rbfox1 Regulates the Expression of Synaptic and Autism-Related Genes. Neuron *89*, 113–128.

Lee, J.-A., Damianov, A., Lin, C.-H., Fontes, M., Parikshak, N.N., Anderson, E.S., Geschwind, D.H., Black, D.L., and Martin, K.C. (2016b). Cytoplasmic Rbfox1 Regulates the Expression of Synaptic and Autism-Related Genes. Neuron *89*, 113–128.

Lee, J., Chung, C., Ha, S., Lee, D., Kim, D.-Y., Kim, H., and Kim, E. (2015). Shank3-mutant mice lacking exon 9 show altered excitation/inhibition balance, enhanced rearing, and spatial memory deficit. Front Cell Neurosci *9*, 94.

Lee, Y., and Rio, D.C. (2015). Mechanisms and Regulation of Alternative Pre-mRNA Splicing. Annu. Rev. Biochem. *84*, 291–323.

Levin, S.I., Khaliq, Z.M., Aman, T.K., Grieco, T.M., Kearney, J.A., Raman, I.M., and

Meisler, M.H. (2006). Impaired motor function in mice with cell-specific knockout of sodium channel Scn8a (NaV1.6) in cerebellar purkinje neurons and granule cells. J. Neurophysiol. *96*, 785–793.

Lewis, B.P., Burge, C.B., and Bartel, D.P. (2005). Conserved seed pairing, often flanked by adenosines, indicates that thousands of human genes are microRNA targets. Cell *120*, 15–20.

Lewis, D.A., Curley, A.A., Glausier, J.R., and Volk, D.W. (2012). Cortical parvalbumin interneurons and cognitive dysfunction in schizophrenia. Trends in Neurosciences *35*, 57–67.

Li, Q., Lee, J.-A., and Black, D.L. (2007). Neuronal regulation of alternative pre-mRNA splicing. Nat. Rev. Neurosci. *8*, 819–831.

Li, Q., Zheng, S., Han, A., Lin, C.-H., Stoilov, P., Fu, X.-D., and Black, D.L. (2014). The splicing regulator PTBP2 controls a program of embryonic splicing required for neuronal maturation. Elife *3*, e01201–e01201.

Li, Z., Zhang, Y., Li, D., and Feng, Y. (2000). Destabilization and mislocalization of myelin basic protein mRNAs in quaking dysmyelination lacking the QKI RNA-binding proteins. Journal of Neuroscience *20*, 4944–4953.

Licatalosi, D.D., Yano, M., Fak, J.J., Mele, A., Grabinski, S.E., Zhang, C., and Darnell, R.B. (2012). Ptbp2 represses adult-specific splicing to regulate the generation of neuronal precursors in the embryonic brain. Genes Dev. *26*, 1626–1642.

Lin, X., Miller, J.W., Mankodi, A., Kanadia, R.N., Yuan, Y., Moxley, R.T., Swanson, M.S., and Thornton, C.A. (2006). Failure of MBNL1-dependent post-natal splicing transitions in myotonic dystrophy. Human Molecular Genetics *15*, 2087–2097.

Linares, A.J., Lin, C.-H., Damianov, A., Adams, K.L., Novitch, B.G., and Black, D.L. (2015). The splicing regulator PTBP1 controls the activity of the transcription factor Pbx1 during neuronal differentiation. Elife *4*, 6778.

Lindsley, R.C., and Ebert, B.L. (2013). Molecular pathophysiology of myelodysplastic syndromes. Annu Rev Pathol *8*, 21–47.

Ling, S.-C., Polymenidou, M., and Cleveland, D.W. (2013). Converging mechanisms in ALS and FTD: disrupted RNA and protein homeostasis. Neuron *79*, 416–438.

Lisman, J.E., and Jensen, O. (2013). The θ-γ neural code. Neuron *77*, 1002–1016.

Liu, D.-Z., Ander, B.P., Tian, Y., Stamova, B., Jickling, G.C., Davis, R.R., and Sharp, F.R. (2012). Integrated analysis of mRNA and microRNA expression in mature neurons, neural progenitor cells and neuroblastoma cells. Gene *495*, 120–127.

Liu, Y., Sugiura, Y., and Lin, W. (2011). The role of synaptobrevin1/VAMP1 in Ca2+-

triggered neurotransmitter release at the mouse neuromuscular junction. The Journal of Physiology *589*, 1603–1618.

Lovci, M.T., Ghanem, D., Marr, H., Arnold, J., Gee, S., Parra, M., Liang, T.Y., Stark, T.J., Gehman, L.T., Hoon, S., et al. (2013). Rbfox proteins regulate alternative mRNA splicing through evolutionarily conserved RNA bridges. Nat. Struct. Mol. Biol.

Lu, Z., Zhang, Y., Ku, L., Wang, H., Ahmadian, A., and Feng, Y. (2003). The quakingviable mutation affects qkI mRNA expression specifically in myelin-producing cells of the nervous system. Nucleic Acids Research *31*, 4616–4624.

Lukong, K.E., and Richard, S. (2003). Sam68, the KH domain-containing superSTAR. Biochim. Biophys. Acta *1653*, 73–86.

Lukong, K.E., and Richard, S. (2008). Motor coordination defects in mice deficient for the Sam68 RNA-binding protein. Behav. Brain Res. *189*, 357–363.

Mackenzie, I.R., Rademakers, R., and Neumann, M. (2010). TDP-43 and FUS in amyotrophic lateral sclerosis and frontotemporal dementia. Lancet Neurol *9*, 995–1007.

Makeyev, E.V., Zhang, J., Carrasco, M.A., and Maniatis, T. (2007). The MicroRNA miR-124 promotes neuronal differentiation by triggering brain-specific alternative pre-mRNA splicing. Mol. Cell *27*, 435–448.

Malmevik, J., Petri, R., Knauff, P., Brattås, P.L., Åkerblom, M., and Jakobsson, J. (2016). Distinct cognitive effects and underlying transcriptome changes upon inhibition of individual miRNAs in hippocampal neurons. Sci Rep *6*, 19879.

Marín, O. (2012). Interneuron dysfunction in psychiatric disorders. Nat. Rev. Neurosci. *13*, 107–120.

Martin, C.L., Duvall, J.A., Ilkin, Y., Simon, J.S., Arreaza, M.G., Wilkes, K., Alvarez-Retuerto, A., Whichello, A., Powell, C.M., Rao, K., et al. (2007). Cytogenetic and molecular characterization of A2BP1/FOX1 as a candidate gene for autism. Am. J. Med. Genet. B Neuropsychiatr. Genet. *144B*, 869–876.

Matera, A.G., and Wang, Z. (2014). A day in the life of the spliceosome. Nat. Rev. Mol. Cell Biol. *15*, 108–121.

Matter, N., Herrlich, P., and König, H. (2002). Signal-dependent regulation of splicing via phosphorylation of Sam68. Nature *420*, 691–695.

Mauger, O., Lemoine, F., and Scheiffele, P. (2016). Targeted Intron Retention and Excision for Rapid Gene Regulation in Response to Neuronal Activity. Neuron *92*, 1266–1278.

McKee, A.E., Minet, E., Stern, C., Riahi, S., Stiles, C.D., and Silver, P.A. (2005). A genome-wide in situ hybridization map of RNA-binding proteins reveals anatomically

restricted expression in the developing mouse brain. BMC Dev Biol *5*, 14.

Meisler, M.H., Kearney, J., Escayg, A., MacDonald, B.T., and Sprunger, L.K. (2001). Sodium channels and neurological disease: insights from Scn8a mutations in the mouse. Neuroscientist *7*, 136–145.

Merkin, J., Russell, C., Chen, P., and Burge, C.B. (2012). Evolutionary dynamics of gene and isoform regulation in Mammalian tissues. Science *338*, 1593–1599.

Meyer, S., Temme, C., and Wahle, E. (2004). Messenger RNA turnover in eukaryotes: pathways and enzymes. Crit. Rev. Biochem. Mol. Biol. *39*, 197–216.

Mulley, J.C., Scheffer, I.E., Petrou, S., and Berkovic, S.F. (2003). Channelopathies as a genetic cause of epilepsy. Curr. Opin. Neurol. *16*, 171–176.

Nakahata, S., and Kawamoto, S. (2005). Tissue-dependent isoforms of mammalian Fox-1 homologs are associated with tissue-specific splicing activities. Nucleic Acids Research *33*, 2078–2089.

Nakamura, T., Matsumoto, J., Takamura, Y., Ishii, Y., Sasahara, M., Ono, T., and Nishijo, H. (2015). Relationships among parvalbumin-immunoreactive neuron density, phase-locked gamma oscillations, and autistic/schizophrenic symptoms in PDGFR-β knock-out and control mice. PLoS ONE *10*, e0119258.

Nakano, Y., Jahan, I., Bonde, G., Sun, X., Hildebrand, M.S., Engelhardt, J.F., Smith, R.J.H., Cornell, R.A., Fritzsch, B., and Bánfi, B. (2012). A mutation in the Srrm4 gene causes alternative splicing defects and deafness in the Bronx waltzer mouse. PLoS Genet. *8*, e1002966.

Nguyen, T.-M., Schreiner, D., Xiao, L., Traunmüller, L., Bornmann, C., and Scheiffele, P. (2016). An alternative splicing switch shapes neurexin repertoires in principal neurons versus interneurons in the mouse hippocampus. Elife *5*, 997.

Nitkin, R.M., Smith, M.A., Magill, C., Fallon, J.R., Yao, Y.M., Wallace, B.G., and McMahan, U.J. (1987). Identification of agrin, a synaptic organizing protein from Torpedo electric organ. The Journal of Cell Biology *105*, 2471–2478.

Nussbacher, J.K., Batra, R., Lagier-Tourenne, C., and Yeo, G.W. (2015). RNA-binding proteins in neurodegeneration: Seq and you shall receive. Trends in Neurosciences *38*, 226–236.

Nystuen, A.M., Schwendinger, J.K., Sachs, A.J., Yang, A.W., and Haider, N.B. (2007). A null mutation in VAMP1/synaptobrevin is associated with neurological defects and prewean mortality in the lethal-wasting mouse mutant. Neurogenetics *8*, 1–10.

O'Brien, J.E., Drews, V.L., Jones, J.M., Dugas, J.C., Ben A Barres, and Meisler, M.H. (2012). Molecular and Cellular Neuroscience. Molecular and Cellular Neuroscience *49*, 120–126.

Palm, K., Metsis, M., and Timmusk, T. (1999). Neuron-specific splicing of zinc finger transcription factor REST/NRSF/XBR is frequent in neuroblastomas and conserved in human, mouse and rat. Brain Res. Mol. Brain Res. *72*, 30–39.

Papale, L.A., Beyer, B., Jones, J.M., Sharkey, L.M., Tufik, S., Epstein, M., Letts, V.A., Meisler, M.H., Frankel, W.N., and Escayg, A. (2009). Heterozygous mutations of the voltage-gated sodium channel SCN8A are associated with spike-wave discharges and absence epilepsy in mice. Human Molecular Genetics *18*, 1633–1641.

Parikshak, N.N., Swarup, V., Belgard, T.G., Irimia, M., Ramaswami, G., Gandal, M.J., Hartl, C., Leppa, V., Ubieta, L. de L.T., Huang, J., et al. (2016). Genome-wide changes in lncRNA, splicing, and regional gene expression patterns in autism. Nature *540*, 423–427.

Parker, R., and Sheth, U. (2007). P bodies and the control of mRNA translation and degradation. Mol. Cell *25*, 635–646.

Parker, R., and Song, H. (2004). The enzymes and control of eukaryotic mRNA turnover. Nat. Struct. Mol. Biol. *11*, 121–127.

Peça, J., Feliciano, C., Ting, J.T., Wang, W., Wells, M.F., Venkatraman, T.N., Lascola, C.D., Fu, Z., and Feng, G. (2011). Shank3 mutant mice display autistic-like behaviours and striatal dysfunction. Nature *472*, 437–442.

Peñagarikano, O., Abrahams, B.S., Herman, E.I., Winden, K.D., Gdalyahu, A., Dong, H., Sonnenblick, L.I., Gruver, R., Almajano, J., Bragin, A., et al. (2011). Absence of CNTNAP2 leads to epilepsy, neuronal migration abnormalities, and core autism-related deficits. Cell *147*, 235–246.

Perycz, M., Urbanska, A.S., Krawczyk, P.S., Parobczak, K., and Jaworski, J. (2011). Zipcode binding protein 1 regulates the development of dendritic arbors in hippocampal neurons. Journal of Neuroscience *31*, 5271–5285.

Plummer, N.W., McBurney, M.W., and Meisler, M.H. (1997). Alternative splicing of the sodium channel SCN8A predicts a truncated two-domain protein in fetal brain and non-neuronal cells. J. Biol. Chem. *272*, 24008–24015.

Poduri, A., Evrony, G.D., Cai, X., and Walsh, C.A. (2013). Somatic mutation, genomic variation, and neurological disease. Science *341*, 1237758–1237758.

Polymenidou, M., Lagier-Tourenne, C., Hutt, K.R., Bennett, C.F., Cleveland, D.W., and Yeo, G.W. (2012). Misregulated RNA processing in amyotrophic lateral sclerosis. Brain Res. *1462*, 3–15.

Polymenidou, M., Lagier-Tourenne, C., Hutt, K.R., Huelga, S.C., Moran, J., Liang, T.Y., Ling, S.-C., Sun, E., Wancewicz, E., Mazur, C., et al. (2011). Long pre-mRNA depletion and RNA missplicing contribute to neuronal vulnerability from loss of TDP-43. Nat Neurosci *14*, 459–468.

Ponthier, J.L., Schluepen, C., Chen, W., Lersch, R.A., Gee, S.L., Hou, V.C., Lo, A.J., Short, S.A., Chasis, J.A., Winkelmann, J.C., et al. (2006). Fox-2 splicing factor binds to a conserved intron motif to promote inclusion of protein 4.1R alternative exon 16. J. Biol. Chem. *281*, 12468–12474.

Pouille, F., and Scanziani, M. (2001). Enforcement of temporal fidelity in pyramidal cells by somatic feed-forward inhibition. Science *293*, 1159–1163.

Poulos, M.G., Batra, R., Charizanis, K., and Swanson, M.S. (2011). Developments in RNA splicing and disease. Cold Spring Harbor Perspectives in Biology *3*, a000778–a000778.

Qiu, Z., Sylwestrak, E.L., Lieberman, D.N., Zhang, Y., Liu, X.-Y., and Ghosh, A. (2012). The Rett syndrome protein MeCP2 regulates synaptic scaling. Journal of Neuroscience *32*, 989–994.

Quesnel-Vallières, M., Dargaei, Z., Irimia, M., Gonatopoulos-Pournatzis, T., Ip, J.Y., Wu, M., Sterne-Weiler, T., Nakagawa, S., Woodin, M.A., Blencowe, B.J., et al. (2016). Misregulation of an Activity-Dependent Splicing Network as a Common Mechanism Underlying Autism Spectrum Disorders. Mol. Cell *64*, 1023–1034.

Quesnel-Vallières, M., Irimia, M., Cordes, S.P., and Blencowe, B.J. (2015). Essential roles for the splicing regulator nSR100/SRRM4 during nervous system development. Genes Dev. *29*, 746–759.

Racca, C., Gardiol, A., Eom, T., Ule, J., Triller, A., and Darnell, R.B. (2010). The Neuronal Splicing Factor Nova Co-Localizes with Target RNAs in the Dendrite. Front Neural Circuits *4*, 5.

Radhu, N., Garcia Dominguez, L., Farzan, F., Richter, M.A., Semeralul, M.O., Chen, R., Fitzgerald, P.B., and Daskalakis, Z.J. (2015). Evidence for inhibitory deficits in the prefrontal cortex in schizophrenia. Brain *138*, 483–497.

Raj, B., and Blencowe, B.J. (2015). Alternative Splicing in the Mammalian Nervous System: Recent Insights into Mechanisms and Functional Roles. Neuron *87*, 14–27.

Raj, B., Irimia, M., Braunschweig, U., Sterne-Weiler, T., O'Hanlon, D., Lin, Z.-Y., Chen, G.I., Easton, L.E., Ule, J., Gingras, A.-C., et al. (2014). A global regulatory mechanism for activating an exon network required for neurogenesis. Mol. Cell *56*, 90–103.

Raj, B., O'Hanlon, D., Vessey, J.P., Pan, Q., Ray, D., Buckley, N.J., Miller, F.D., and Blencowe, B.J. (2011). Cross-regulation between an alternative splicing activator and a transcription repressor controls neurogenesis. Mol. Cell *43*, 843–850.

Raman, I.M., and Bean, B.P. (1997). Resurgent sodium current and action potential formation in dissociated cerebellar Purkinje neurons. J. Neurosci. *17*, 4517–4526.

Raman, I.M., Sprunger, L.K., Meisler, M.H., and Bean, B.P. (1997). Altered

subthreshold sodium currents and disrupted firing patterns in Purkinje neurons of Scn8a mutant mice. Neuron *19*, 881–891.

Ray, D., Kazan, H., Cook, K.B., Weirauch, M.T., Najafabadi, H.S., Li, X., Gueroussov, S., Albu, M., Zheng, H., Yang, A., et al. (2013). A compendium of RNA-binding motifs for decoding gene regulation. Nature *499*, 172–177.

Reist, N.E., Werle, M.J., and McMahan, U.J. (1992). Agrin released by motor neurons induces the aggregation of acetylcholine receptors at neuromuscular junctions. Neuron *8*, 865–868.

Rice, D.S., and Curran, T. (2001). Role of the reelin signaling pathway in central nervous system development. Annu. Rev. Neurosci. *24*, 1005–1039.

Rice, D.S., Sheldon, M., D'Arcangelo, G., Nakajima, K., Goldowitz, D., and Curran, T. (1998). Disabled-1 acts downstream of Reelin in a signaling pathway that controls laminar organization in the mammalian brain. Development *125*, 3719–3729.

Richard, S., Torabi, N., Franco, G.V., Tremblay, G.A., Chen, T., Vogel, G., Morel, M., Cléroux, P., Forget-Richard, A., Komarova, S., et al. (2005). Ablation of the Sam68 RNA binding protein protects mice from age-related bone loss. PLoS Genet. *1*, e74.

Rogelj, B., Easton, L.E., Bogu, G.K., Stanton, L.W., Rot, G., Curk, T., Zupan, B., Sugimoto, Y., Modic, M., Haberman, N., et al. (2012). Widespread binding of FUS along nascent RNA regulates alternative splicing in the brain. Sci Rep *2*, 603.

Rossbach, O., Hung, L.-H., Schreiner, S., Grishina, I., Heiner, M., Hui, J., and Bindereif, A. (2009). Auto- and cross-regulation of the hnRNP L proteins by alternative splicing. Molecular and Cellular Biology *29*, 1442–1451.

Ruggiu, M., Herbst, R., Kim, N., Jevsek, M., Fak, J.J., Mann, M.A., Fischbach, G., Burden, S.J., and Darnell, R.B. (2009). Rescuing Z+ agrin splicing in Nova null mice restores synapse formation and unmasks a physiologic defect in motor neuron firing. Proceedings of the National Academy of Sciences *106*, 3513–3518.

Sakai, K., Gofuku, M., Kitagawa, Y., Ogasawara, T., Hirose, G., Yamazaki, M., Koh, C.S., Yanagisawa, N., and Steinman, L. (1994). A hippocampal protein associated with paraneoplastic neurologic syndrome and small cell lung carcinoma. Biochem. Biophys. Res. Commun. *199*, 1200–1208.

Sanes, J.R., and Lichtman, J.W. (1999). Development of the vertebrate neuromuscular junction. Annu. Rev. Neurosci. *22*, 389–442.

Sasaki, Y., Welshhans, K., Wen, Z., Yao, J., Xu, M., Goshima, Y., Zheng, J.Q., and Bassell, G.J. (2010). Phosphorylation of zipcode binding protein 1 is required for brain-derived neurotrophic factor signaling of local beta-actin synthesis and growth cone turning. Journal of Neuroscience *30*, 9349–9358.

Sawicka, K., Bushell, M., Spriggs, K.A., and Willis, A.E. (2008). Polypyrimidine-tract-binding protein: a multifunctional RNA-binding protein. Biochem. Soc. Trans. *36*, 641–647.

Schoch, S., Deák, F., Königstorfer, A., Mozhayeva, M., Sara, Y., Südhof, T.C., and Kavalali, E.T. (2001). SNARE function analyzed in synaptobrevin/VAMP knockout mice. Science *294*, 1117–1122.

Sebat, J., Lakshmi, B., Malhotra, D., Troge, J., Lese-Martin, C., Walsh, T., Yamrom, B., Yoon, S., Krasnitz, A., Kendall, J., et al. (2007). Strong association of de novo copy number mutations with autism. Science *316*, 445–449.

Sephton, C.F., Good, S.K., Atkin, S., Dewey, C.M., Mayer, P., Herz, J., and Yu, G. (2010). TDP-43 is a developmentally regulated protein essential for early embryonic development. J. Biol. Chem. *285*, 6826–6834.

Shi, Y., and Manley, J.L. (2015). The end of the message: multiple protein-RNA interactions define the mRNA polyadenylation site. Genes Dev. *29*, 889–897.

Shi, Z., Luo, G., Fu, L., Fang, Z., Wang, X., and Li, X. (2013). miR-9 and miR-140-5p target FoxP2 and are regulated as a function of the social context of singing behavior in zebra finches. Journal of Neuroscience *33*, 16510–16521.

Shibasaki, T., Tokunaga, A., Sakamoto, R., Sagara, H., Noguchi, S., Sasaoka, T., and Yoshida, N. (2013). PTB deficiency causes the loss of adherens junctions in the dorsal telencephalon and leads to lethal hydrocephalus. Cereb. Cortex *23*, 1824–1835.

Shibayama, M., Ohno, S., Osaka, T., Sakamoto, R., Tokunaga, A., Nakatake, Y., Sato, M., and Yoshida, N. (2009). Polypyrimidine tract-binding protein is essential for early mouse development and embryonic stem cell proliferation. Febs J. *276*, 6658–6668.

Shimojo, M., Lee, J.H., and Hersh, L.B. (2001). Role of zinc finger domains of the transcription factor neuron-restrictive silencer factor/repressor element-1 silencing transcription factor in DNA binding and nuclear localization. J. Biol. Chem. *276*, 13121–13126.

SIDMAN, R.L., Cowen, J.S., and Eicher, E.M. (1979). Inherited muscle and nerve diseases in mice: a tabulation with commentary. Ann. N. Y. Acad. Sci. *317*, 497–505.

SIDMAN, R.L., DICKIE, M.M., and APPEL, S.H. (1964). MUTANT MICE (QUAKING AND JIMPY) WITH DEFICIENT MYELINATION IN THE CENTRAL NERVOUS SYSTEM. Science *144*, 309–311.

Sim, S.-E., Lim, C.-S., Kim, J.-I., Seo, D., Chun, H., Yu, N.-K., Lee, J., Kang, S.J., Ko, H.-G., Choi, J.-H., et al. (2016). The Brain-Enriched MicroRNA miR-9-3p Regulates Synaptic Plasticity and Memory. Journal of Neuroscience *36*, 8641–8652.

Simo, S., Jossin, Y., and Cooper, J.A. (2010). Cullin 5 regulates cortical layering by

modulating the speed and duration of Dab1-dependent neuronal migration. Journal of Neuroscience *30*, 5668–5676.

Sobkowicz, H.M., Inagaki, M., August, B.K., and Slapnick, S.M. (1999). Abortive synaptogenesis as a factor in the inner hair cell degeneration in the Bronx Waltzer (bv) mutant mouse. J. Neurocytol. *28*, 17–38.

Sommeijer, J.-P., and Levelt, C.N. (2012). Synaptotagmin-2 is a reliable marker for parvalbumin positive inhibitory boutons in the mouse visual cortex. PLoS ONE *7*, e35323.

Spassky, N., Merkle, F.T., Flames, N., Tramontin, A.D., García-Verdugo, J.M., and Alvarez-Buylla, A. (2005). Adult ependymal cells are postmitotic and are derived from radial glial cells during embryogenesis. Journal of Neuroscience *25*, 10–18.

Spellman, R., Llorian, M., and Smith, C.W.J. (2007). Crossregulation and functional redundancy between the splicing regulator PTB and its paralogs nPTB and ROD1. Mol. Cell *27*, 420–434.

Sprunger, L.K., Escayg, A., Tallaksen-Greene, S., Albin, R.L., and Meisler, M.H. (1999). Dystonia associated with mutation of the neuronal sodium channel Scn8a and identification of the modifier locus Scnm1 on mouse chromosome 3. Human Molecular Genetics *8*, 471–479.

Srikantan, S., and Gorospe, M. (2012). HuR function in disease. Front Biosci (Landmark Ed) *17*, 189–205.

Suckale, J., Wendling, O., Masjkur, J., Jäger, M., Münster, C., Anastassiadis, K., Stewart, A.F., and Solimena, M. (2011). PTBP1 is required for embryonic development before gastrulation. PLoS ONE *6*, e16992.

Sun, A.X., Crabtree, G.R., and Yoo, A.S. (2013a). MicroRNAs: regulators of neuronal fate. Current Opinion in Cell Biology *25*, 215–221.

Sun, S., Zhang, Z., Sinha, R., Karni, R., and Krainer, A.R. (2010). SF2/ASF autoregulation involves multiple layers of post-transcriptional and translational control. Nat. Struct. Mol. Biol. *17*, 306–312.

Sun, W., Wagnon, J.L., Mahaffey, C.L., Briese, M., Ule, J., and Frankel, W.N. (2013b). Aberrant sodium channel activity in the complex seizure disorder of Celf4 mutant mice. The Journal of Physiology *591*, 241–255.

Swanson, K.C.K.-Y.L.R.B.M.G.C.Z.Y.Y.L.S.M.C.M.S.G.X.A.K.T.A.H.N.C.T.K.M.T.H.F.K.J.H.Y.M.G.-P.G.G.N.S.S.N.T.F.M.A.J.R.D.M., Lee, K.-Y., Batra, R., Goodwin, M., Zhang, C., Yuan, Y., Shiue, L., Cline, M., Scotti, M.M., Xia, G., et al. (2012). Muscleblind-like 2-Mediated Alternative Splicing in the Developing Brain and Dysregulationin Myotonic Dystrophy. Neuron *75*, 437–450.

Szabo, A., Dalmau, J., Manley, G., Rosenfeld, M., Wong, E., Henson, J., Posner, J.B., and Furneaux, H.M. (1991). HuD, a paraneoplastic encephalomyelitis antigen, contains RNA-binding domains and is homologous to Elav and Sex-lethal. Cell *67*, 325–333.

Sørensen, J.B., Nagy, G., Varoqueaux, F., Nehring, R.B., Brose, N., Wilson, M.C., and Neher, E. (2003). Differential control of the releasable vesicle pools by SNAP-25 splice variants and SNAP-23. Cell *114*, 75–86.

Tabuchi, A., Yamada, T., Sasagawa, S., Naruse, Y., Mori, N., and Tsuda, M. (2002). REST4-mediated modulation of REST/NRSF-silencing function during BDNF gene promoter activation. Biochem. Biophys. Res. Commun. *290*, 415–420.

Tabuchi, K., and Südhof, T.C. (2002). Structure and evolution of neurexin genes: insight into the mechanism of alternative splicing. Genomics *79*, 849–859.

Tang, Z.Z., Zheng, S., Nikolic, J., and Black, D.L. (2009). Developmental Control of CaV1.2 L-Type Calcium Channel Splicing by Fox Proteins. Molecular and Cellular Biology *29*, 4757–4765.

Tollervey, J.R., Curk, T., Rogelj, B., Briese, M., Cereda, M., Kayikci, M., König, J., Hortobágyi, T., Nishimura, A.L., Zupunski, V., et al. (2011). Characterizing the RNA targets and position-dependent splicing regulation by TDP-43. Nat Neurosci *14*, 452–458.

Trapnell, C., Roberts, A., Goff, L., Pertea, G., Kim, D., Kelley, D.R., Pimentel, H., Salzberg, S.L., Rinn, J.L., and Pachter, L. (2012). Differential gene and transcript expression analysis of RNA-seq experiments with TopHat and Cufflinks. Nat Protoc *7*, 562–578.

Traunmüller, L., Bornmann, C., and Scheiffele, P. (2014). Alternative splicing coupled nonsense-mediated decay generates neuronal cell type-specific expression of SLM proteins. Journal of Neuroscience *34*, 16755–16761.

Tremblay, R., Lee, S., and Rudy, B. (2016). GABAergic Interneurons in the Neocortex: From Cellular Properties to Circuits. Neuron *91*, 260–292.

Trommsdorff, M., Gotthardt, M., Hiesberger, T., Shelton, J., Stockinger, W., Nimpf, J., Hammer, R.E., Richardson, J.A., and Herz, J. (1999). Reeler/Disabled-like disruption of neuronal migration in knockout mice lacking the VLDL receptor and ApoE receptor 2. Cell *97*, 689–701.

Tronche, F., Kellendonk, C., Kretz, O., Gass, P., Anlag, K., Orban, P.C., Bock, R., Klein, R., and Schütz, G. (1999). Disruption of the glucocorticoid receptor gene in the nervous system results in reduced anxiety. Nat Genet *23*, 99–103.

Turrigiano, G. (2011). Too many cooks? Intrinsic and synaptic homeostatic mechanisms in cortical circuit refinement. Annu. Rev. Neurosci. *34*, 89–103.

Uemura, T., Lee, S.-J., Yasumura, M., Takeuchi, T., Yoshida, T., Ra, M., Taguchi, R., Sakimura, K., and Mishina, M. (2010). Trans-synaptic interaction of GluRdelta2 and Neurexin through Cbln1 mediates synapse formation in the cerebellum. Cell *141*, 1068–1079.

Uhlhaas, P.J., and Singer, W. (2010). Abnormal neural oscillations and synchrony in schizophrenia. Nat. Rev. Neurosci. *11*, 100–113.

Ule, J., Jensen, K.B., Ruggiu, M., Mele, A., Ule, A., and Darnell, R.B. (2003). CLIP identifies Nova-regulated RNA networks in the brain. Science *302*, 1212–1215.

Underwood, J.G., Boutz, P.L., Dougherty, J.D., Stoilov, P., and Black, D.L. (2005). Homologues of the Caenorhabditis elegans Fox-1 Protein Are Neuronal Splicing Regulators in Mammals. Molecular and Cellular Biology *25*, 10005–10016.

van Kouwenhove, M., Kedde, M., and Agami, R. (2011). MicroRNA regulation by RNA-binding proteins and its implications for cancer. Nat. Rev. Cancer *11*, 644–656.

Vanden Broeck, L., Callaerts, P., and Dermaut, B. (2014). TDP-43-mediated neurodegeneration: towards a loss-of-function hypothesis? Trends in Molecular Medicine *20*, 66–71.

Voineagu, I., Wang, X., Johnston, P., Lowe, J.K., Tian, Y., Horvath, S., Mill, J., Cantor, R.M., Blencowe, B.J., and Geschwind, D.H. (2011). Transcriptomic analysis of autistic brain reveals convergent molecular pathology. Nature *474*, 380–384.

Wagnon, J.L., Mahaffey, C.L., Sun, W., Yang, Y., Chao, H.-T., and Frankel, W.N. (2011). Etiology of a genetically complex seizure disorder in Celf4 mutant mice. Genes Brain Behav. *10*, 765–777.

Wagnon, J.L., Briese, M., Sun, W., Mahaffey, C.L., Curk, T., Rot, G., Ule, J., and Frankel, W.N. (2012). CELF4 regulates translation and local abundance of a vast set of mRNAs, including genes associated with regulation of synaptic function. PLoS Genet. *8*, e1003067.

Wahl, M.C., Will, C.L., and Lührmann, R. (2009). The spliceosome: design principles of a dynamic RNP machine. Cell *136*, 701–718.

Wamsley, B., and Fishell, G. (2017). Genetic and activity-dependent mechanisms underlying interneuron diversity. Nat. Rev. Neurosci. *18*, 299–309.

Wang, V.Y., and Zoghbi, H.Y. (2001). Genetic regulation of cerebellar development. Nat. Rev. Neurosci. *2*, 484–491.

Weyn-Vanhentenryck, S.M., Mele, A., Yan, Q., Sun, S., Farny, N., Zhang, Z., Xue, C., Herre, M., Silver, P.A., Zhang, M.Q., et al. (2014a). HITS-CLIP and integrative modeling define the Rbfox splicing-regulatory network linked to brain development and autism. Cell Rep *6*, 1139–1152.

Weyn-Vanhentenryck, S.M., Mele, A., Yan, Q., Sun, S., Farny, N., Zhang, Z., Xue, C., Herre, M., Silver, P.A., Zhang, M.Q., et al. (2014b). HITS-CLIP and integrative modeling define the Rbfox splicing-regulatory network linked to brain development and autism. Cell Rep *6*, 1139–1152.

Whitlon, D.S., Gabel, C., and Zhang, X. (1996). Cochlear inner hair cells exist transiently in the fetal Bronx Waltzer (bv/bv) mouse. J. Comp. Neurol. *364*, 515–522.

Will, C.L., and Lührmann, R. (2011). Spliceosome structure and function. Cold Spring Harbor Perspectives in Biology *3*, a003707–a003707.

Wu, J., Akerman, M., Sun, S., McCombie, W.R., Krainer, A.R., and Zhang, M.Q. (2011). SpliceTrap: a method to quantify alternative splicing under single cellular conditions. Bioinformatics *27*, 3010–3016.

Wu, J.I., Reed, R.B., GRABOWSKI, P.J., and Artzt, K. (2002). Function of quaking in myelination: regulation of alternative splicing. Proc. Natl. Acad. Sci. U.S.a. *99*, 4233–4238.

Wu, L.-S., Cheng, W.-C., Hou, S.-C., Yan, Y.-T., Jiang, S.-T., and Shen, C.-K.J. (2010). TDP-43, a neuro-pathosignature factor, is essential for early mouse embryogenesis. Genesis *48*, 56–62.

Xie, J., Ameres, S.L., Friedline, R., Hung, J.-H., Zhang, Y., Xie, Q., Zhong, L., Su, Q., He, R., Li, M., et al. (2012). Long-term, efficient inhibition of microRNA function in mice using rAAV vectors. Nat Meth *9*, 403–409.

Xue, M., Atallah, B.V., and Scanziani, M. (2014). Equalizing excitation-inhibition ratios across visual cortical neurons. Nature *511*, 596–600.

Xue, Q., Yu, C., Wang, Y., Liu, L., Zhang, K., Fang, C., Liu, F., Bian, G., Song, B., Yang, A., et al. (2016). miR-9 and miR-124 synergistically affect regulation of dendritic branching via the AKT/GSK3β pathway by targeting Rap2a. Sci Rep *6*, 26781.

Xue, Y., Ouyang, K., Huang, J., Zhou, Y., Ouyang, H., Li, H., Wang, G., Wu, Q., Wei, C., Bi, Y., et al. (2013). Direct conversion of fibroblasts to neurons by reprogramming PTB-regulated microRNA circuits. Cell *152*, 82–96.

Yamamoto, J., Suh, J., Takeuchi, D., and Tonegawa, S. (2014). Successful execution of working memory linked to synchronized high-frequency gamma oscillations. Cell *157*, 845–857.

Yang, C., Wang, H., Qiao, T., Yang, B., Aliaga, L., Qiu, L., Tan, W., Salameh, J., McKenna-Yasek, D.M., Smith, T., et al. (2014). Partial loss of TDP-43 function causes phenotypes of amyotrophic lateral sclerosis. Proceedings of the National Academy of Sciences *111*, E1121–E1129.

Yang, Y.Y., Yin, G.L., and Darnell, R.B. (1998). The neuronal RNA-binding protein

Nova-2 is implicated as the autoantigen targeted in POMA patients with dementia. Proc. Natl. Acad. Sci. U.S.a. *95*, 13254–13259.

Yang, Y., Mahaffey, C.L., Bérubé, N., Maddatu, T.P., Cox, G.A., and Frankel, W.N. (2007). Complex seizure disorder caused by Brunol4 deficiency in mice. PLoS Genet. *3*, e124.

Yano, M., Hayakawa-Yano, Y., Mele, A., and Darnell, R.B. (2010). Nova2 regulates neuronal migration through an RNA switch in disabled-1 signaling. Neuron *66*, 848–858.

Yap, K., and Makeyev, E.V. (2013). Regulation of gene expression in mammalian nervous system through alternative pre-mRNA splicing coupled with RNA quality control mechanisms. Mol. Cell. Neurosci. *56*, 420–428.

Yap, K., Lim, Z.Q., Khandelia, P., Friedman, B., and Makeyev, E.V. (2012). Coordinated regulation of neuronal mRNA steady-state levels through developmentally controlled intron retention. Genes Dev. *26*, 1209–1223.

Ying, Y., Wang, X.-J., Vuong, C.K., Lin, C.-H., Damianov, A., and Black, D.L. (2017). Splicing Activation by Rbfox Requires Self-Aggregation through Its Tyrosine-Rich Domain. Cell *170*, 312–323.e10.

Yizhar, O., Fenno, L.E., Prigge, M., Schneider, F., Davidson, T.J., O'Shea, D.J., Sohal, V.S., Goshen, I., Finkelstein, J., Paz, J.T., et al. (2011). Neocortical excitation/inhibition balance in information processing and social dysfunction. Nature *477*, 171–178.

Yoo, A.S., Sun, A.X., Li, L., Shcheglovitov, A., Portmann, T., Li, Y., Lee-Messer, C., Dolmetsch, R.E., Tsien, R.W., and Crabtree, G.R. (2011). MicroRNA-mediated conversion of human fibroblasts to neurons. Nature *476*, 228–231.

Yoshida, K., and Ogawa, S. (2014). Splicing factor mutations and cancer. Wiley Interdiscip Rev RNA *5*, 445–459.

Yoshida, K., Sanada, M., Shiraishi, Y., Nowak, D., Nagata, Y., Yamamoto, R., Sato, Y., Sato-Otsubo, A., Kon, A., Nagasaki, M., et al. (2011). Frequent pathway mutations of splicing machinery in myelodysplasia. Nature *478*, 64–69.

Zapata, A., Capdevila, J.L., Tarrason, G., Adan, J., Martínez, J.M., Piulats, J., and Trullas, R. (1997). Effects of NMDA-R1 antisense oligodeoxynucleotide administration: behavioral and radioligand binding studies. Brain Res. *745*, 114–120.

Zhang, Y.-J., Xu, Y.-F., Cook, C., Gendron, T.F., Roettges, P., Link, C.D., Lin, W.-L., Tong, J., Castanedes-Casey, M., Ash, P., et al. (2009). Aberrant cleavage of TDP-43 enhances aggregation and cellular toxicity. Proceedings of the National Academy of Sciences *106*, 7607–7612.

Zhao, C., Sun, G., Li, S., and Shi, Y. (2009). A feedback regulatory loop involving microRNA-9 and nuclear receptor TLX in neural stem cell fate determination. Nat.

Struct. Mol. Biol. *16*, 365–371.

Zhao, L., Tian, D., Xia, M., Macklin, W.B., and Feng, Y. (2006). Rescuing qkV dysmyelination by a single isoform of the selective RNA-binding protein QKI. Journal of Neuroscience *26*, 11278–11286.

Zheng, S., and Black, D.L. (2013). Alternative pre-mRNA splicing inneurons: growing up and extendingits reach. Trends in Genetics 1–7.

Zheng, S., Gray, E.E., Chawla, G., Porse, B.T., O'Dell, T.J., and Black, D.L. (2012). PSD-95 is post-transcriptionally repressed during early neural development by PTBP1 and PTBP2. Nat Neurosci *15*, 381–8–S1.

Zimmermann, J., Trimbuch, T., and Rosenmund, C. (2014). Synaptobrevin 1 mediates vesicle priming and evoked release in a subpopulation of hippocampal neurons. J. Neurophysiol. *112*, 1559–1565.

Zinszner, H., Sok, J., Immanuel, D., Yin, Y., and Ron, D. (1997). TLS (FUS) binds RNA in vivo and engages in nucleo-cytoplasmic shuttling. J. Cell. Sci. *110 (Pt 15)*, 1741–1750.